

AD-A038 632

AVCO EVERETT RESEARCH LAB INC EVERETT MASS  
TURBULENCE ENVIRONMENT CHARACTERIZATION.(U)  
MAR 77 M G MILLER, P L ZIESKE

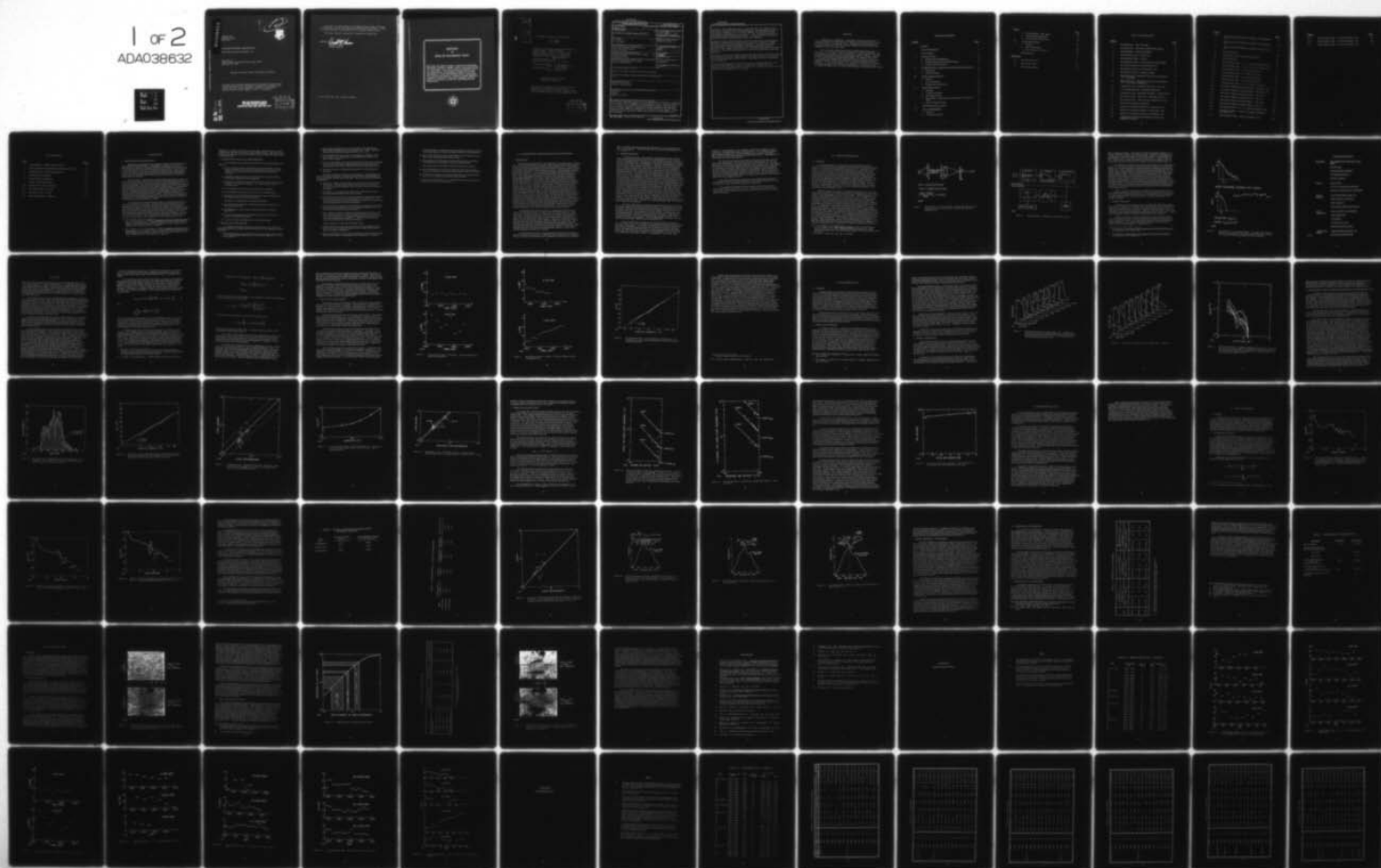
F/G 4/1

UNCLASSIFIED

RADC-TR-77-70

F30602-76-C-0054  
NL

1 of 2  
ADA038632





AD A 038632

RADC-TR-77-70  
Technical Report  
March 1977



## TURBULENCE ENVIRONMENT CHARACTERIZATION

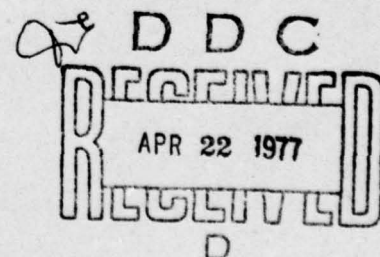
AVCO Everett Research Laboratory, Inc.

Sponsored by  
Defense Advanced Research Projects Agency (DoD)  
ARPA Order No. 2646

Approved for public release; distribution unlimited.

The views and conclusions contained in this document are those of the authors and should not be interpreted as necessarily representing the official policies, either expressed or implied, of the Defense Advanced Research Projects Agency or the U. S. Government.

ROME AIR DEVELOPMENT CENTER  
AIR FORCE SYSTEMS COMMAND  
GRIFFISS AIR FORCE BASE, NEW YORK 13441

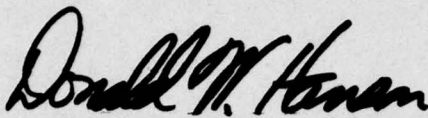


AD No. \_\_\_\_\_  
DDC FILE COPY

This report has been reviewed by the RADC Information Office (OI) and is releasable to the National Technical Information Service (NTIS). At NTIS it will be releasable to the general public including foreign nations.

This report has been reviewed and is approved for publication.

APPROVED:

A handwritten signature in dark ink, appearing to read "Donald W. Hanson". The signature is fluid and cursive, with the first name "Donald" being more prominent.

DONALD W. HANSON  
Project Engineer

Do not return this copy. Retain or destroy.



*MISSION  
of  
Rome Air Development Center*

RADC plans and conducts research, exploratory and advanced development programs in command, control, and communications (C<sup>3</sup>) activities, and in the C<sup>3</sup> areas of information sciences and intelligence. The principal technical mission areas are communications, electromagnetic guidance and control, surveillance of ground and aerospace objects, intelligence data collection and handling, information system technology, ionospheric propagation, solid state sciences, microwave physics and electronic reliability, maintainability and compatibility.





UNCLASSIFIED

SECURITY CLASSIFICATION OF THIS PAGE (When Data Entered)

19 REPORT DOCUMENTATION PAGE		READ INSTRUCTIONS BEFORE COMPLETING FORM	
1. REPORT NUMBER RADC-TR-77-70	2. GOVT ACCESSION NO.	3. RECIPIENT'S CATALOG NUMBER	
4. TITLE (and Subtitle) TURBULENCE ENVIRONMENT CHARACTERIZATION.		5. TYPE OF REPORT & PERIOD COVERED Interim Report. 15 Oct 75—15 Sep 76.	
7. AUTHOR(s) M. G. Miller P. L. Zieske		6. PERFORMING ORG. REPORT NUMBER N/A	
9. PERFORMING ORGANIZATION NAME AND ADDRESS AVCO Everett Research Laboratory, Inc. 2385 Revere Beach Parkway Everett MA 02149		8. CONTRACT OR GRANT NUMBER(s) F30602-76-C-0054 new	
11. CONTROLLING OFFICE NAME AND ADDRESS Defense Advanced Research Projects Agency 1400 Wilson Blvd Arlington VA 22209		10. PROGRAM ELEMENT, PROJECT, TASK AREA & WORK UNIT NUMBERS 62301E 26460115 101 112P.	
14. MONITORING AGENCY NAME & ADDRESS (if different from Controlling Office) Rome Air Development Center (OCSE) Griffiss AFB NY 13441		12. REPORT DATE March 1977	
		13. NUMBER OF PAGES 107	
		15. SECURITY CLASS. (of this report) UNCLASSIFIED	
		15a. DECLASSIFICATION/DOWNGRADING SCHEDULE N/A	
16. DISTRIBUTION STATEMENT (of this Report)  Approved for public release; distribution unlimited.			
17. DISTRIBUTION STATEMENT (of the abstract entered in Block 20, if different from Report) Same			
18. SUPPLEMENTARY NOTES RADC Project Engineer: Donald W. Hanson (OCSE)			
19. KEY WORDS (Continue on reverse side if necessary and identify by block number) Turbulence Seeing Atmospheric Optics			
20. ABSTRACT (Continue on reverse side if necessary and identify by block number) This report covers some aspects of our investigations of atmospheric turbulence as it relates to the propagation of electromagnetic waves. The major emphasis in this report is a presentation and discussion of data obtained during the last year with a variety of experimental systems deployed at the ARPA Maui Optical Station (AMOS) atop Haleakala on the island of Maui, Hawaii. A brief discussion of the operational aspects and status of the instrumentation is also included. —> next page (cont'd)			

UNCLASSIFIED

SECURITY CLASSIFICATION OF THIS PAGE(When Data Entered)

cont  
→ Estimates of the correlation scale,  $r_0$ , were obtained on 24 nights (a total data set of 228 points) using the Seeing Monitor. The measured mean value is 9.6 cm with a range of (5.3 - 17.8) cm at 5000 Å. The uncertainty in the measurements is estimated to be of order (5 - 10)%. Absolute calibration of the entire system is the major uncertainty. A variety of effects including trends and apparent nonstationarity effects were observed.

0.00058 Estimates of high altitude turbulence profiles obtained with the Star Sensor indicate a flattening and in some cases an increase in turbulent strength in the vicinity of the meteorological tropopause. Log-Amplitude variances integrated over the 36 cm aperture of this device have a mean value of  $5.8 \times 10^{-4}$  and a range of  $(1.5 - 28) \times 10^{-4}$ . Nonstationarity effects were often observed. Comparative and simultaneous scintillation measurements show good agreement.  
0.00015 - 0.00028

Internal agreement of the optical observations with empirical turbulence profile information is not good. Rough agreement exist with theoretical calculations using the Hufnagel wind correlated model. Agreement with other observations is reasonable.

↑ Data collected during the initial AMOS testing of the RTAM indicates a performance level sufficient to obtain an independent estimate of  $r_0$  for comparison with the Seeing Monitor. However, it is unlikely that high frequency MTF and phase information can be obtained.

UNCLASSIFIED

SECURITY CLASSIFICATION OF THIS PAGE(When Data Entered)



## PREFACE

This report is submitted in compliance with the requirements of Contract F30602-76-C-0054 and covers work carried out during the period 15 October 1975 to 15 September 1976. Related work under a previous contract (F30602-75-C-0012) is reported in RADC-TR-75-185 (July 1976) and RADC-TR-76-189 (June 1976).

We would like to thank the staff of the AMOS observatory and, in particular, R. Taft and W. Zane for assistance in collecting the data. We acknowledge the assistance and cooperation of J. Spenser and D. Tarazano of RADC where the meteorological and profile data was reduced. Copies of the radiosonde data were provided by RADC. We thank J. Ochs and R. Lawrence of the NOAA Environmental Research Laboratories for providing us with the results of their airborne experiments and numerical modeling. H. Yura of Aerospace, Inc., was very cooperative in providing us with the results of his theoretical calculations. A. MacGovern and J. LeFebvre of Itek, Inc., were particularly helpful with regard to the RTAM.



## TABLE OF CONTENTS

<u>Section</u>	<u>Page</u>
Preface	1
List of Illustrations	4
List of Tables	7
I. INTRODUCTION	8
1. Background and Objectives	8
2. Program Status and Accomplishments	9
3. Results and Conclusions	9
II. EXPERIMENTAL OPERATIONS AND INSTRUMENTATION	12
1. Operations	12
2. Instrumentation	13
III. SEEING MONITOR DATA	15
1. General	15
2. Error Estimates	18
3. Results and Conclusions	24
IV. STAR SENSOR DATA	29
1. General	29
2. Turbulent Profiles	29
3. Scintillation Data	30
4. Star Sensor - Small Aperture Photometer Comparative Data	34
5. Noise Evaluation Tests	40
V. METEOROLOGICAL DATA	45
VI. DATA COMPARISONS	47
1. General	47
2. Turbulence Profile	47

<u>Section</u>	<u>Page</u>
3. Seeing Monitor - Star Sensor	58
4. Theoretical Comparisons	59
5. Experimental Comparisons	59
VII. RTAM AMOS TESTS	63
1. General	63
2. MTF Performance	63
3. Phase Transfer Function	65
REFERENCES	70
<u>Appendices</u>	
A. Seeing Monitor Data	72
B. Star Sensor Data	82
C. Meteorological Data	99

## LIST OF ILLUSTRATIONS

<u>Figure</u>		<u>Page</u>
1	Seeing Monitor - Basic Concept	16
2	Seeing Monitor - Electronic and Data Processing	17
3	Seeing Monitor - Theoretical Model	21
4	Seeing Monitor Data - Variability	25
5	Seeing Monitor Data - Trends	26
6	Seeing Monitor Data - Correlation Scale Distribution	27
7	Star Sensor Profiles of 18 November 1975	31
8	Star Sensor Profiles of 15 November 1975	32
9	Star Sensor Profiles - Monthly Average	33
10	Star Sensor Log - Amplitude Variance of 18 November 1975 - Histogram	35
11	Star Sensor Log - Amplitude Variance of 18 November 1975 - Cumulative Probability	36
12	Comparative Log - Amplitude Variances - Raw Data	37
13	b-29 Photometer Data - Bandwidth Dependence	38
14	Comparative Log - Amplitude Variances - Adjusted Data	39
15	Star Sensor Noise - Total Log - Amplitude Variance	41
16	Star Sensor Noise - Filtered Log - Amplitude Variance	42
17	Star Sensor Operation Conditions	44
18	Empirical Turbulence Profile of 17 November 1975	48
19	Empirical Turbulence Profile of 18 November 1975	49
20	Empirical Turbulence Profile of 21 November 1975	50
21	Comparison of Measured and Profile Derived Log - Amplitude Variances	54

<u>Figure</u>		<u>Page</u>
22	Two Dimensional Turbulence Contours of 17 November 1975	55
23	Two Dimensional Turbulence Contours of 18 November 1975	56
24	Two Dimensional Turbulence Contours of 20 November 1975	57
25	RTAM-MTF Data	64
26	RTAM-Reduction in High-Frequency (S/N)	66
27	RTAM-PTF Data	68
A-1	Seeing Monitor Data - 11, 12, 14 and 15 November 1975	75
A-2	Seeing Monitor Data - 17, 18, 19 and 21 November 1975	76
A-3	Seeing Monitor Data - 6, and 8 December 1975	77
A-4	Seeing Monitor Data - 12, 13 and 27 May 1976	78
A-5	Seeing Monitor Data - 10, 18 and 21 June 1976	79
A-6	Seeing Monitor Data - 24, 29 and 30 June 1976	80
A-7	Seeing Monitor Data - 6, 8, 9, 12 and 13 July 1976	81
B-1	Star Sensor Nightly Averaged Profiles - November 1975	93
B-2	Star Sensor Nightly Averaged Profiles - December 1975	94
B-3	Star Sensor Nightly Averaged Profiles - April 1976	95
B-4	Star Sensor Nightly Averaged Profiles - May 1976	96
B-5	Star Sensor Nightly Averaged Profiles - June 1976	97
B-6	Star Sensor Nightly Averaged Profiles - July 1976	98
C-1	Microthermal Data - 14, 15, 17 and 18 November 1975	102
C-2	Microthermal Data - 19 and 21 November and 6 and 8 December 1975	103
C-3	Meteorological Data - 14 and 15 November 1975	104

<u>Figure</u>		<u>Page</u>
C-4	Meteorological Data - 17 and 18 November 1975	105
C-5	Meteorological Data - 19 and 20 November 1975	106
C-6	Meteorological Data - 21 and 22 November 1975	107



## LIST OF TABLES

<u>Table</u>		<u>Page</u>
1	Seeing Monitor - System Characteristics	19
2	Optical Parameters Obtained from Empirical Profiles	52
3	Seeing Monitor - Profile Comparisons	53
4	Theoretical Comparisons	60
5	Experimental Comparisons	62
6	RTAM - MTF Performance	67
A-1	Seeing Monitor Data - Summary	74
B-1	Star Sensor Data - Summary	84
B-2	Star Sensor Data - Profile	85
C-1	Microthermal Data - Summary	101

## I. INTRODUCTION

### 1. BACKGROUND AND OBJECTIVES

Atmospheric turbulence has a significant impact on the operation of large aperture optical systems. Degradations observed include loss of resolution when imaging, increased difficulty in detecting dim objects, loss of tracking accuracy, as well as a number of other effects. The evaluation of the performance of any system and the specification of operating parameters for systems designed to eliminate or minimize these degradations require detailed empirical information about the turbulent environment in which they must operate.

This program, Turbulence Environment Characterization, has as its objective the collection, processing, analysis and interpretation of data from a variety of experiments in order to provide a characterization of the turbulent environment. The site of the measurements is the ARPA Maui Optical Station (AMOS) atop Haleakala on the island of Maui, Hawaii. Experimental instrumentation which has been or will be employed include the Seeing Monitor, the Real Time Atmospheric Measuring System (RTAM), the Star Sensor, a differential Hartmann sensor, a small aperture photometer, microthermal probes and an acoustic sounder. During a previous program, Turbulence Characterization and Control, much of this instrumentation was installed and several periods of data collection were carried out. Details of this work can be found in Refs. 1 and 2.

During the period covered by this report, a considerable amount of data was collected and analyzed. In addition, several upgrades to the instrumentation were accomplished and an initial series of tests with the RTAM were completed. The overall program status, accomplishments and the most significant results and conclusions are given below. More detailed discussions are given in the balance of the report. Section II summarizes the experimental operations and the status of all instrumentation. Sections III, IV and V summarize the Seeing Monitor, Star Sensor and meteorological data, respectively. The complete and detailed data is given in the

1. M. G. Miller and P. F. Kellen, Turbulence Characterization and Control, Interim Technical Report, Contract #F30602-75-C-0012 (Avco Everett Research Laboratory), Rome Air Development Center Technical Report #RADC-TR-75-185 (July 1975), (A015759).
2. M. G. Miller, P. L. Zieske and G. Dryden, Turbulence Characterization and Control, Final Technical Report, Contract #F30602-75-C-0012 (Avco Everett Research Laboratory), Rome Air Development Center Technical Report #RADC-TR-76-189 (June 1976), (A027155).

Appendices. Section VI discusses various data comparisons and includes comparisons with theory and other experimental results. The final section gives a brief analysis of some of the data collected during the initial period of RTAM testing.

## 2. PROGRAM STATUS AND ACCOMPLISHMENTS

As of the date of this report, the status of the instrumentation is as follows.

- Data collection with the meteorological instrumentation, Seeing Monitor and Star Sensor has been reduced to a level such that the normal observatory personnel can operate these systems as scheduled.
- The PDP-8 data processing system has been operating reliably. Input/output capability will be upgraded.
- Because of operational failures, the acoustic sounder was returned to RADC for complete evaluation. It is expected back early in November 1976.
- The new tape recorder has been installed and evaluated.
- The RTAM has undergone an initial period of AMOS testing.
- Operations with the differential Hartmann sensor and small aperture photometer have been discontinued.

Important accomplishments include the following:

- An intensive period of data collection during late November and early December 1975.
- Establishment of routine data collection activities starting in April 1976.
- A series of comparative measurements between the Star Sensor and small aperture photometer.
- A series of noise evaluation tests with the Star Sensor.

## 3. RESULTS AND CONCLUSIONS

Two hundred and twenty-eight ten minute samples of  $r_0$  have been obtained on twenty-four nights with the Seeing Monitor yielding the following information.

- The ensemble has an approximate Gaussian distribution with a mean of 9.6 cm, a standard deviation of 2.2 cm and a range of (5.3 - 17.8) cm at 5000 Å.

- The statistical significance of a given value is estimated to be better than  $\pm 2\%$  with a precision of better than  $\pm 1/2\%$ . Estimated relative uncertainty due to known errors is (5 - 10)%.
- A potentially major uncertainty is the absolute calibration of the entire system. No simultaneous and independent measure of  $r_0$  has yet been obtained.
- A variety of behavior over periods of hours has been seen, including near constant conditions, large variability over time periods of minutes and trends towards both improving and degrading seeing.
- On some occasions, substantial atmospheric non-stationarity is indicated.

Star Sensor data was collected on 30 occasions. One hundred and twenty-six upper atmospheric profiles and 218 twenty-minute samples of the log-amplitude variance were collected. These data yield the following information.

- Significant changes in the profiles are seen in time scales of 20 to 40 minutes. Profiles tend to flatten and in some cases indicate increased levels of turbulence in the vicinity of the meteorological tropopause.
- Atmospheric non-stationarity effects were sufficiently strong to invalidate approximately 40% of the profiles.
- The aperture average (36 cm) twenty minute log-amplitude variances have a mean of  $5.8 \times 10^{-4}$  with a range of  $(1.5 - 28) \times 10^{-4}$ . The ensemble of twenty-four second variances collected on a single night show an approximate Gaussian distribution.
- Simultaneous Star Sensor and small aperture photometer data show agreement in log-amplitude variances of approximately  $0.5 \times 10^{-4}$  for the most directly comparable results.
- The results of the noise evaluation tests have lead to a more complete characterization of noise properties than previously existed. The operational limit for reliable information has been established as third to fourth stellar magnitude. The effect of noise on the reduced profile has not yet been determined.

Data comparisons lead to the following results.

- Agreement between the empirical profile and the Seeing Monitor data is not good. Spatial variability of the turbulent field could be the cause of this discrepancy.
- Some correlation is seen in the Seeing Monitor and Star Sensor data, particularly relative to atmospheric non-stationarity. However,

because these two instruments tend to emphasize different portions of the atmosphere, a strong correlation should not be anticipated.

- Theoretical modeling of the profile based on gross meteorological data, yields rough agreement with the data.
- The agreement of this data for both scintillation and correlation scale agrees quite reasonably with other reported data.

The initial tests of the RTAM yield the following conclusions:

- Current performance levels would provide data which would be extremely difficult to process for high frequency MTF information.
- It should be possible to implement RTAM for an independent measure of  $r_0$  for comparison with the Seeing Monitor.
- Because of several effects, it is unlikely that useful high-frequency phase information can be obtained.



## II. EXPERIMENTAL OPERATIONS AND INSTRUMENTATION

### 1. OPERATIONS

During the contract period, several types of operations were carried out. The first of these was an intensive data collection period which started in early November and continued until early December 1975. The measurement systems used during this period were the microthermal probes, acoustic sounder, Star Sensor, Seeing Monitor and the b-29 photometer equipped with a small aperture. The microthermal probes, Seeing Monitor and photometer outputs were processed using the PDP-8 data processing system. The analog signals from these sensors were sampled 1350 times during approximately 8.25 minutes followed by a data printout which required approximately 1.75 minutes. This resulted in a basic 10 minute data processing cycle. More detailed discussions of these various systems can be found in Ref. 2. The Seeing Monitor and photometer were mounted on the b-37 and b-29 telescopes, respectively. Because these two telescopes share a common mount, data from these systems could not be collected simultaneously. Hence, alternate 10 minute cycles were used to obtain data with these two devices. The twenty minute Star Sensor cycle was synchronized with the other systems yielding a single data cycle for every two PDP-8 cycles. Typical data runs lasted for three hours and were started at various times during the night. Successful data runs with some or all of these systems were accomplished on ten occasions. During the week of 17-21 November, personnel from the NOAA Environmental Research Laboratories collected data with a light aircraft instrumented with a microthermal probe. Coupled with other instrumentation, this yields an empirical estimate of the turbulence profile above the site which can then be compared with the direct optical measurements. The results obtained during this period are discussed in other sections of this report.

Subsequent to the above activities, a routine data collection procedure was established using the Star Sensor and Seeing Monitor. Data runs were typically two hours in length and were implemented using the same basic 10 minute collection cycle discussed above. Operations were generally scheduled on two nights a week but were often preempted by higher priority operations or bad weather. Data was collected on an additional twenty-one nights during the period 16 April to 13 July 1976. Near the end of this period, atmospheric data using the technique of speckle interferometry was also collected by a different experimental group. Some simultaneous data using the Seeing Monitor was obtained. When reduced, this data (speckle) may provide an independent measure of  $r_0$  for comparison with the Seeing Monitor results.

A third type of activity carried out during this period were special operations whose objective was to establish proper operation of instrumentation, collection of simultaneous and comparative data and noise evaluation

tests. Systems involved included the Star Sensor, b-29 photometer and the acoustic sounder. Details of this work are discussed in Sections II.2, IV.4, and IV.5.

## 2. INSTRUMENTATION

The Seeing Monitor, Star Sensor, meteorological sensor and the PDP-8 data processing system have been established as routine systems and their operation can be carried out by the normal observatory personnel on an as scheduled basis. Maintenance, while time consuming on occasion, has not been a major source of difficulty. Several modifications and additions to some of the systems have been carried out or are being planned. Minor software changes have been made to the Star Sensor to facilitate output presentation and remote fine drive controls have been installed so that optimization of this instrument's operation can be carried out without entering the dome. A problem with the Seeing Monitor which has become more severe is the unbalance in the two seeing angle outputs. The source of this appears to be difficulties with the optical alignment of the dove prism. Because studies of potential non-isotropic effects is not a high priority item, the prism will be removed before mounting on the 1.6 meter telescope. It is expected that this will eliminate much of the problem and thus allow other effects such as wavelength scaling to be studied. The routine meteorological sensor outputs have been connected (in parallel to the PDP-8 A/D converter) to a digital meter equipped with a sequencing switch and scaling electronics located in the observatory control room. This allows a direct visual reading of the gross meteorological conditions (wind direction and speed, temperature and dew point) without resorting to data reduction with the PDP-8. It is also expected that an automatic, remotely read barometric sensor will be added in the near future. The PDP-8 has been operating reliably. However, the existing teletype input/output has proved restrictive for certain types of work. Therefore, a high speed paper tape reader/punch will be obtained and installed.

The major difficulty encountered has been with the acoustic sounder. Although it appeared that proper operation had been established prior to the November-December experiments and raw data was collected and recorded during the entire period, the data processing yielded results which were dominated by noise. Subsequently, a variety of tests, modifications, data collection attempts and other remedial actions were taken, none of which yielded usable data. Hence the instrument was returned to RADC for a complete checkout and evaluation. It is now apparently operating correctly and will be returned to AMOS in early November 1976.

The b-29 photometer equipped with a one-inch effective aperture, while operating correctly, provided very marginal data during the November-December experiments. The reason for this was the excessive amount of noise seen in the data (approximately 90% of the total measured variance) without the capability of a sufficiently accurate measurement of this effect. The causes were probably the high electrical bandwidth ( $\approx 4$  kHz) used and a low efficiency of the entire system. Consequently, only a very rough

estimate of the atmospheric log-amplitude variance was obtained. Later in the year, the photometer was reconfigured to a 36 cm effective aperture and scintillation data was collected simultaneously with the Star Sensor. The results of these experiments are given in Section IV.4. Operations with this system have been discontinued.

The new Bell and Howell VR3700B tape recorder has been received and is now operational. This machine has a fourteen channel record (one direct and 13 FM) and five channel reproduce (one 2 MHz direct, two 80 kHz FM and two 400 kHz FM) capability with one inch magnetic tape. Nine speeds are available covering the range from 15/16 to 120 ips. This instrument provides a data recording and reproduce compatibility between AMOS, the Everett Laboratory and other facilities such as RADC. Initial applications will be for recording acoustic sounder raw data for on-site processing at a later time and full bandwidth (1 kHz) recording of the Seeting Monitor angular outputs for processing at Everett.

The initial AMOS testing of the Real Time Atmospheric Measurement System (RTAM) have been completed. A summary of these tests and an analysis of some of the data is given in Section VII.

The portable differential Hartmann device has not been used to collect data since August 1974. Because of higher priority tasks and the availability of other instrumentation, no activity with this system is anticipated at this time.

### III. SEEING MONITOR DATA

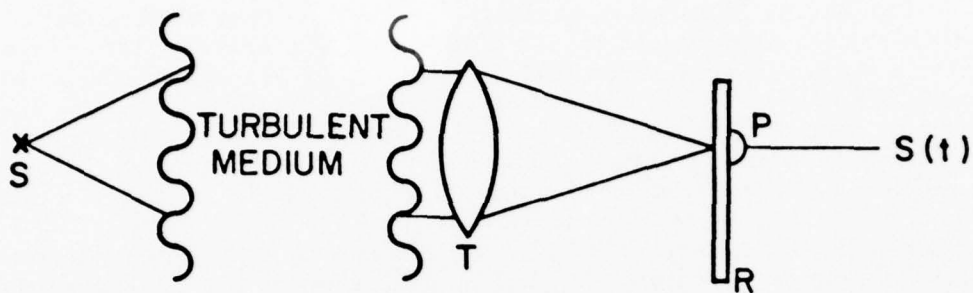
#### 1. GENERAL

The Seeing Monitor is basically a variable-spatial-frequency spinning-reticle photometer mounted in the focal plane of a large telescope imaging a distant star through turbulence (Figure 1). Assuming a reticle intensity transmission ( $T$ ) which is a spatially-varying sine wave, the output of a photomultiplier (PM) placed behind the reticle will include a term whose envelope is proportional to the Fourier transform of the star image ( $|\tilde{I}(f)|$ ) at the spatial frequency ( $f$ ) of the reticle. Properly normalized, this quantity is just the Modulation Transfer Function (MTF) of the combined atmosphere-telescope optical system which is related to the Mutual Coherence Function. By utilizing a variable spatial-frequency reticle, the entire MTF can be scanned as the reticle rotates. In actual practice, a logarithmic-varying, square-wave pattern is used, however, the basic effect remains the same. A more complete description of this instrument is given in Refs. 2 and 3.

While a number of outputs are available from this device, the one used in this experiment is a single parameter characterization of the width of the MTF or equivalently, the size of the image. The development of this signal is indicated in the top portion of Figure 2. The PM output is an oscillating signal whose modulation decreases with time (increasing spatial frequency). At the beginning of each scan, the modulation is maximum because the reticle bars are larger than the image. As the scan continues, modulation decreases as a result of the image being larger than the reticle bars. The signal is demodulated resulting in an envelope which is proportional to the MTF. This signal decreases as a function of scan time. Analog electronics are used to determine the time (i.e., spatial-frequency) at which the MTF drops to one-half its initial (zero spatial frequency) value. A voltage proportional to this half-MTF frequency is developed and provided as an output from the instrument. This voltage changes with each successive scan of the reticle indicating the changing size of the image as a result of the variable atmosphere. The system is duplicated for an orthogonal channel. Data processing is shown in the lower portion of the figure. While tape-recording of the raw data will be utilized in the future for detailed temporal characterization, at present the outputs are fed directly to a real

3. C. R. Giuliano, et al, Space Object Imaging, Final Technical Report, Contract #F30602-74-C-0227 (Hughes Research Laboratory), Rome Air Development Center Technical Report #RADC-TR-76-54 (March 1976), (A023497).
4. D. Fried, J. Opt. Soc. Am. 56, 1372 (1966).





$$S(t) \sim \int dx I(x) T(x,t)$$

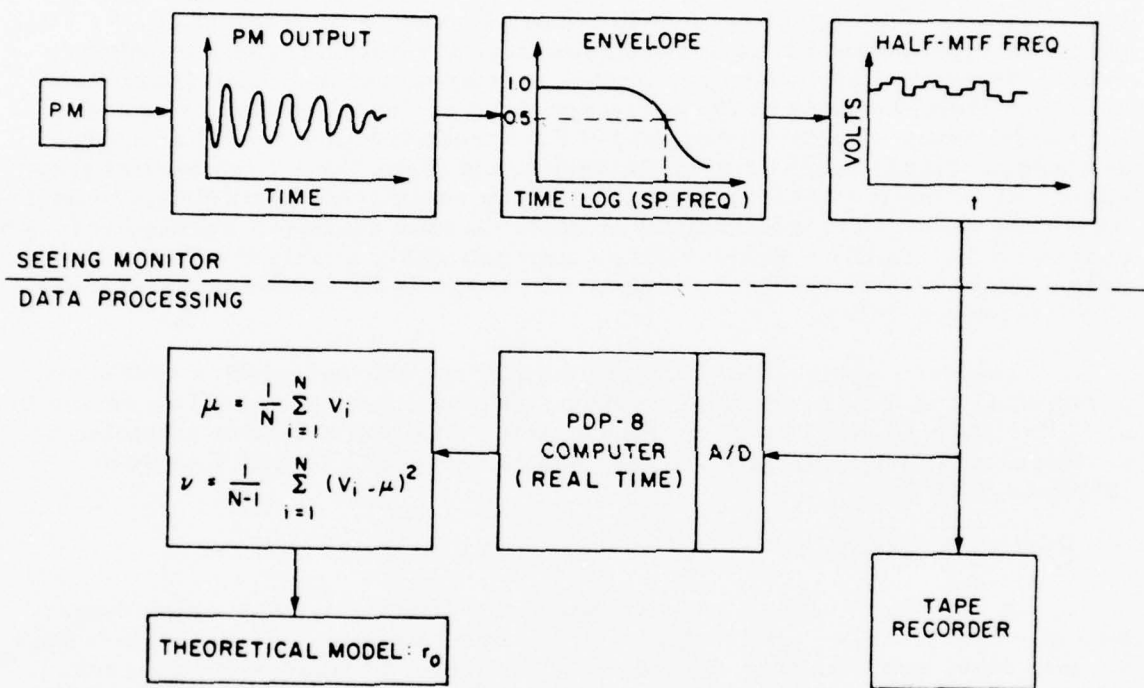
$$T(x) \sim 1 + \sin(2\pi f x + w t)$$

$$\left| \frac{S(t) - S(0)}{S(0)} \right| \sim |\tau(f)|$$

G5569

Figure 1. Seeing Monitor - Basic Concept. Components shown are the Stellar Source (S), Telescope (T), Reticle (R) and Photo Multiplier (P).





G5565

Figure 2. Seeing Monitor - Electronic and Data Processing

time processing system. This system includes an analog to digital converter, PDP-8/I computer and teletype output. The PDP-8 is programmed to calculate the mean and variance of the input signals. Total sample size and sampling rate are variable and control the total cycle time of the system. The average voltage calculated by the processing system is then fit to a theoretical model to provide an estimate of the correlation scale ( $r_0$ ).

The theoretical model used to obtain an estimate of  $r_0$  is indicated in Figure 3. The data processing system averages a voltage which is proportional to the spatial-frequency at which the MTF decreases to one-half its initial value. The model used is the Short Exposure Average MTF. (4) This model is appropriate because the Seeing Monitor automatically eliminates overall image wander. The parameter  $\alpha$  is assumed to be one (near field approximation) because of the large aperture of the telescope. However, the model deals with the averaged MTF whereas the processing actually averages a signal which is proportional to the logarithm of the spatial frequency at which the MTF on a realization by realization basis drops to half its initial value. The assumption is made that the spatial-frequency ( $\langle f_{1/2} \rangle$ ) corresponding to the average voltage approximately equals the spatial frequency ( $f_0$ ) at which the short exposure average MTF decreases to half its zero frequency value.

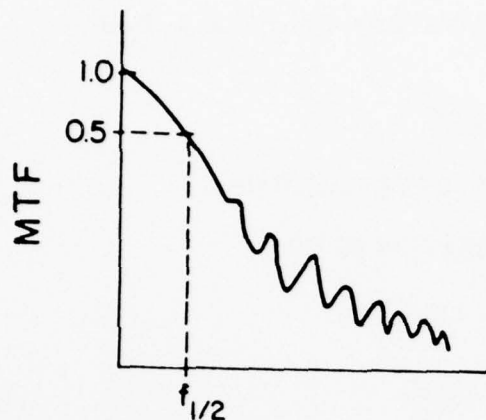
Table 1 summarizes the most significant characteristics of the experimental and data processing system. These conditions yield an estimate of  $r_0$  for each 10 minutes of operating time. While the data is collected at a central wavelength of 6200 Å, the results have been scaled with wavelength to 5000 Å.

## 2. ERROR ESTIMATES

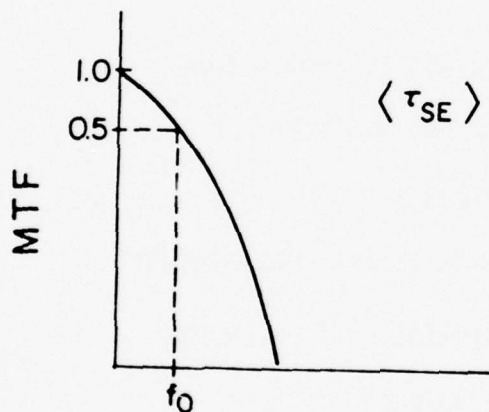
A variety of effects are present in the Seeing Monitor which contribute to errors and/or uncertainties in the reduced data. These include finite sample size, quantization, quantum fluctuations, internal noise sources, telescope MTF and voltage averaging. Another important aspect of the data reduction is the absolute calibration of the angular size of the image. Ideally, error estimates should be associated with each of these sources.

In the processing, a random voltage is averaged which potentially has contributions not only from the atmosphere but also the noise sources. A basic question is the level of statistical significance associated with the finite sample size. Assuming independent samples, theory<sup>(5)</sup> yields a variance of the sample mean ( $\mu$  - see Figure 2),

- 
5. A. Papoulis, Probability, Random Variables and Stochastic Processes (McGraw-Hill, N. Y. 1965), 245.
  6. D. Middleton, An Introduction to Statistical Communication Theory, (McGraw-Hill, N. Y. 1960), 426.



SHORT EXPOSURE AVERAGE MTF (FRIED)



$$\langle \tau_{SE} \rangle = e^{-3.44 (\lambda f / r_0)^{5/3} [1 - (\lambda f / D)^{1/3}]} \tau_0(f)$$

ASSUMPTION:  $\langle f_{1/2} \rangle \approx f_0$

WHERE:  $\langle \tau_{SE}(f_0) \rangle = 0.5$

G5568

Figure 3. Seeing Monitor - Theoretical Model. The upper figure approximates the Seeing Monitor operation and the lower one indicates the Theoretical Model assuming near-field conditions.

## SYSTEM CHARACTERISTICS

TELESCOPE:	AMOS OBSERVATORY-HALEAKALA, MAUI, HAWAII
	3KM ALTITUDE
	1.22M APERTURE CASSEGRAIN
	0.27 OBSCURATION RATIO
	19M FOCAL LENGTH
SOURCE:	SINGLE STARS
	+2 VISUAL MAGNITUDE OR BRIGHTER
	NOMINAL ELEVATION OF 60° OR GREATER
SEEING MONITOR:	1 MILLISECOND RESOLUTION TIME
	6200Å CENTRAL WAVELENGTH
	1200Å BANDPASS
	TWO CHANNEL SEEING ANGLE OUTPUT
DATA PROCESSING :	SUBMILLISECOND A D CONVERSION
	10 BIT RESOLUTION
	1350 SAMPLES
	10 MINUTE CYCLE TIME
	MEAN AND VARIANCE OUTPUT
THEORETICAL MODEL:	SHORT EXPOSURE AVERAGED MTF
	NEAR FIELD APPROXIMATION

G5570

$$\sigma_{\mu}^2 = \sigma^2/N \quad (1)$$

where  $\sigma^2$  is the true statistical variance and  $N$  is the sample size (1350). The sample variance,  $v$ , is an estimate of  $\sigma^2$ . For the data reported here,  $v$  was almost always less than 1 (volts)<sup>2</sup> and the sample mean was typically in the range (4-6) volts. Hence, the statistical significance of the average voltage (one sigma) is better than  $\pm 1\%$ . Tracing this level of fluctuation through the instrumental calibration and theoretical model<sup>(4)</sup> yields an estimated statistical significance in  $r_0$  of better than  $\pm 2\%$ . In many cases it was better than  $\pm 1\%$ .

Instrumental noise sources and quantum fluctuations become significant because of two effects. One is the degradation in statistical significance due to the addition of a large noise variance to the total variance which is not adequately reduced by the sample size. The data supports the conclusion that this does not occur. In addition, a theoretical calculation<sup>(3)</sup> for quantum fluctuation indicates a single realization (one millisecond) root variance to mean ratio of better than 1% for a second magnitude star. This value is well below the actual ratio seen in the data. The other effect is an addition to the average voltage (i.e., bias) which is not due to the atmosphere. As far as is known, this effect does not occur.

A noise source which is not averaged by the sample size is the quantization associated with the data processing. This is really not noise, but rather the precision of the measurement. The ten bit resolution of the PDP-8 yields a precision in the voltage output of approximately 0.01 volts. This in turn, for typical conditions, yields a precision in the  $r_0$  estimate of better than  $\pm 1/2\%$ .

More important than the above effects are unknowns which change the calibration of the system. One of the more important of these is the telescope MTF ( $\tau_0$  in Figure 3). In fitting the data to theory, an aberration-free, clear aperture of 1.22 M was assumed. This is obviously not the case. Because of the low frequencies involved, the central obscuration of the telescope does not contribute. Aberrations may be important. Hartmann testing of the telescope indicates an 80% encircled energy diameter of (0.7 - 1.3) arc sec with a scatter in the data of approximately 0.4 arc sec. This information by itself is not sufficient to evaluate the effect on the estimate of  $r_0$  because the detailed shape of the MTF is not known. Over the entire experimental period, the maximum averaged one-half MTF spatial-frequency observed was approximately 1 (arc sec)<sup>-1</sup>. This in turn implies that the telescope MTF had to be at least 0.5 at this spatial-frequency. Fitting this value to a Gaussian function and calculating the 80% encircled energy diameter yields a value of 0.6 arc sec. While this value is low, it is not inconsistent with the Hartmann data. Using the same Gaussian function to estimate  $r_0$  leads to the result that aberrations are not important



(< 10%) for values lower than 13 cm. However, for values of  $r_0$  in excess of 15 cm, aberrations could result in estimates substantially lower than actual. Hence these large values should probably only be viewed as lower bounds.

The theoretical model used to fit the data corresponds to the spatial-frequency at which the averaged MTF with overall tilt removed is reduced to one-half of its initial value. In practice, the voltage averaged is logarithmically related to the spatial-frequency at which single, short exposure MTF's decrease to 0.5. Clearly, these two (theory and practice) are different. Depending on the type of statistics involved and parameter values, the difference could be substantial. If the voltage statistics are assumed Gaussian then

$$\langle f_{1/2} \rangle = 0.035 \exp \left[ \frac{(0.46)^2}{2} \sigma_v^2 + (0.46) \langle v \rangle \right] \quad (2)$$

and

$$\frac{\sigma_f^2}{\langle f_{1/2} \rangle^2} = \exp \left[ (0.46)^2 \sigma_v^2 \right] - 1 \quad (3)$$

where  $\langle v \rangle$  is the average voltage,  $\sigma_v^2$  is the voltage variance,  $\langle f_{1/2} \rangle$  is the average frequency and  $\sigma_f^2$  is the frequency variance. The numerical constants arise from the instrumental calibration. For most of the data reported, the voltage variance was small enough so that its effect on the average frequency was less than 10%; typically, in the range of (1-3)%. A similar effect occurs in the estimate of  $r_0$ .

Evaluating the effect of frequency averaging is, in general, complicated. It is related to the zero crossing problem which is common in statistical theory. (6) However, because of the low-frequencies involved, a simple first-order analysis can be developed. At these low frequencies, the MTF can be characterized by the sum of the averaged short exposure MTF and a small, mean-zero fluctuation. (7) Because of the small variances involved, the averaged short-exposure MTF at the frequency detected by the device ( $f_{1/2}$  in Figure 3) can be expanded in Taylor series about the frequency at which it drops to one-half its initial value ( $f_0$  in Figure 3). This yields

---

7. Actually, the random fluctuation is more appropriately modeled as having a small, but non-zero mean (see Ref. 8). However, this should not significantly effect the first order analysis.

8. D. Korff, G. Dryden and M. G. Miller, Optics Comm. 5, 187 (1972).

$$\begin{aligned}
|\tau(f_{1/2})| = 0.5 \approx & \langle \tau_{SE}(f_{1/2}) \rangle + (f_{1/2} - f_o) \frac{d}{df} \langle \tau_{SE}(f_{1/2}) \rangle \\
& + \frac{1}{2} (f_{1/2} - f_o)^2 \frac{d^2}{df^2} \langle \tau_{SE}(f_o) \rangle + \dots \\
& + \hat{A}(f_{1/2})
\end{aligned} \tag{4}$$

where  $A$  is the mean-zero fluctuation. Averaging this result and maintaining terms through second order yields

$$f_o \approx \langle f_{1/2} \rangle + \frac{\langle (f_{1/2} - f_o)^2 \rangle}{2} \frac{\frac{d^2}{df^2} \langle \tau_{SE}(f) \rangle}{\frac{d}{df} \langle \tau_{SE}(f_o) \rangle} + \dots \tag{5}$$

Carrying out the indicated averages and derivatives yields

$$f_o \approx \langle f_{1/2} \rangle \left\{ 1 - (1/4) \sigma_f^2 / \langle f_{1/2} \rangle^2 \right\} \tag{6}$$

Assuming the Gaussian model of Eq. (3) yields a maximum effect of 10% with typical values of less than 2%.

A number of other effects can also cause uncertainties in the system calibration. These include defocus, error in the value of the telescope focal length, mechanical, optical and electronic misalignments of the instrument and the assumption of near field turbulence. However, none of these are considered to be significant.

It would be very desirable to have an independent measure of image size (or  $r_o$ ) to provide a check on overall system calibration. This is of particular interest because the laboratory calibration<sup>(3)</sup> was done against a pinhole image which is substantially different than an atmospherically degraded image. In addition, the laboratory measurements indicated an internal inconsistency. Unfortunately, no reduced, comparative data exist. While some potentially comparative speckle interferometry data exist, it has not yet been reduced. Once the RTAM becomes operational, it may

also be possible to obtain true simultaneous and independent estimates of the half-MTF frequency under identical conditions. However, this will not provide a complete system (including telescope) calibration. Data collection against planets could provide such a calibration, at least for the large image sizes that would be involved.

In summary, the statistical significance of a given value of  $r_0$  is estimated to be better than  $\pm 2\%$  with a precision of better than  $\pm 1/2\%$ . Known and estimated error sources yield a maximum uncertainty in  $r_0$  of 10% with 5% being more typical. Because of telescope aberrations, large values of  $r_0$  ( $>15$  cm) may only represent a lower bound. A potentially major uncertainty in the results is the absolute calibration of the entire system. However, existing and anticipated data may be able to provide an independent measure of the correlation scale.

### 3. RESULTS AND CONCLUSIONS

During the period 11 November 1975 to 13 July 1976, Seeing Monitor data was collected on twenty-four nights. These data are summarized in Appendix A. Table A-1 gives the dates, collection period, number of points and the mean and range of  $r_0$  at 5000 Å for each data run. The various graphs in the Appendix give the temporal behavior of the data runs. In total, 228 data points were collected.

A variety of temporal behavior are seen in the results. This ranges from almost a constant value of  $r_0$  over a three hour period to large fluctuations between points separated by twenty minutes. Extremes of this type of behavior are shown in Figure 4. The data of 6 December 1975 is essentially constant (i.e., less than 5% variation about the mean) while that of 8 December 1975 shows large fluctuation (almost  $\pm 30\%$ ). More typically, variations over a given data run are less than  $\pm 20\%$ .

Another type of behavior seen were trends towards improving (increasing  $r_0$ ) and degrading (decreasing  $r_0$ ) conditions. Examples of this are shown in Figure 5. On 8 July 1976, except for several points, seeing conditions degraded in essentially a monotonic fashion from a high of 11.6 cm near the beginning of the run to a low of 8.1 cm near the end of the run, a variation of (+ 21%, - 16%) about the mean value. Just the opposite effect occurred on 12 July 1976. During this three hour run,  $r_0$  changed from a low of 7.6 cm near the beginning of the run to 14.4 cm near the end of the run, a variation of (- 32%, + 30%) about the mean value. Again, the trend (towards improved seeing) is reasonably monotonic.

The total data sample is summarized in Figure 6. The mean value of the 228 member ensemble is 9.6 cm with a standard deviation of 2.2 cm. The range of measurements were from 5.3 to 17.8 cm. Thirteen percent of the values lie below 7.5 cm and eighteen percent are above 11.5 cm. The straight line in the figure is a theoretical Gaussian distribution with the empirical mean and variance. As can be seen, the fit is quite reasonable.

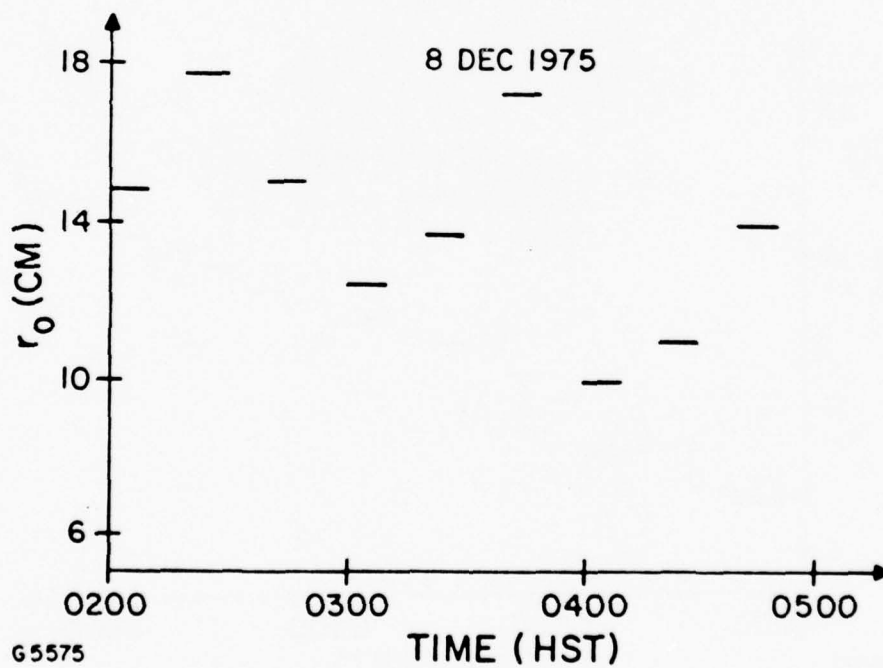
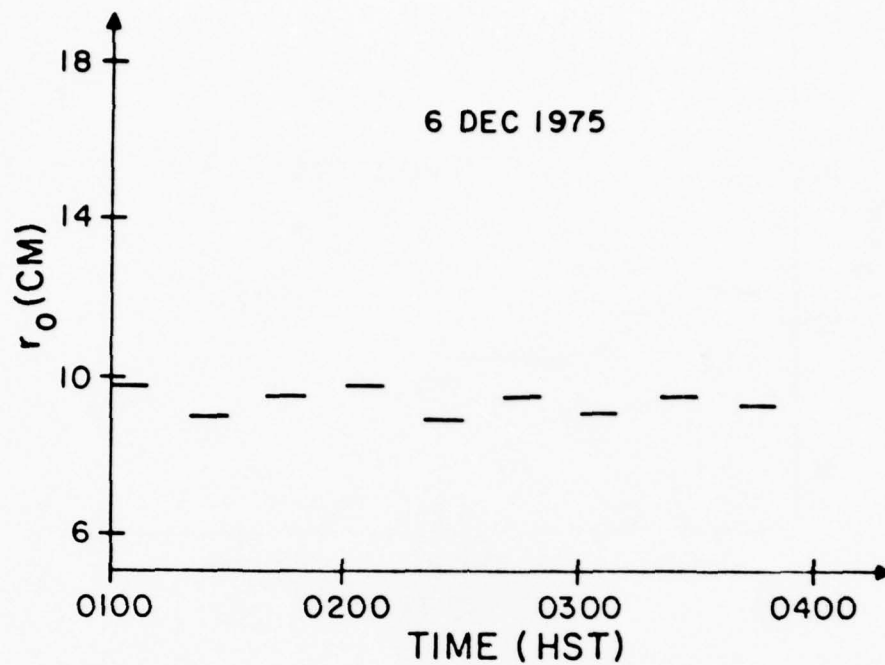


Figure 4. Seeing Monitor Data - Variability. The bars indicate the data averaging period.

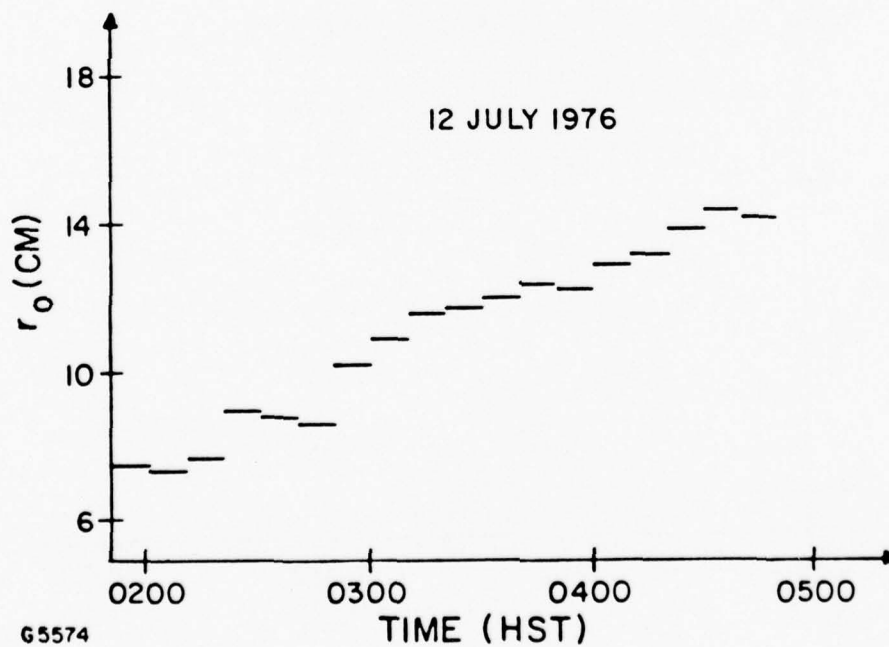
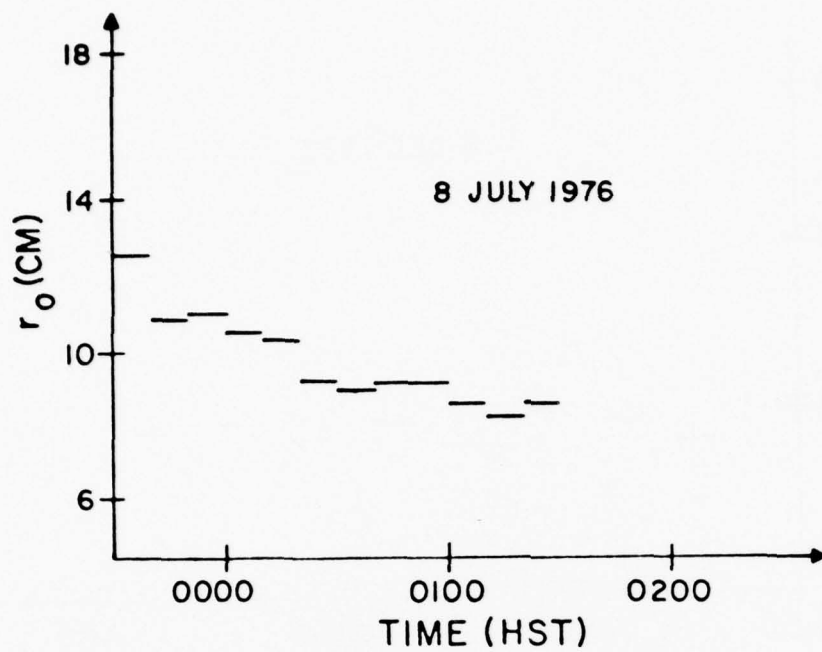


Figure 5. Seeing Monitor Data - Trends. The bars indicate the data averaging period



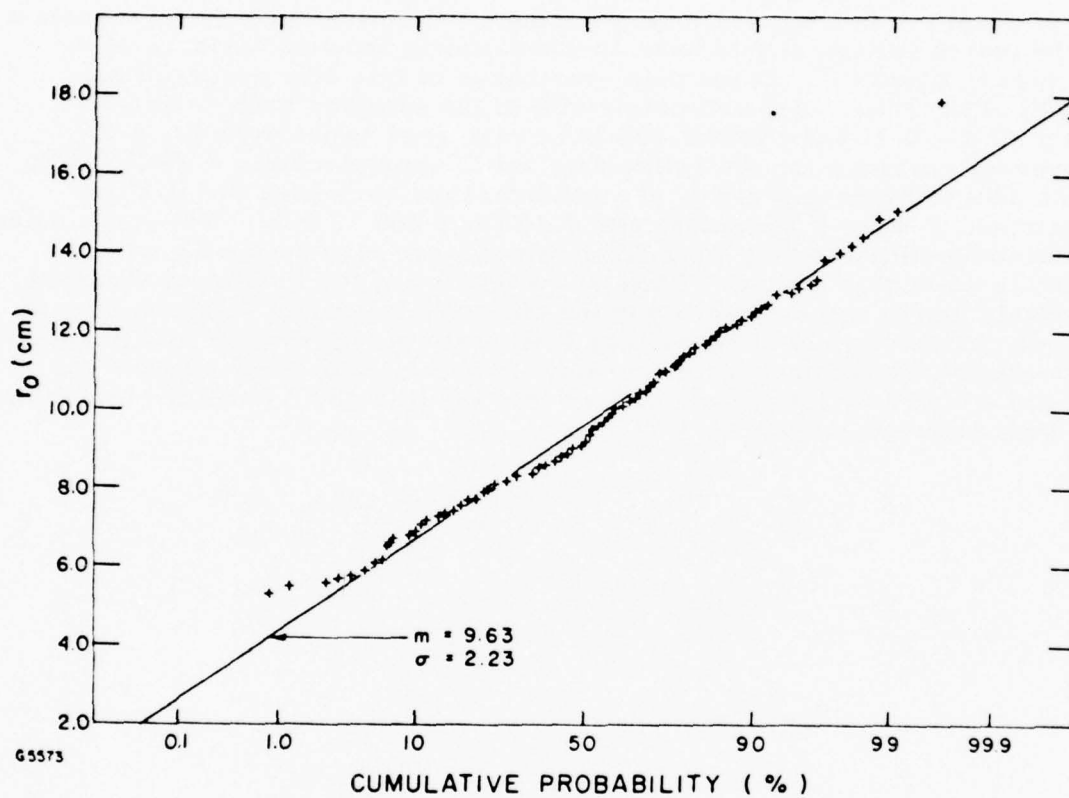


Figure 6. Seeing Monitor Data - Correlation Scale Distribution. The straight line is for a Gaussian distribution with the empirical mean and variance.

Another interesting aspect of the data is the level of fluctuation seen in the output voltage during a given ten minute collection cycle. If the single frame MTF is modeled as the sum of a low-frequency deterministic portion (i. e., averaged short exposure MTF) and a Rayleigh distributed random fluctuation which is band limited by the telescope aperture, (8) then the variance of the MTF is controlled by the latter term and is proportional to  $(r_0/D)^2$ . Tracing this through the data processing yields the conclusion<sup>(9)</sup> that if the atmosphere is truly stationary during a collection cycle (i. e., constant  $r_0$ ), the output voltage should have an atmospheric induced variance of no more than 0.1 (volts)<sup>2</sup>. In the data, variances of this size occurred less than 10% of the time. Approximately 40% of the samples have variances between (0.1 - 0.2) and another 30% have variances between (0.2 - 0.3). The average variance for the entire data set is approximately 0.25 (volts)<sup>2</sup>. For the data of Figures 5 and 6, the run averaged variances are 0.2 for 6 December, 1.4 for 8 December and 0.15 for 8 and 12 July. The large value of 8 December implies that large fluctuations were also occurring within a ten minute collection period. While some portion of the measured variance is probably due to noise, theory and the observed minimum value imply that the noise contribution is no more than 0.05 (volts)<sup>2</sup>. Hence the data supports the conclusion that atmospheric non-stationarity effects occur much of the time with a characteristic scale of less than ten minutes. Similar conclusions have been reported elsewhere. (10)

---

9. Gaussian voltage statistics are assumed.

10. D. Karo and A. Schneiderman, J. Opt. Soc. Am. 66, 1065A (1976).

## IV. STAR SENSOR DATA

### 1. GENERAL

The Star Sensor is a variable spatial-frequency photometer which scans the scintillation pattern in the aperture of a 36cm telescope and provides a measure of the aperture averaged log-amplitude variance and the log-amplitude variance associated with a specific spatial-frequency which is varied as a function of time. The assumption of a theoretical model allows these data to be interpreted in terms of the strength of the turbulent fluctuations,  $C_n^2$ , at seven different levels in the upper atmosphere. In addition, the aperture-averaged log-amplitude variance is available as an output. A complete data collection cycle requires approximately twenty minutes yielding a reduced profile at the end of this time period. A more complete description of this device is given in Ref. 11 and 12.

During the period 11 November 1975 to 13 July 1976, operations with this instrument were carried out on thirty-one nights. Valid profiles were obtained on twenty-seven occasions and scintillation data only on an additional three. A summary of these data are given in Appendix B. Included are the average and range of scintillation, the complete set of valid turbulent profiles and graphs of the nightly averaged profiles.

### 2. TURBULENT PROFILES

As shown in Table B-1, a total of 229 turbulent profiles have been obtained. Of these, 24 are not valid because of mechanical malfunctions or saturation of the photomultipliers, leaving a total of 205 for which the instrument was apparently operating correctly. The data processing is such that each 24 sec an average value of the aperture averaged log-amplitude variance is obtained and recorded. During the twenty-minute cycle required to carry out the complete spatial frequency scan, approximately forty such values are accumulated. A final step in the processing (before determination of the profile) is to calculate the mean and standard deviation to mean ratio for this forty member ensemble. This latter quantity is a measure of several effects. Two of the more important are non-stationarity of the turbulent-statistics and the existence of cloud obscuration during a portion of the data run. Both of these effects have serious consequences in the

11. G.R. Ochs, R.S. Lawrence, T. Wang and P. Zieske, SPIE Proceedings 75, 48 (1976).
12. G.R. Ochs, T. Wang, R.S. Lawrence and S.F. Clifford, Applied Optics 15, 2504 (1976).

profile determination because they can cause the data collection conditions to change substantially during a cycle and violate one of the basic assumptions of the theoretical model. Hence a large value of the standard deviation to mean ratio indicates a profile of questionable significance.

For operational purposes, a value of this ratio in excess of 0.2 has been established as unacceptably high. Based on this criteria, 79 profiles were eliminated leaving a total of 126 collected during the period on twenty-seven nights. These are tabulated in Table B-2 and include the data, start time of each cycle, elevation angle, the seven reduced values of  $C_n^2$ , (at nominal altitudes above the observatory of 2.25, 3.75, 5.25, 7.5, 9.75, 12.75, and  $> 14.5$  km), the twenty minute mean log-amplitude variance and the standard deviation to mean ratio. As an indication of the relative amount of non-stationarity, the ratio of the number of valid profiles to the total collected (yield) is included in Table B-1. Graphs of the nightly average of the valid profiles are also included in the Appendix. While, in fact, the instrument calculates a value appropriate to an altitude range, the results are plotted as a function of the peak of the various weighing functions used in the theory.<sup>(12)</sup> Because of the small zenith angles involved, the data has not been corrected for this effect.

Several interesting properties can be seen in the results. For many of the profiles lower values of  $C_n^2$ , are indicated at intermediate levels. However, these levels also tend to fluctuate more rapidly in time and have relatively greater magnitude variations than the high and low levels. Not only do the results vary substantially from night to night but large changes also occur during a single night. Noticeable changes are seen in some cases between two profiles adjacent in time. Examples of this are shown in Figures 7 and 8.

In Figure 9, the average profiles for each month in which data was collected are shown. Again, they are plotted as a function of the nominal altitudes. The number of profiles averaged for each curve varies as a result of the varying amount of data collected during each month.

### 3. SCINTILLATION DATA

Measurements of the aperture averaged log-amplitude variances were obtained on thirty nights during the experimental period. Table B-1 summarizes these data giving the date, experimental time period, number of samples and the mean and variance of the twenty minute averages obtained on each occasion. Because most of the data was collected at zenith angles of less than  $30^\circ$ , corrections were not made for this effect. The mean value for the entire 218 member ensemble is  $5.85 \times 10^{-4}$  with a range of  $(1.55 - 28.3) \times 10^{-4}$ .

To provide a more detailed look at the statistics of scintillation, the complete set of 24 second (as opposed to the 20 minute data of Table B-1) log-amplitude variances taken during the single four hour run of 18 November 1975 has been analyzed as a single ensemble. The resulting

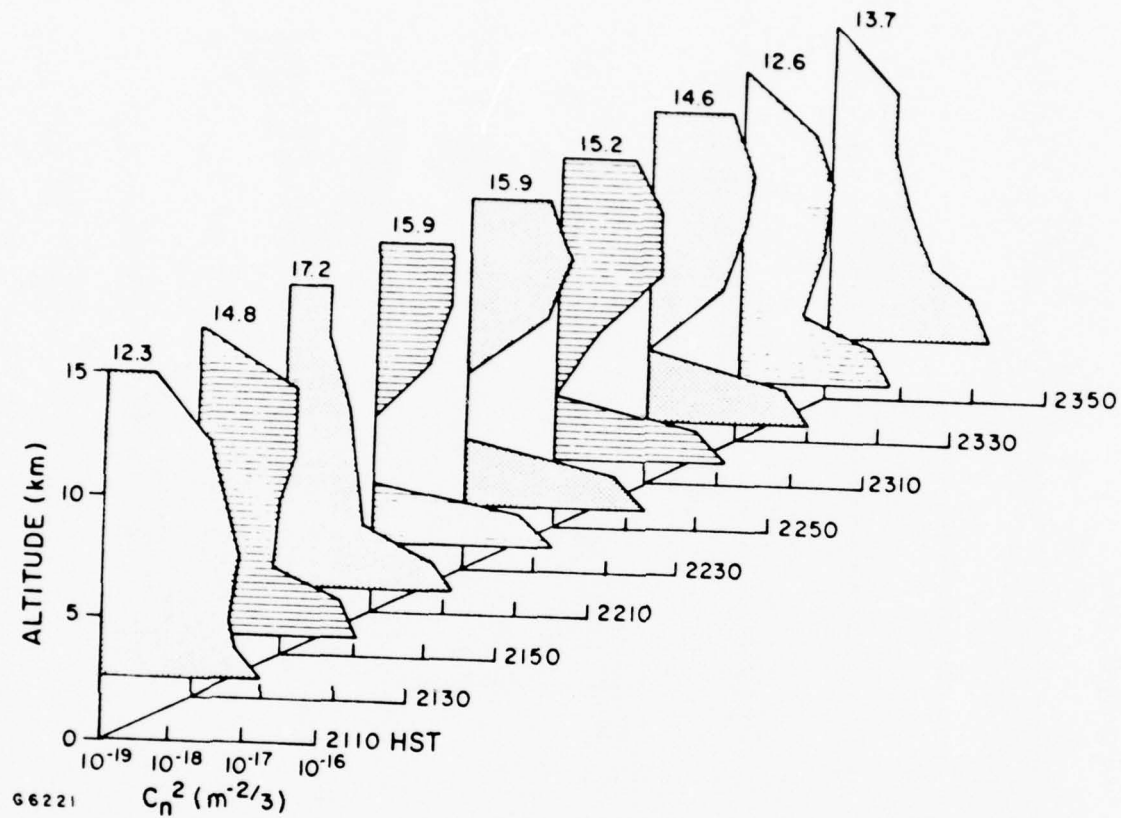


Figure 7. Star Sensor Profiles of 18 November 1975. Altitude is in meters above the site and the numbers above each profile indicate the measured value of  $r_0$  (in cm) obtained with the Seeing Monitor within each cycle.



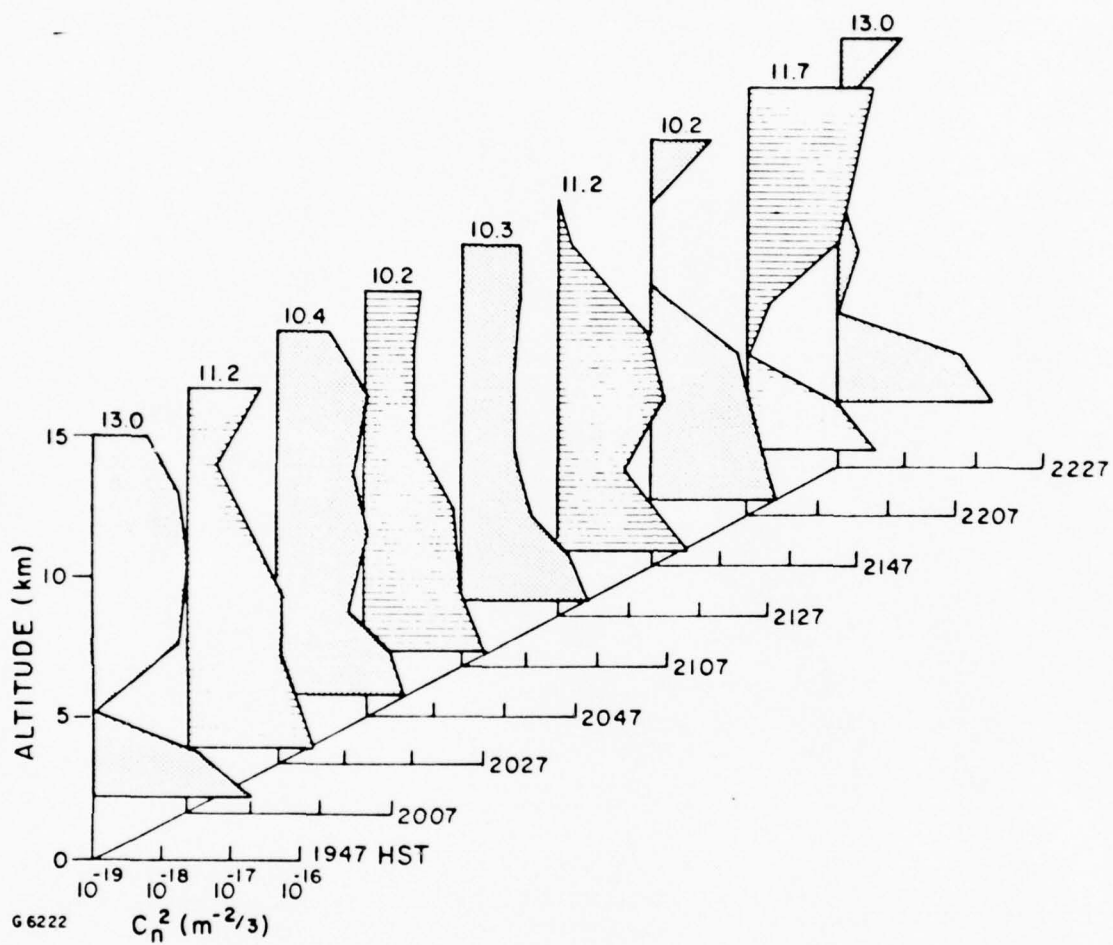


Figure 8. Star Sensor Profiles of 15 November 1975. Same as 7.

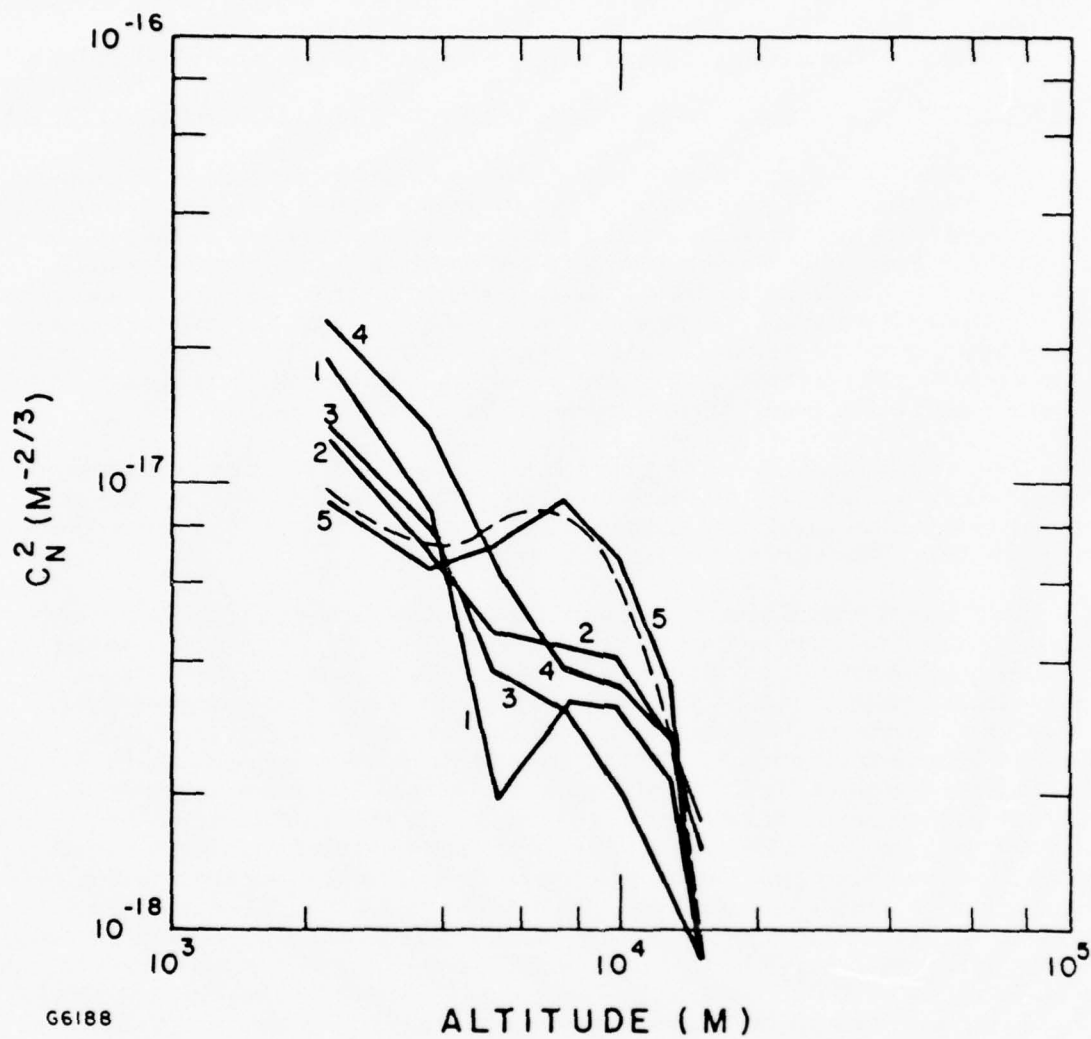


Figure 9. Star Sensor Profiles - Monthly Average for Nov-Dec (1), April (2), May (3), June (4) and July (5). Altitude is in meters above the site. The dashed line is from the Hufnagel wind correlated model with an average wind speed of 15 m/s.

histogram and cumulative probability density are shown in Figures 10 and 11. This ensemble contains 534 points and has a mean and root variance of  $3.76 \times 10^{-4}$  and  $0.93 \times 10^{-4}$ , respectively. The smooth curves represent a Gaussian distribution with mean and variance equal to the empirical values.

#### 4. STAR SENSOR - SMALL APERTURE PHOTOMETER COMPARATIVE DATA

In order to obtain direct and simultaneous observations of the log-amplitude variance, the photometer system on the AMOS b-29 telescope was equipped with an equivalent 36cm aperture to correspond to that of the Star Sensor. A central obscuration was not used, but this should be only a small effect. The b-29 data was reduced using the PDP-8 data processing system. Operations were carried out during nine nights. On two occasions (26 May and 9 June 1976) synchronous twenty-four second average variances were obtained. The rest of the data corresponds to 10 min averaged b-29 data taken within the basic 20 min cycle of the Star Sensor.

The complete data set is given in Figure 12. If the agreement were perfect, all data would lie on the solid line. The dashed lines indicate a factor of two difference in the measurements. While there is some dispersion in the data, the agreement is reasonably good.

One effect which is not accounted for in the data of Figure 12 is the contribution due to noise. To investigate this effect, b-29 data was taken at a variety of bandwidths. The results of one such data run (taken on 26 May) is shown in Figure 13. Assuming the noise is due to photoelectron fluctuations and that the bandwidth of significant atmospheric fluctuations is below 1000 Hz (and stationary), the higher bandwidth data should be describable by a constant plus linear frequency term. The smooth curve in the figure represents a least squares fit of this model to the three wide bandwidth data points. The fit is very good (better than 5%). This result implies that the noise contribution to the b-29 data is approximately  $2 \times 10^{-4}$ . Similar results were also obtained on the night of 9 June, however, there was more dispersion in the data. Subtracting this level of fluctuation from the b-29 data would place most of the points to the left of the solid line in Figure 12. There is, of course, also a noise contribution to the Star Sensor data. Assuming this to be of order  $10^{-4}$ , one-half of the derived b-29 noise was subtracted from the data and the 24 sec average data replotted. The results are given in Figure 14. It should be noted that the "adjustment" was derived from one data set, but fits the other data set equally well. As can be seen from this figure, most of the data lies quite close to the equal magnitude solid line. The dashed lines represent a  $\pm 10\%$  difference. The maximum difference seen is (+27.8, -27.4)%.

The conclusion that can be drawn from this analysis is that the Star Sensor log-amplitude variance has a noise contribution of order  $10^{-4}$ . An independent set of noise evaluation tests carried out on the Star Sensor (and reported in the next section) indicate that for the operating conditions of these experiments, the noise level is no larger than  $0.5 \times 10^{-4}$ . While there is a discrepancy of approximately a factor of two, the combined

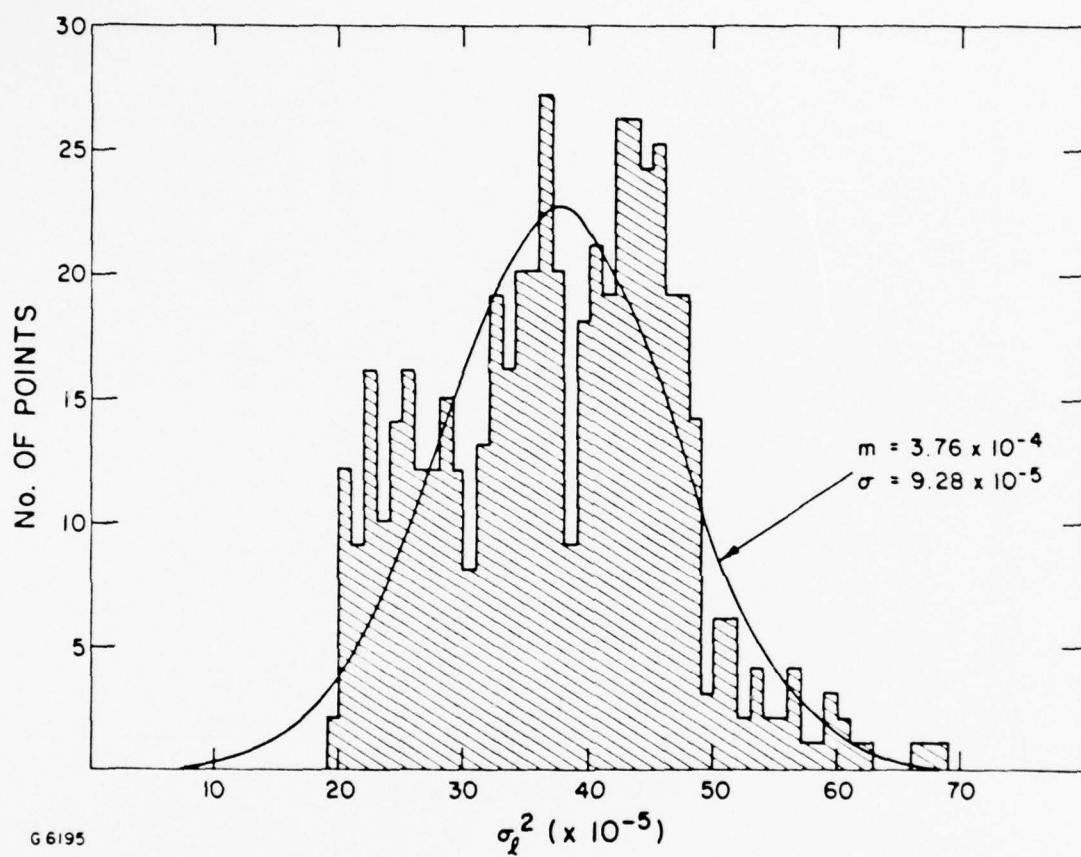


Figure 10. Star Sensor Log - Amplitude Variance of 18 November 1975 - Histogram. The smooth line is for a Gaussian distribution with the empirical mean and variance.

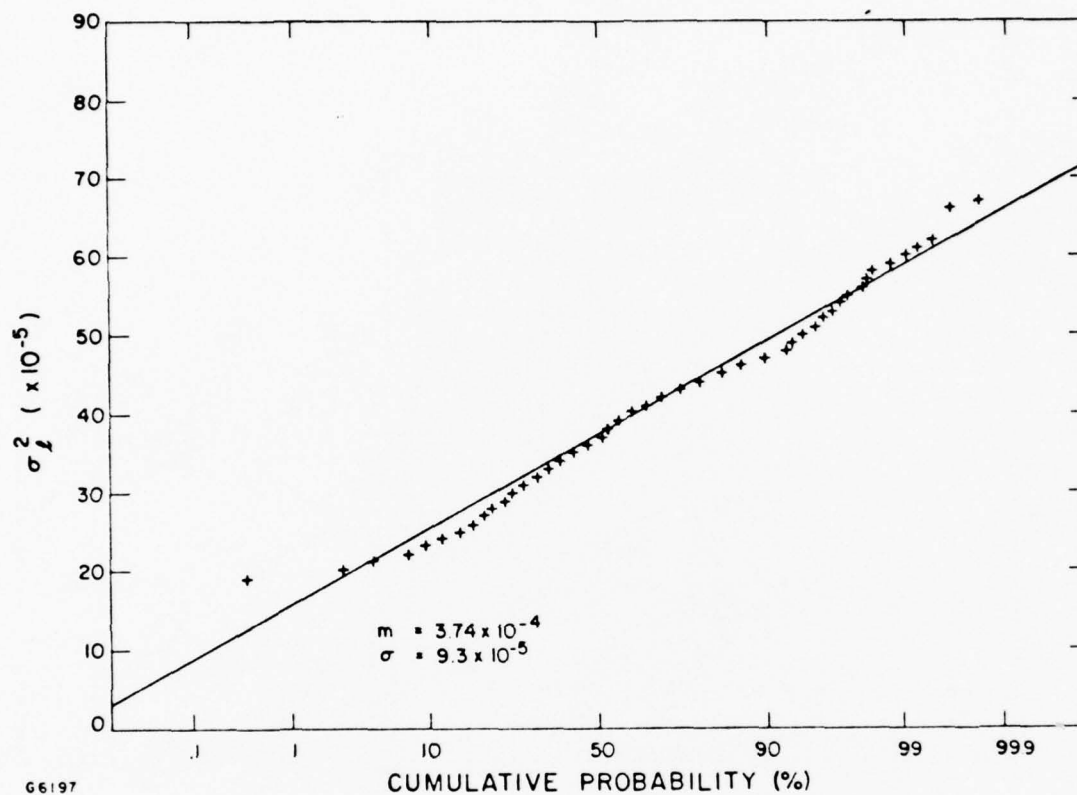


Figure 11. Star Sensor Log - Amplitude Variance of 18 November 1975 - Cumulative Probability. The straight line is for a Gaussian distribution with the empirical mean and variance.



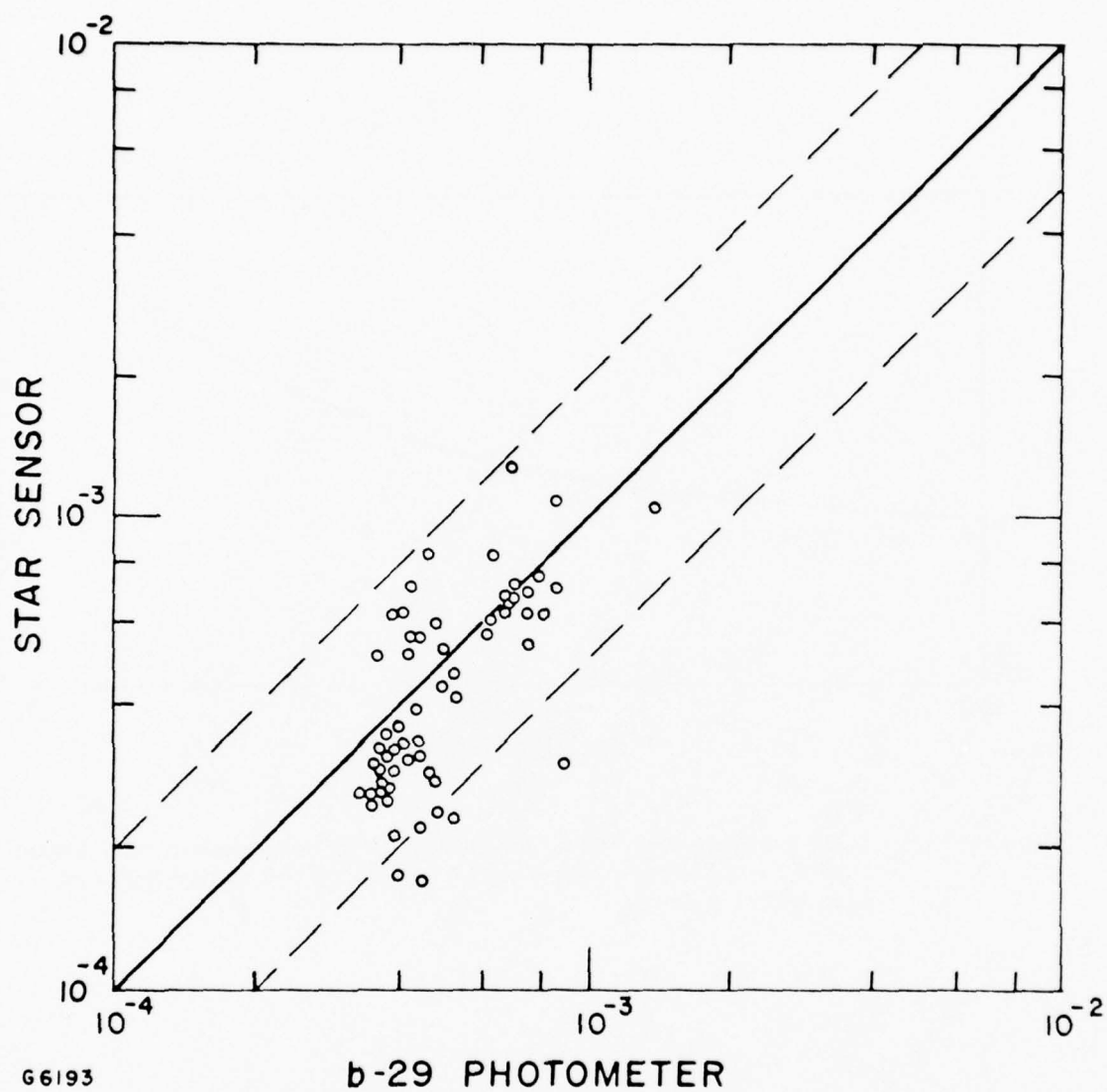


Figure 12. Comparative Log - Amplitude Variances - Raw Data. Data includes 24 sec averages and 10 min b-29 averages taken within a 20 min Star Sensor cycle.

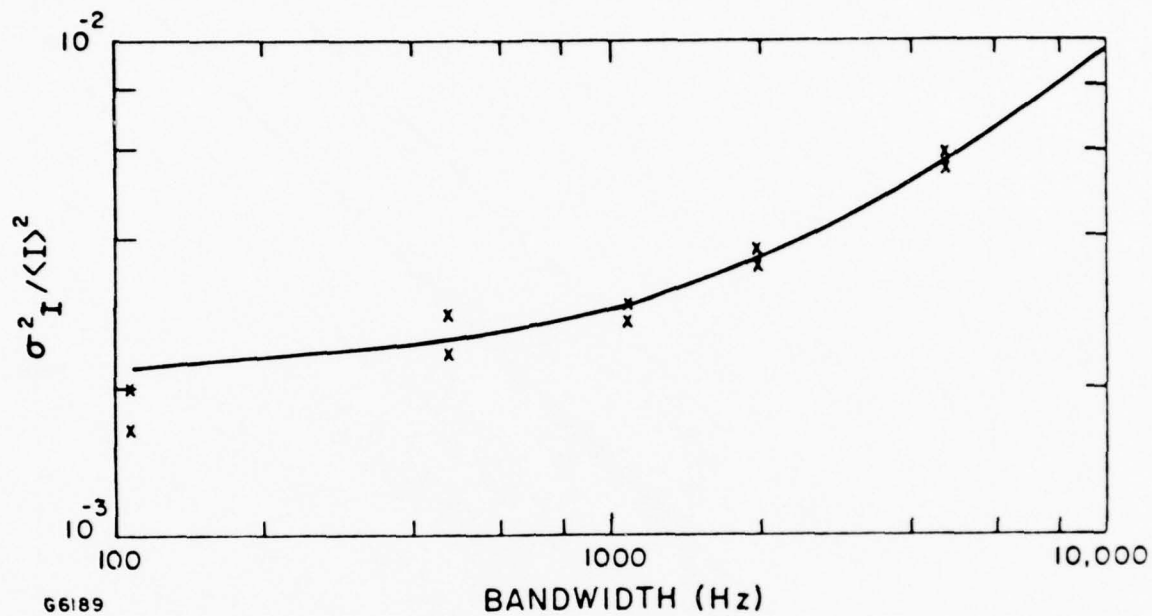


Figure 13. b-29 Photometer Data - Bandwidth Dependence. The smooth curve is a least-square fit of  $a + bf$  to the three highest bandwidth points.

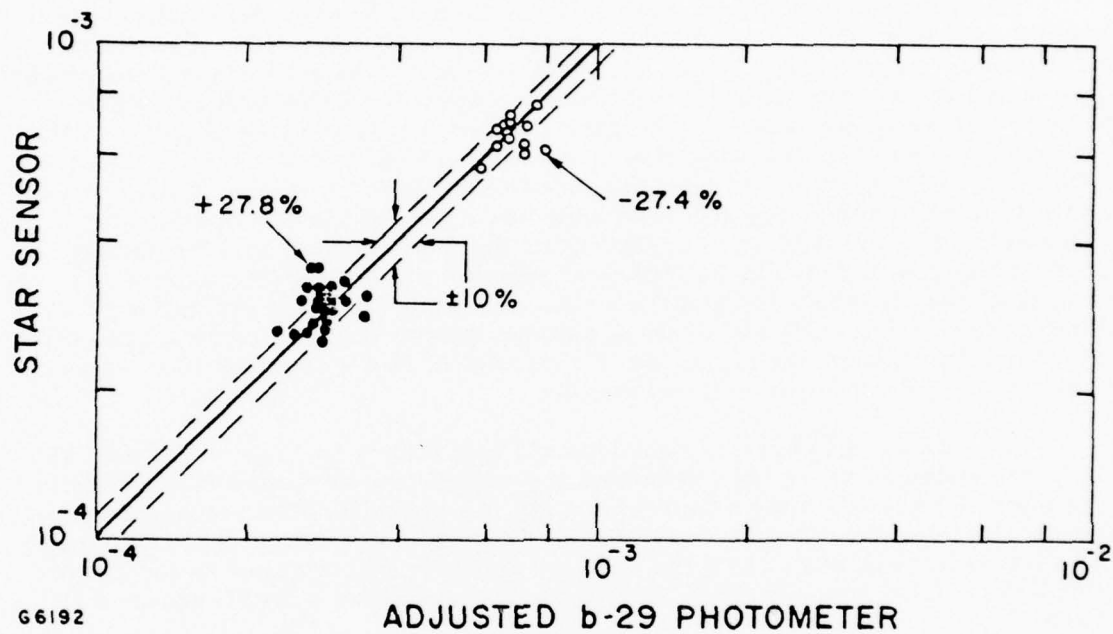


Figure 14. Comparative Log - Amplitude Variances - Adjusted Data.  
Data includes 24 sec averages taken on 26 May (o) and 9 June (●).

results certainly established considerable confidence in the basic operation of the Star Sensor, particularly when the measured log-amplitude variance is significantly above a value of  $(0.5-1.0) \times 10^{-4}$ .

## 5. NOISE EVALUATION TESTS

To provide for a direct estimate of the Star Sensor noise characteristics, a second and different set of measurements were carried out. For these experiments, a low voltage light bulb was connected to a regulated DC power supply and located such that it illuminated a portion of the diffuse, white interior surface of the dome. The Star Sensor telescope was pointed at the illuminated dome, the tracking motor was turned off and the mount was locked in position. The instrument was operated with photomultiplier voltages and outputs typical of the range of conditions seen during stellar operations. A laboratory photometer was located near the light source and its analog output was connected to the PDP-8 data processing system to provide a measure of the illumination fluctuations. All other lights were turned off and personnel were excluded from the dome during periods of data collection. Data was collected on six nights over a period of two weeks with the spatial-frequency scanning motor both on and off.

The results of these measurements are shown in Figures 15 and 16. E(1) is the value of the total aperture log-amplitude variance while E(2) is the log-amplitude variance associated with the spatially filtered signal (i.e., the data required for profile reduction). E(3) is the average photomultiplier output (in arbitrary units) and the voltage given is that applied to the photomultipliers. The straight lines in Figure 15 represent a least-squares fit to form

$$E(2) = A e^{bV} [E(3)]^{-1} + C \quad (7)$$

The inverse proportionality to E(3) is consistent with an instrumental noise dominated by photoelectron fluctuations. The constant term is assumed to be a contribution due to the light source. In the least-square fit several points which obviously did not fall close to the straight line were excluded. The data actually plotted has been reduced by the empirically derived constant value. As can be seen, the fit is quite good except for a few points. The empirical fit gave  $A = 6.75 \times 10^{-6}$  and  $B = 0.01037$ .

The assumed source contribution (C) was found to be in the range  $(1-3) \times 10^{-5}$  except for the data taken on 25 August which was of order  $5.5 \times 10^{-5}$ . The lower values are consistent with the estimates obtained from the photometer. There was indications that due to unknown causes, the line voltage in the dome was low and variable during the nights of 23 and 25 August which could have effected the light source and/or the Star Sensor and resulted in a higher level of noise. This level of source noise could also explain the higher dispersion in the data at low voltage and high E(3).

The straight lines in Figure 16 also represent a least-square fit to the model given in Eq. (7). This fit gives  $A = 2.47 \times 10^{-5}$  and  $B = 0.01075$ .

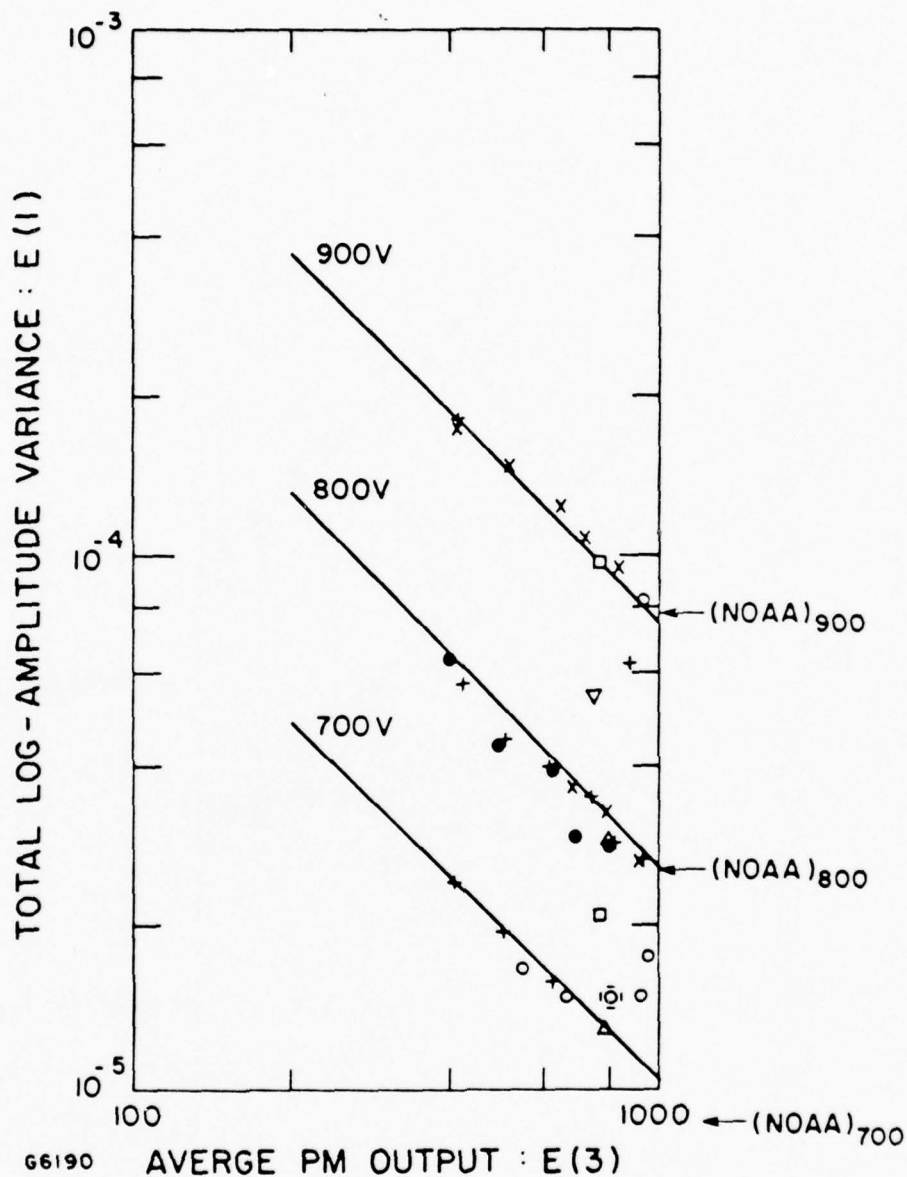


Figure 15. Star Sensor Noise - Total Log - Amplitude Variance. Included is motor off data of 25 August (●), 26 August (x), 27 August (+), 31 August (o) and 1 September (□) as well as motor on data of 23 August (▽), 31 August (Δ) and 1 September (□). The straight lines are least-square fits of Eq. (7) to the data for the PM voltage indicated. The three points marked (NOAA) are the values used in the noise compensation subroutine at the voltage indicated.



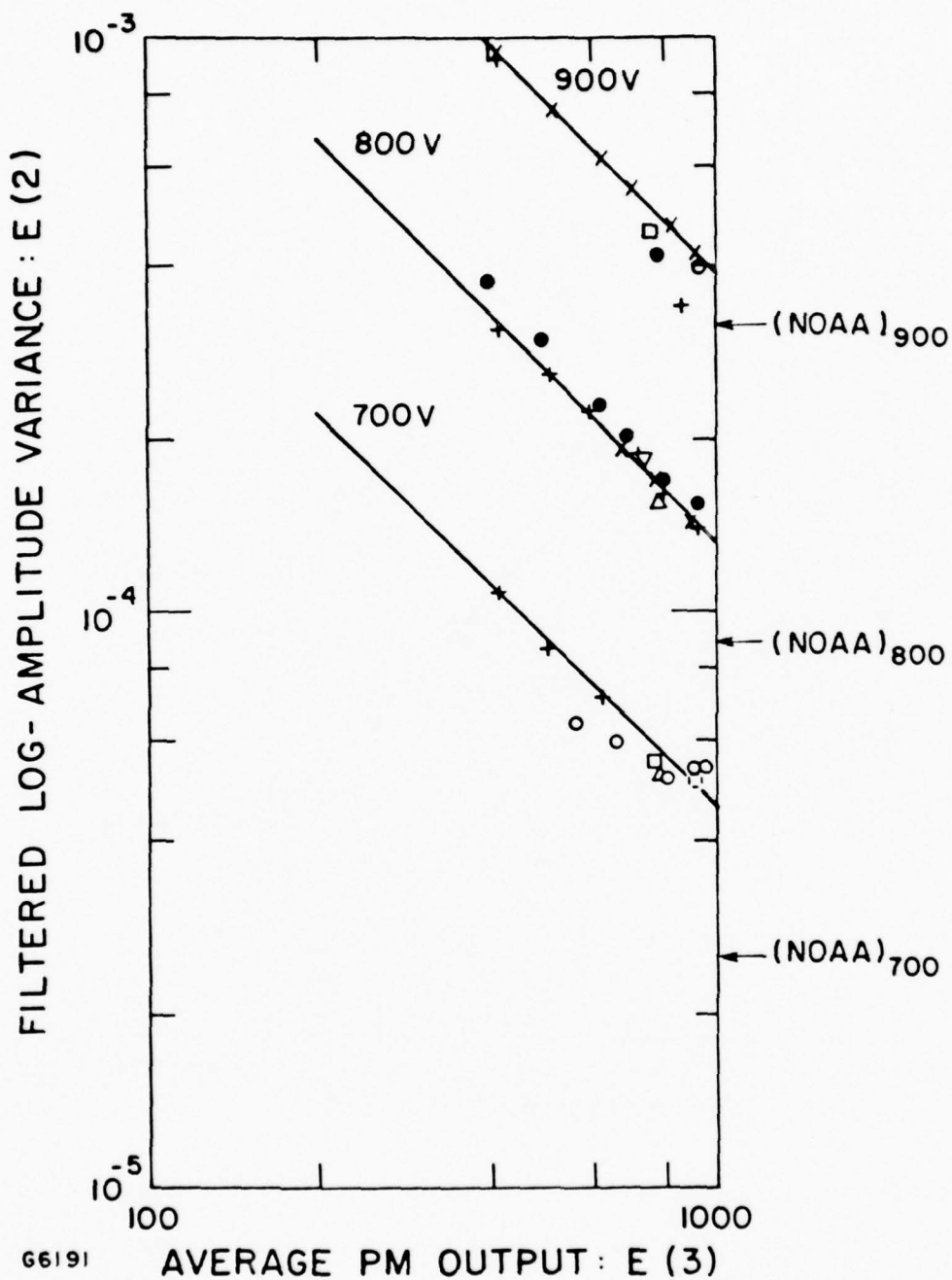


Figure 16. Star Sensor Noise - Filtered Log - Amplitude Variance. Same as Fig. 15.

The empirical values of  $C$  were much smaller (below  $10^{-5}$ ) and hence were set to zero. This includes the data of 25 August which showed relatively higher levels in the values of  $E(1)$ . As can be seen, there are also fewer points well off the curves than in Figure 15. All of these observations are very consistent with the interpretation of the constant factor as a light source fluctuation. The reason for this is that  $E(2)$  is derived from the difference in outputs of the two photomultipliers, each collecting approximately one-half of the light. Hence, any overall temporal (but spatially stationary) fluctuation in the illumination should cancel.

Another issue is the spatial uniformity of the illumination. If this effect were present,  $E(2)$  might indeed be measuring a real spatial variation which should have varied as the spatial frequency was changed. No evidence of this was seen as is indicated by the data taken with the filter drive motor on.

Experiments similar to these were carried out by NOAA before the instrument was shipped to AMOS and a noise cancellation routine was programmed into the software. Only a voltage dependence was included. The numerical values are indicated in the figures. The constants ( $b$ ) are quite close (0.01103 for  $E(2)$  and 0.0126 for  $E(2)$ ) but the overall level of noise is somewhat higher in the present experiment. While there is no definite explanation for this, it could be attributed to a variety of causes including different operating environment, aging, etc. However, the illumination level dependence found in the present experiments was expected and probably should be incorporated into the noise cancellation routine.

Complete twenty minute cycles were also run, resulting in turbulent profiles derived in this experimental configuration. While differences are seen in profiles taken in sequence, insufficient data exist to obtain a real estimate of the errors associated with the  $C_n^2$  values. Subjective impressions tend to support a  $\pm 10\%$  accuracy but a more complete theoretical and/or experimental assessment is required to establish any firm conclusion.

A rough estimate of the range of reliable operation of the Star Sensor can also be obtained from these results. The operations carried out over the past year were surveyed to obtain an estimate of operating conditions as a function of stellar magnitude. The results for applied PM voltage vs. magnitude are given in Figure 17. The operating range for  $E(3)$  was typically (600-900). These results imply that a magnitude 3 star would require an operating voltage of 900 V while a magnitude 4 star would require 1000 V (maximum allowed). The results of Figure 15 indicate that for the  $E(3)$  operating range the noise contribution to the total log-amplitude variance would be  $(1.4-2.1) \times 10^{-4}$  and  $(2.4-3.6) \times 10^{-4}$  for a magnitude 3 and 4 star, respectively. These values are within the range of measured atmospheric log-amplitude variances. While the data reduction software does subtract out the estimated noise contribution, an experimental result which has a spurious contribution of magnitude equal to that of the signal should be viewed with caution. This is particularly true of the Star Sensor because a complete evaluation of the effect of noise on the profile is not yet available. Therefore, for operational purposes, the threshold for useful data has been set at stellar magnitude 3 to 4.

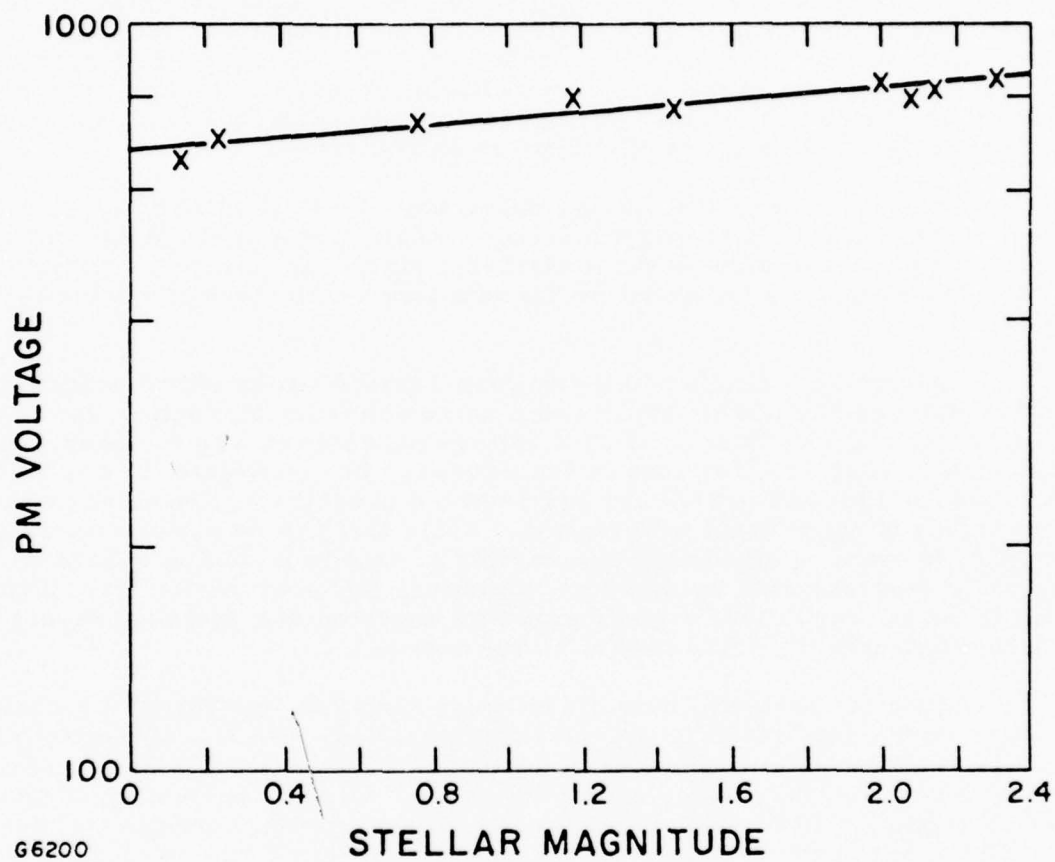


Figure 17. Star Sensor Operating Conditions. The straight line is a least-square fit of an exponential to the data.

## V. METEOROLOGICAL DATA

The AMOS Observatory is equipped with two 18-meter towers instrumented with routine meteorological instruments and microthermal probes. Some of the meteorological data is necessary for the reduction of microthermal and acoustic sounder data. In addition, routine measurements are desirable for establishing the gross meteorology of the site. While some of this latter data has been collected and will be in the future, results are not reported here.

Mounted on each tower is a triad of microthermal probes with a nominal one meter separation. The analog outputs from these probes are connected to the PDP-8 data processing system which calculates a mean, variance and covariance matrix for each array. The latter two quantities are required for the calculation of  $C_T^2$  and  $C_n^2$  values. For all data reported the averaging time was set at approximately 10 min. While six values are calculated, one is preferred. The selection was based on the probe pair whose axis was closest to normal to the wind direction on the windward tower. The first requirement is based on geometrical considerations while the second is to avoid a potentially turbulent wake due to the observatory domes. However, an often overriding consideration to pair selection was an obviously broken sensor. If this occurred, the single active pair remaining on the windward tower was used.

While data was collected on a number of occasions, only that obtained during November and December of 1975 is reported. There were several reasons for this. One is that this period represents a major data collection effort while the 1976 measurements were more routine. More importantly, was the failure of the acoustic sounder to provide reduced data. Without the additional profiling device, a single value of  $C_n^2$  at ground level was judged to be of marginal significance, particularly when viewed relative to maintenance and manpower requirements.

Appendix C summarizes the data. Table C-1 gives the dates, time period, number of samples and mean value and range of the reduced  $C_n^2$  values. The graphs show the temporal behavior of the reduced data. For the total data set of 143 points, the mean value of  $C_n^2$  is  $5.26 \times 10^{-15} \text{ M}^{-2/3}$ . As can be seen from the various figures, temporal behavior varied from a relatively constant value over a three hour period (17 November) to fluctuations over a similar time period of almost a factor of 10 (19 and 21 November). One run (14 November) show a tendency towards increasing values of  $C_n^2$  while one run (6 December) shows a tendency towards decreasing values of  $C_n^2$ . However, the existing data set is not sufficient to establish any firm conclusions regarding these types of effects. When compared to direct optical data, no obvious correlation is apparent.

Also included in the Appendix is gross meteorological information obtained from radiosonde data of the U.S. Weather Bureau at Hilo, Hawaii, a distance of approximately 100 miles southeast of AMOS. The launch time was 0200 HST and the dates indicate the mission date as given in Table B-2. The existence of an upper atmospheric disturbance from 17 November to 23 November is indicated by the presence of a jet stream at approximately 12,000 M (this jet is usually found farther north) and the replacement of the usual northeast trade winds by roughly southwest winds at altitudes below 12,000 M. While detailed studies of the correlation of this type of data with optical data has not been carried out, some comparisons have been made and are reported in Section VI.



## VI. DATA COMPARISONS

### 1. GENERAL

In this section a number of comparative studies of the data are reported. Several types are included. The first is a direct comparison of optical parameters with theoretical values calculated on the basis of the empirical turbulence profile information. Others include Seeing Monitor-Star Sensor non-stationarity and variability, experimental vs theory and comparisons with other experimental data reported in the literature. In general, the data appears to be consistent in some aspects but with poor agreement between the profile and direct optical measurements.

### 2. TURBULENCE PROFILE

Turbulence profiles averaged over the complete data runs taken on 17, 18 and 21 November 1975 are shown in Figures 18, 19 and 20. The lowest altitude data points were obtained from the ground based microthermal sensors (Appendix C). Data from 37 m to 2.5 km was provided by NOAA from a reduction of airborne microthermal data they collected using an instrumented light aircraft. (11) The line segments from 1 km to 24 km were derived from Star Sensor profiles (Appendix B) and represent the approximate widths of the weighing functions used in the data reduction. (12) The horizontal scale is in height (meters) above the observatory. The tropopause height was estimated from the temperature profiles obtained from the U.S. Weather Bureau (Appendix C).

Values of  $r_o$  and  $\sigma_1^2$  (point aperture) were calculated from these profiles using the expressions (4), (13).

$$r_o = \left[ 0.42 (2\pi/\lambda)^2 \int_{\text{path}} d h C_n^2(h) \right]^{-3/5} \quad (8)$$

$$\sigma_1^2 = 0.56 (2\pi/\lambda)^2 \int_{\text{path}} d n h^{5/6} C_n^2(h) \quad (9)$$

---

13. R. S. Lawrence and J. W. Strohbehn, Proc. of IEEE 58, 1523 (1970).

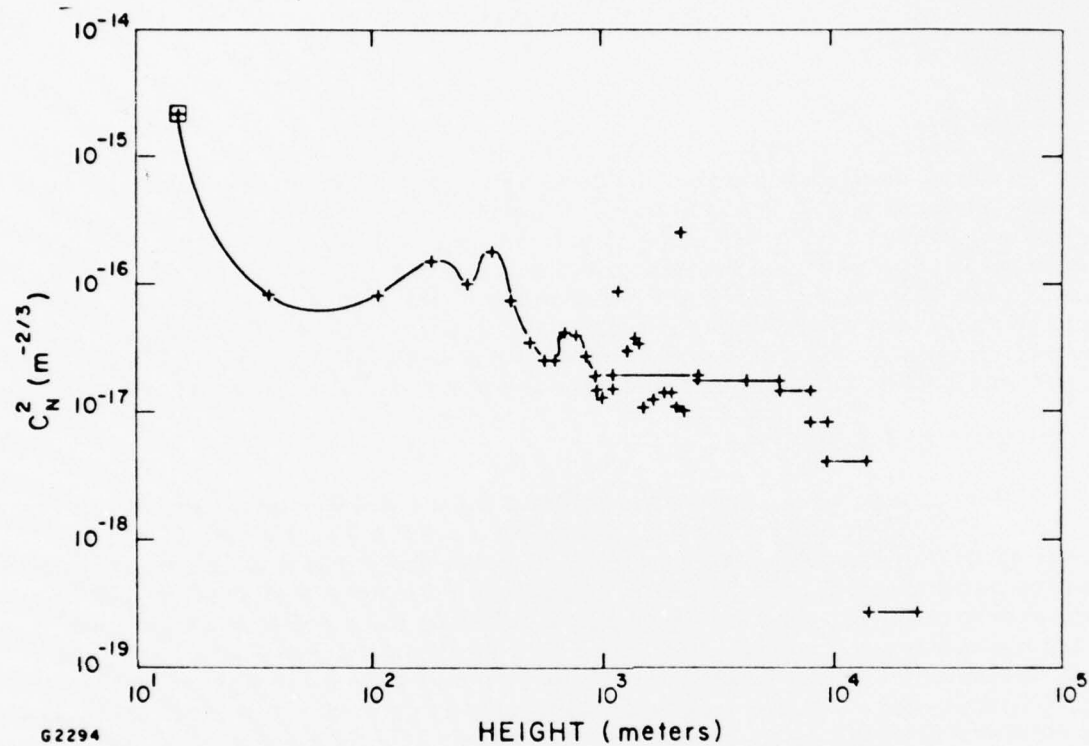


Figure 18. Empirical Turbulence Profile of 17 November 1975. Altitude is in height above the observatory. Based on ground level microthermal data ( $\square$ ), airborne microthermal data (+) and Star Sensor data ( $\text{---}\rightarrow$ ). Estimated tropopause height of 11 to 15.5 km.

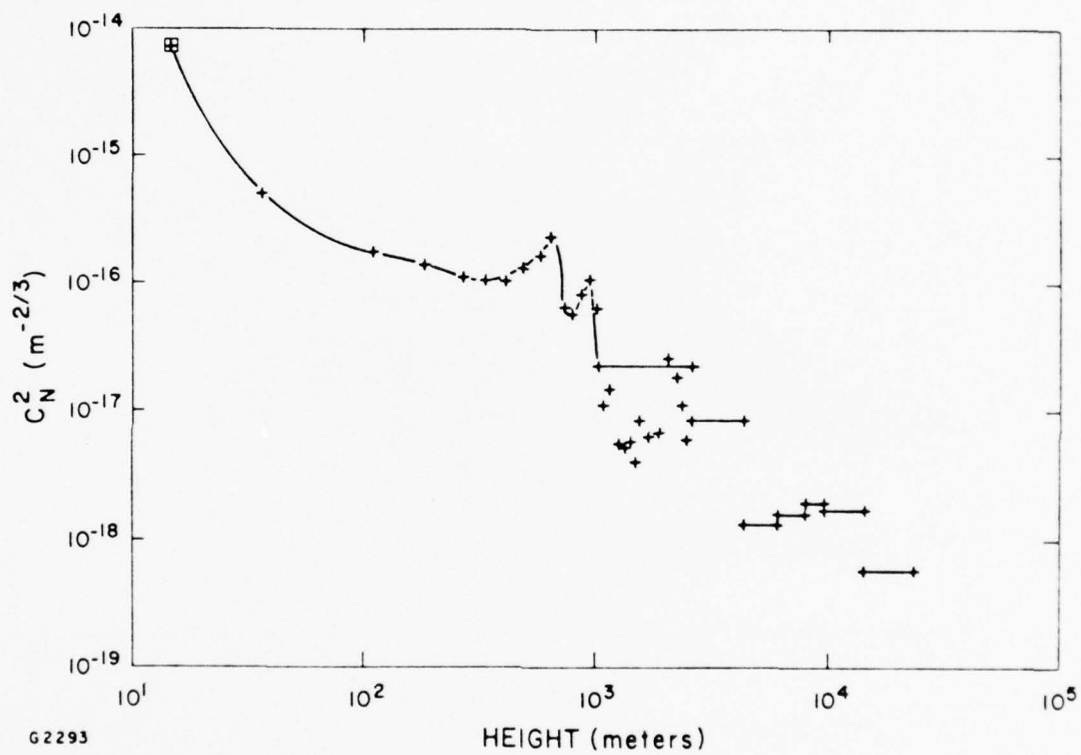


Figure 19. Empirical Turbulence Profile of 18 November 1975. Same as Fig. 18. Estimated tropopause height of 9.0 to 15.5 km.

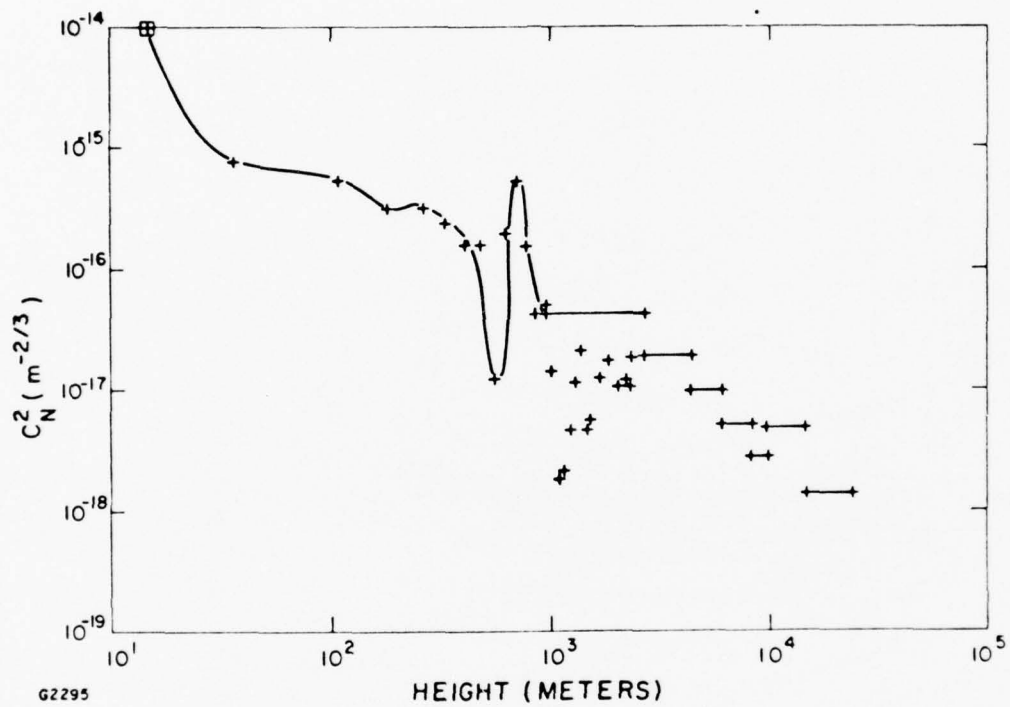


Figure 20. Empirical Turbulence Profile of 21 November 1975. Same as Fig. 18. Estimated tropopause height of 9.1 to 15 km.

The calculation was carried out (at RADC) on a Hewlett Packard 9810 desk top calculator using a 45 point Riemann sum in the region between 15 m and 25 k. Where experimental data overlaps, the Star Sensor results were used. All results are scaled to a wavelength of 5000 Å and are given in Table 2.

Comparative values of  $r_0$  and  $\sigma_1^2$  ( $D = 36$  cm) are given in Table 3. Profile values of  $\sigma_1^2$  ( $D = 36$  cm) were obtained from the results of Table 2 by multiplying by the theoretical aperture averaging factor of 0.019.<sup>(14)</sup> The Seeing Monitor values are slightly higher than those reported in Appendix A. The reason for this is two-fold. The first is that all values were corrected for zenith angle and the second is that each value of  $r_0$  was reduced to the equivalent value of the  $C_n^2$  integral before averaging to obtain a more direct comparison with the profile information. Table 3 also includes the factor by which the  $r_0$  profile integral would have to be multiplied to obtain agreement.

Comparisons between Star Sensor profiles and the direct measurement of  $\sigma_1^2$  have been carried out by NOAA.<sup>(15)</sup> The results are given in Figure 21. These two values are independent because except for a minor normalization procedure, the measured log-amplitude variance is not used in the profile data reduction.

As can be seen from these results, agreement between the profile and Seeing Monitor data is not good. A possible explanation for this is that significant amounts of turbulence was missed by the profiling instrumentation. Assuming this to be the case, the good agreement of the scintillation data would indicate that the missing turbulence is at low altitudes. It should be noted that the low altitude airborne data was not taken directly over the observatory but over a region on a lower portion of the mountain. Therefore, the data obtained may not be representative of conditions at the observatory because the relative distance to the ground was greater.

The required increase of the  $C_n^2$  integral to bring the two values into agreement could, for example, be accounted for by a turbulent layer of order 20-80 meter thick of average strength  $C_n^2 = 10^{-14} \text{ m}^{-2/3}$ . These values are not unreasonable. If such a layer existed in the first 300 meters above the observatory, it could have been seen by the acoustic sounder. Unfortunately, quantitative reduction of this data was not successful.

The possibility that spatial variability of turbulence is a potential cause of the discrepancy is clearly demonstrated by the data of Figures 22 to 24. These profiles were obtained by NOAA from airborne data they

---

14. H. Yura, Aerospace Technical Report #TR0077(2756)-1, 1976.

15. R.S. Lawrence, private communication.



TABLE 2. OPTICAL PARAMETERS OBTAINED FROM  
EMPIRICAL PROFILES

<u>Date</u>	<u>Correlation Scale <math>r_0</math> (cm)</u>	<u>Log-Amplitude Variance <math>\sigma_1^2</math> (point aperture)</u>
17 November	19.9	0.028
18 November	19.2	0.012
21 November	12.8	0.029

TABLE 3. SEEING MONITOR - PROFILE COMPARISONS

Date	Seeing Monitor $r_0$ (cm)	Profile $r_0$ (cm)	Profile Integral Multiplier	Star Sensor $\sigma_1^2$ ( $\times 10^{-4}$ )	Profile $\sigma_1^2$ ( $\times 10^{-4}$ )
17 November	8.0	19.9	4.5	7.9	5.32
18 November	11.9	19.2	2.2	3.8	2.28
21 November	9.0	12.8	1.8	6.0	5.51

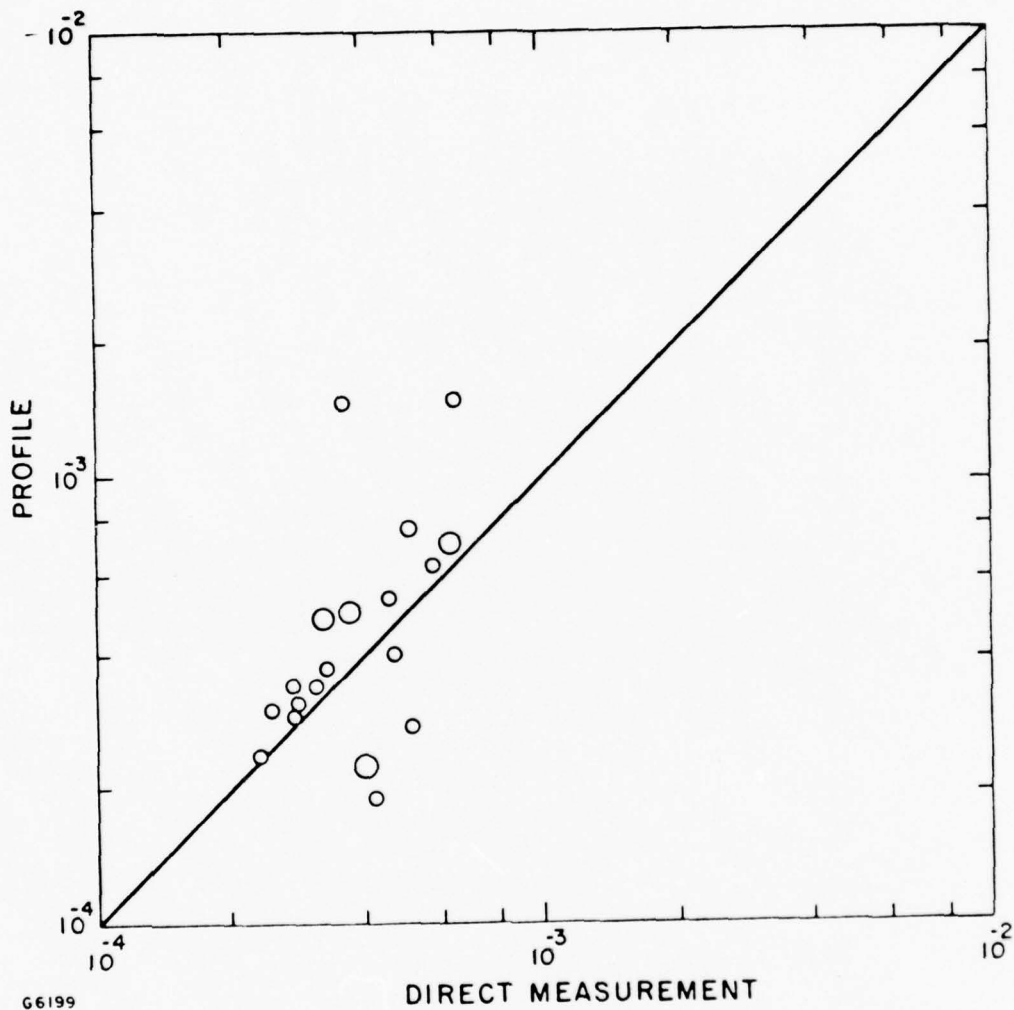


Figure 21. Comparison of Measured and Profile Derived Log - Amplitude Variances. Only valid profiles are used. Big dots are nightly averages and the small dots are for single 20 min cycles.

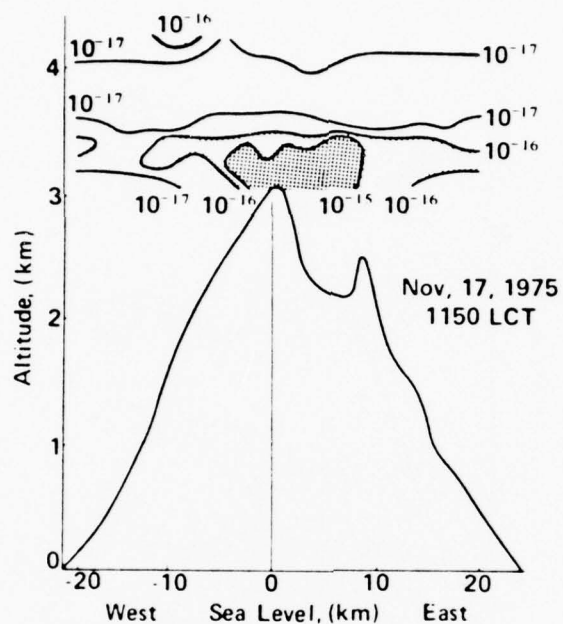


Figure 22. Two Dimensional Turbulence Contours of 17 November 1975. Based on daytime microthermal data. The observatory is approximately 0.5 km west of the peak. Winds are from the trade direction.

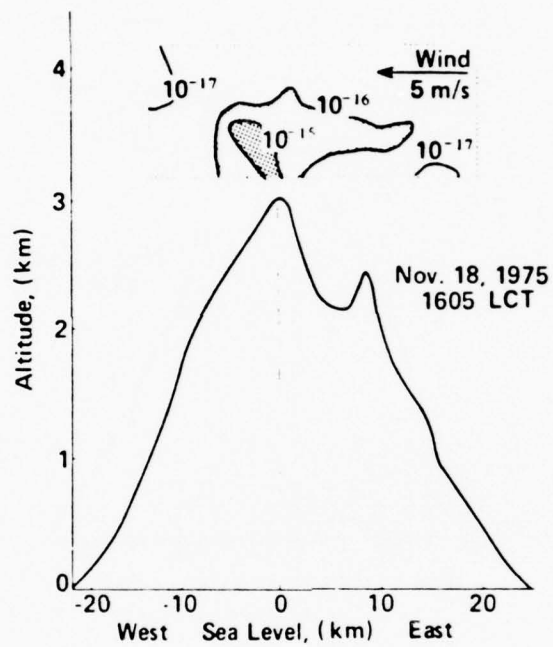


Figure 23. Two Dimensional Turbulence Contours of 18 November 1975. Same as Fig. 22.



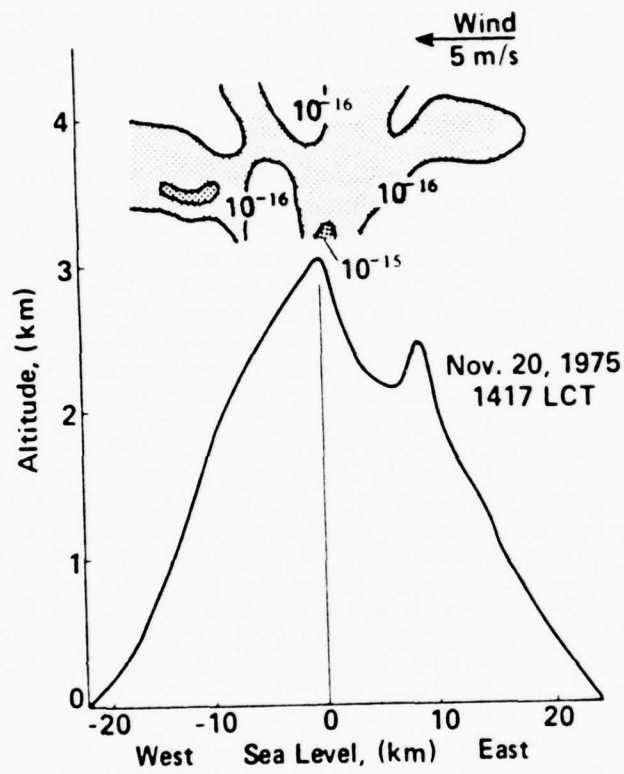


Figure 24. Two Dimensional Turbulence Contours of 20 November 1975.  
Same as Fig. 22.

collected during the daytime. If nighttime conditions are similar, then it is quite possible that the aircraft sensor was sampling substantially different turbulence than the optical measurements. In these profiles, the observatory is located slightly to the west of the peak ( $\approx 0.5$  km) and the winds are from the predominant trade direction (northeast).

### 3. SEEING MONITOR - STAR SENSOR

Several comparisons can also be made between Seeing Monitor and Star Sensor data. One such comparison is given in Figures 7 and 8. The numbers given at the top of each profile are the optical values of  $r_0$  obtained during a 10 min data collection cycle within the 20 min Star Sensor cycle. There appears to be a rough correlation between these two results (i. e.,  $r_0$  larger for profiles with smaller area), at least for the run of 18 November. Of course, a strong correlation would be expected only if the high altitude portion of the profile dominates and/or the turbulence levels under 1 km are relatively constant. The former assumption is generally not valid and, in fact, the data supports this conclusion. The average profiles given in Figure 9 yields a value for the integral of  $C_n^2$  for altitudes above 1 km of the order of  $2 \times 10^{-13} \text{ m}^{1/3}$ . Using the theoretical expression for  $r_0$  and the average value of  $9.6 \text{ cm}$  at  $5000 \text{ \AA}$  yields a value for the integral of  $C_n^2$  over the entire atmospheric path of approximately  $7 \times 10^{-13} \text{ m}^{1/3}$ . Therefore, based on these averages, turbulence above 1 km accounts for roughly 35% of the total. Furthermore, based on the airborne microthermal data, the region between 300 m and 1 km contributes roughly  $10^{-13} \text{ m}^{1/3}$  or 20% of the total. These values lead to the conclusion that approximately 45% of the total contribution to the integrated turbulence is associated with low levels (under 300 m).

Correlation also exist in non-stationary effects seen in the two data sets. For example, the Star Sensor yields for 6 and 8 December were 82% and 30%, respectively (see Figure 4 for Seeing Monitor data). On a cycle by cycle basis, the standard deviation to mean ratio for the Seeing Monitor output voltage had an average of 0.08 and a range of (0.05-0.16) on 6 December. For 8 December, the values were 0.17 and (0.08-0.21). The comparable Star Sensor data is the twenty minute standard-deviation to mean ratio of the log-amplitude variance. The average and range of this parameter was 0.16 (0.11-0.21) and 0.27 (0.13-0.46) for 6 and 8 December, respectively. Hence both sets of data display higher levels of variability on 8 December.

Similar trends are sometimes apparent in the data. For example, the Star Sensor log-amplitude variance, except for one point, decreased in a monotonic fashion during the run of 12 July indicating improving conditions in agreement with the Seeing Monitor data of Figure 5. In contrast, no obvious trend was seen in the log-amplitude variance during the run of 8 July. Because scintillation tends to be dominated by higher altitude turbulence while seeing ( $r_0$ ) is usually dominated by lower altitudes, the two sets of data should not necessarily show the same trends.

#### 4. THEORETICAL COMPARISONS

H. Yura<sup>(14)</sup> has carried out a number of theoretical calculations with regard to these measurements. The theory uses a combination of the Hufnagel wind correlated model<sup>(16)</sup> for high altitudes and a low altitude model based on the work of Bufton<sup>(17)</sup> and Koprov and Tsuang.<sup>(18)</sup> The results of these calculations are given in Table 4. The input to the theoretical model is the average wind velocity which was derived from the meteorological data of Appendix C. The empirical values for this parameter are 21.3 m/s, 20.5 m/s, and 30.8 m/s for 17, 18 and 21, November, respectively. As can be seen, the theoretical results are higher than the experimental data in all cases. It is interesting to note that for  $r_0$ , the theoretical values are in better agreement than the values derived from the empirical profile (Table 3).

The Hufnagel model can also be compared to the Star Sensor high altitude profile data. In Figure 9, the dashed curve is based on the model assuming an altitude averaged velocity of 15 m/s. Several observations are obvious. All of the experimental results have a reasonable shape. In addition, all show a tendency to flatten out at intermediate altitudes and then fall off rapidly. Only two of the five averaged results show an increase in turbulence strength in the vicinity of (6-9 km) above the site (9-12 km above sea level). In general, the data appears to support the existence of a turbulent tropopause but one which is not always strong. The data also indicates relatively higher levels of turbulence at lower altitudes than the theoretical mode. This could possibly be due to the application of the model outside its range of stated validity (ground + 3000 M to 24,000 M). A rather dramatic result is the close agreement between the model and the averaged data for July 1976. Because a detailed study of the available meteorological data on upper atmospheric winds has not yet been carried out, great significance cannot be attached to this agreement.

#### 5. EXPERIMENTAL COMPARISONS

Scintillation data has been collected for a considerable period of time at a number of different sites. A number of average properties associated with this data base are given in Ref. 16. Several can be compared with the data reported here. Results are given in terms of the parameter  $S$ , defined as  $\sigma_p^2 / \langle p \rangle^2$  where  $\sigma_p^2$  is the variance and  $\langle p \rangle$  is the mean value of the integrated irradiance seen by a 10 cm aperture viewing near zenith stars. In particular, over a year long period  $\log S$  is approximately a Gaussian random variable with  $\sigma = \log 2.1$ . The year round median value of  $S$  is about 0.06 for all sites. The complete set of

16. R. E. Hufnagel, OSA Topical Meeting on Optical Propagation Through Turbulence (Boulder, Colorado, 1974), paper WA1.
17. J. L. Bufton, Appl. Opt. 12, 1785 (1973).
18. V. M. Koprov and L. R. Tsuang, Atmos. and Oceanic. Phys. 22, 1142 (1966).

TABLE 4. THEORETICAL COMPARISONS

Date	$\sigma_1^2 (\times 10^{-4})$				$r_o$ (cm) @ 5000 Å				$\int C_n^2 dz (\times 10^{-13} M^{1/3})$			
	Experimental <sup>1</sup>		Theory <sup>2</sup>	Seeing Monitor			Theory <sup>2</sup>	Seeing Monitor		Theory <sup>2</sup>		
Range	Average	Range	Average	Range	Average	Range	Average					
17 Nov.	2.8-18.2	7.9	5.4	6.8-9.8	7.7	12.75	6.8-13.0	10.0	4.7			
18 Nov.	2.3-5.0	3.8	5.0	9.7-13.2	11.3	13.0	4.1-6.9	5.4	4.5			
21 Nov.	5.2-8.2	6.0	10.7	6.6-12.4	8.6	11.0	6.3-14.0	8.7	6.0			

1. Direct measurement from Star Sensor with 35.6 cm aperture.

2. Yura results, based on Hufnagel and low altitude model.

twenty minute log-amplitude variances given in Appendix B has a mean, median and variance of approximately  $5.9 \times 10^{-4}$ ,  $5.6 \times 10^{-4}$  and  $1.9 \times 10^{-7}$ , respectively. However, these values are for a 36 cm aperture. Assuming the approximate large aperture theoretical scaling ( $D^{-7/3}$ ) and the usual Gaussian relationship between irradiance and log-amplitude<sup>(13)</sup> yields a median value for  $S$  of 0.04 and a root variance for log  $S$  of approximately log 2.

A number of other measurements of  $r_0$  have been carried out. At AMOS, techniques implemented have included Speckle Interferometry,<sup>(19)</sup> a differential Hartmann method,<sup>(20)</sup> and a shearing interferometer.<sup>(21)</sup> Data has also been collected at the Mauna Kea Observatory (altitude  $\approx 14,000$  ft) on the island of Hawaii, a distance of approximately 75 miles southeast of AMOS. The instrument used was a coherent interferometer.<sup>(22)</sup> All of these results are given in Table 5. The reported shearing interferometer data is limited to a single plot of the long exposure MTF. The shape varies somewhat from the theoretical expectation. The value of  $r_0$  in the table represents an approximate fit of the theory to the data. The speckle data also indicates non-stationarity effects and approximate Gaussian statistics similar to those reported here.

19. A. Schneiderman and D. Karo, OSA Topical Meeting on Speckle Phenomena (Pacific Grove, California, 1976), paper ThC6 and private communication.
20. M. G. Miller and P. F. Kellen, AAS/SAO/OSA/SPSE Topical Meeting on Imaging in Astronomy (Cambridge, Mass., 1975), paper WB 3.
21. D. Kelsall, J. Opt. Soc. Am. 63, 1472 (1973).
22. J. C. Dainty and R. J. Scaddan, Mon. Not. R. Astr. Soc. 170, 519 (1975).



TABLE 5. EXPERIMENTAL COMPARISONS OF  $r_o$

<u>Technique</u>	<u>Mean (cm)</u>	<u>Range (cm)</u>
Seeing Monitor	9.6	5.3-17.8
Speckle Interferometry (Schneiderman and Karo)		
June 1975		4.1-6.4
June 1976		10
Differential Hartmann, August 1974 (Miller and Kellen)	10.3	3.0-18.0
Coherent Interferometer, June 1974 (Dainty and Scadden-Mauna Kea)	12.7	4.0-18.5
Shearing Interferometer, 1972 (Kelsall)		3

## VII. RTAM AMOS TESTS

### 1. GENERAL

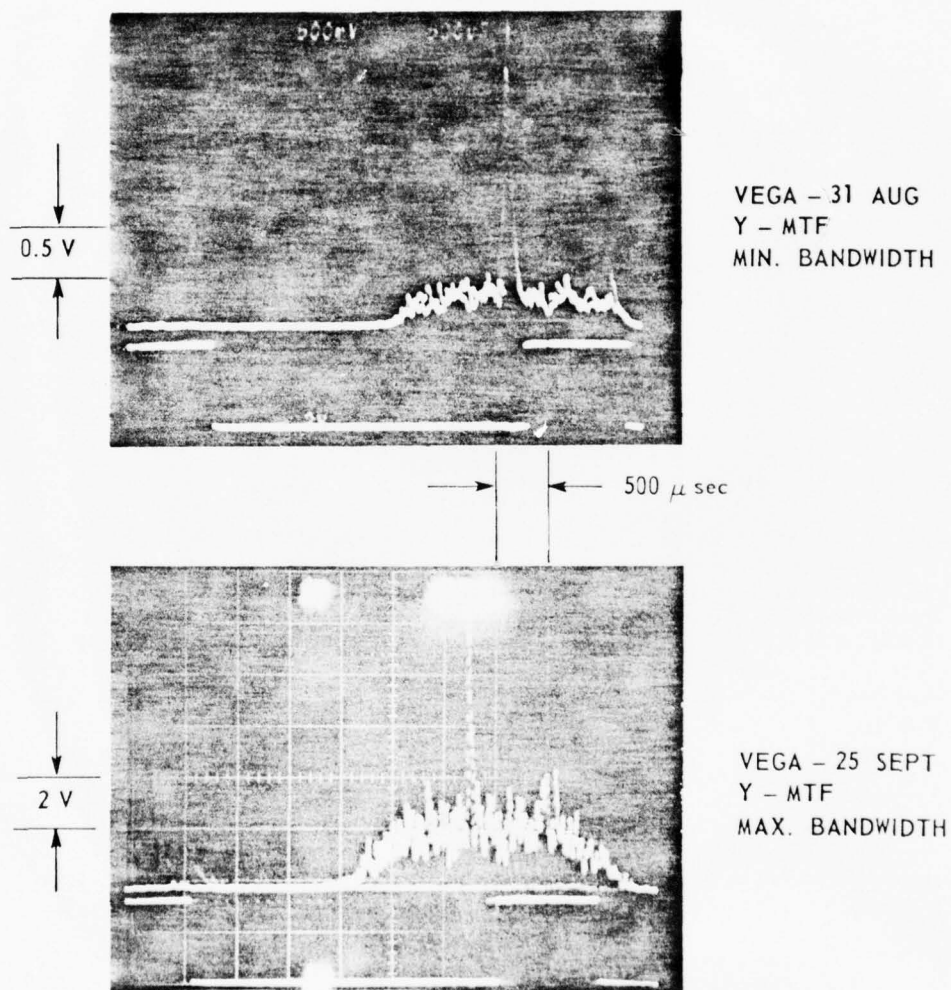
The Real Time Atmospheric Measurement System (RTAM) underwent AMOS testing during the period 16 August to 3 September, 1976. Initially, it was set up on an optical bench and its performance checked using a He-Ne laser source. Results were similar to those seen in the laboratory. After installation on the 1.6 M telescope, a series of diagnostic tests and adjustments were carried out. Successful operation of the instrument was established. However, several problems were found but not eliminated. The first of these was a very narrow field of view (less than four arc seconds) which, if not widened, will be a severe restriction to any future operations, requiring very good tracking and low wind velocity. The second was a low signal to noise ratio which has significant impact on the ability of the RTAM to produce a detailed characterization of the OTF.

### 2. MTF PERFORMANCE

In general, the MTF's seen were consistent with expectation, i.e., a central peak which fell off at low spatial frequency to a low signal level which included large variations.<sup>(8)</sup> These variations are due both to the atmosphere and system noise. Examples are shown in Figure 25. The width of the peak can be used to obtain a rough estimate of seeing conditions (i.e.,  $r_0$ ), while the relative levels of the zero and high spatial frequency portion of the MTF can be used to obtain an estimate of the signal to noise ratio.

Seeing conditions were determined by measuring the width of the MTF at 50% of its initial value. A fit of this frequency to theory yields the desired estimate of  $r_0$ . Because the modulus of the OTF is measured, the appropriate model is the short-exposure averaged MTF.<sup>(4)</sup> The data analyzed in this fashion are short exposures (single realizations) which are corrupted with noise and hence these results are only approximate. The estimated values of  $r_0$  were of order 15 cm on 31 August and in the range 8 to 12 cm on 2 September. These results are reasonable, based on previous experience.

For the purpose of carrying out a detailed characterization of the MTF, an important consideration is the inherent signal to noise ratio of the MTF at high spatial frequencies (i.e., greater than the atmospheric cutoff  $f_A \sim r_0$ ). If this quantity is too small, useful information will be obtained at low spatial frequencies only. It is important to note that this high-frequency (S/N) is different than the (S/N) considered in various RTAM documents which is more characteristic of zero-frequency behavior. Provided various statistical assumptions are made, both can be related to



G 6194

Figure 25. RTAM-MTF Data. Source was Vega ( $m \approx 0$ ). Upper trace is with minimum bandwidth (31 August) and lower trace is with maximum bandwidth (2 September).

the ratio of the average MTF to the average noise level at zero spatial frequency. In the current case, this latter quantity can be estimated from the data because the high-frequency behavior is dominated by noise. Theory<sup>(8)</sup> predicts a high-frequency (S/N) for a single realization of order one due to atmospheric fluctuations only. A theoretical estimate<sup>(23)</sup> (assuming an  $r_0$  of 10 cm) of the multiplicative factor by which this ideal value is reduced by noise as a function of the zero-frequency MTF to average-noise ratio is given in Figure 26. Also included in the figure is the estimated range of operation seen on 31 August and 2 September as well as the theoretically predicted range of operation against a first magnitude star. The former was established by analyzing data taken against several bright stars while the latter is based on theoretical estimates of system characteristics. (24)

Two other quantities are of interest in determining the data processing requirements. The first of these is the number of frames required to obtain a given accuracy in the final average. Assuming that independent realizations are averaged the (S/N) is proportional to the square root of the number of frames. The second is the fraction of the total average high-frequency signal which is due to the MTF. If this fraction is small, processing becomes more difficult due to the existence of a large spurious signal. These three characteristics of the data are tabulated in Table 6 for both the actual performance seen and the theoretically estimated performance.

These results indicate that performing at its current level, the RTAM would provide data which would be extremely difficult to process for useful MTF information at high-spatial frequencies. This is particularly true at the lower end of the operational range where several thousand frames of data would be required and still result in a high frequency signal which would be more than 90% spurious. If the theoretically predicted performance were to be achieved, processing should yield useful results for brighter stars under reasonable conditions.

### 3. PHASE TRANSFER FUNCTION

The situation regarding the phase outputs is more difficult to analyze. While the RTAM did generate signals in these channels, their interpretation is not obvious for a number of reasons. Examples of the PTF taken against Vega on 2 September are shown in Figure 27. Maximum excursions seen were of order  $\pm 10 \pi$  radians with rms values of order  $2 \pi$  radians. These values do not conflict with any fundamental understanding. However, a number of non-atmospheric effects are probably contributing including a systematic error, tracking induced image wander, noise and loss of phase-lock in the detection process. The systematic error was observed in the laboratory. While its presence complicates processing, it can be eliminated (if it is constant in time) by subtracting a known phase (as a

---

23. Based on an analysis similar to that given by F. Roddier (reference 20, paper ThC6), A. Schneidman and D. Karo (reference 11, pg. 70) and M. G. Miller (reference 19, paper ThC4).

24. A. MacGovern, private communication.

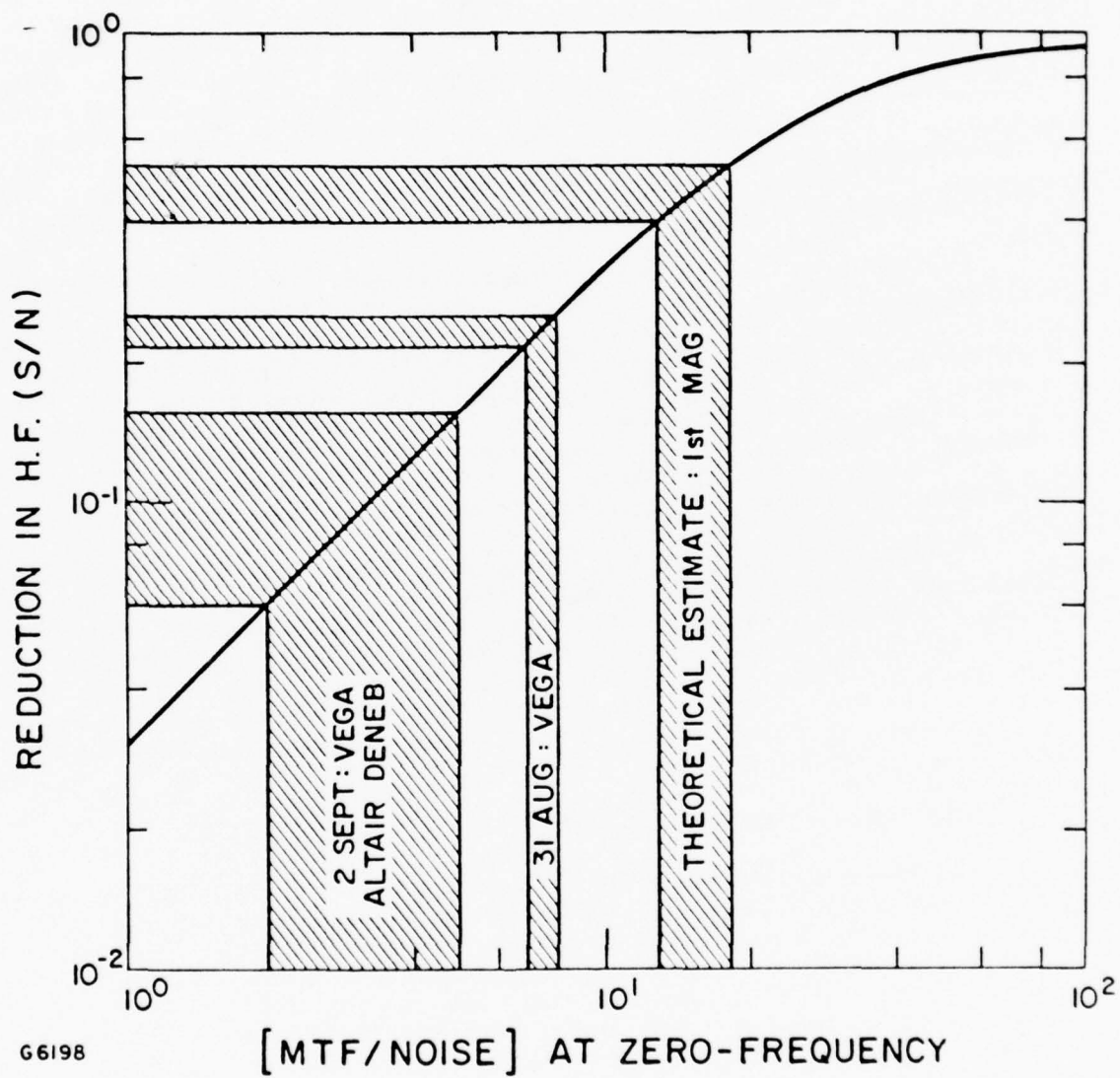


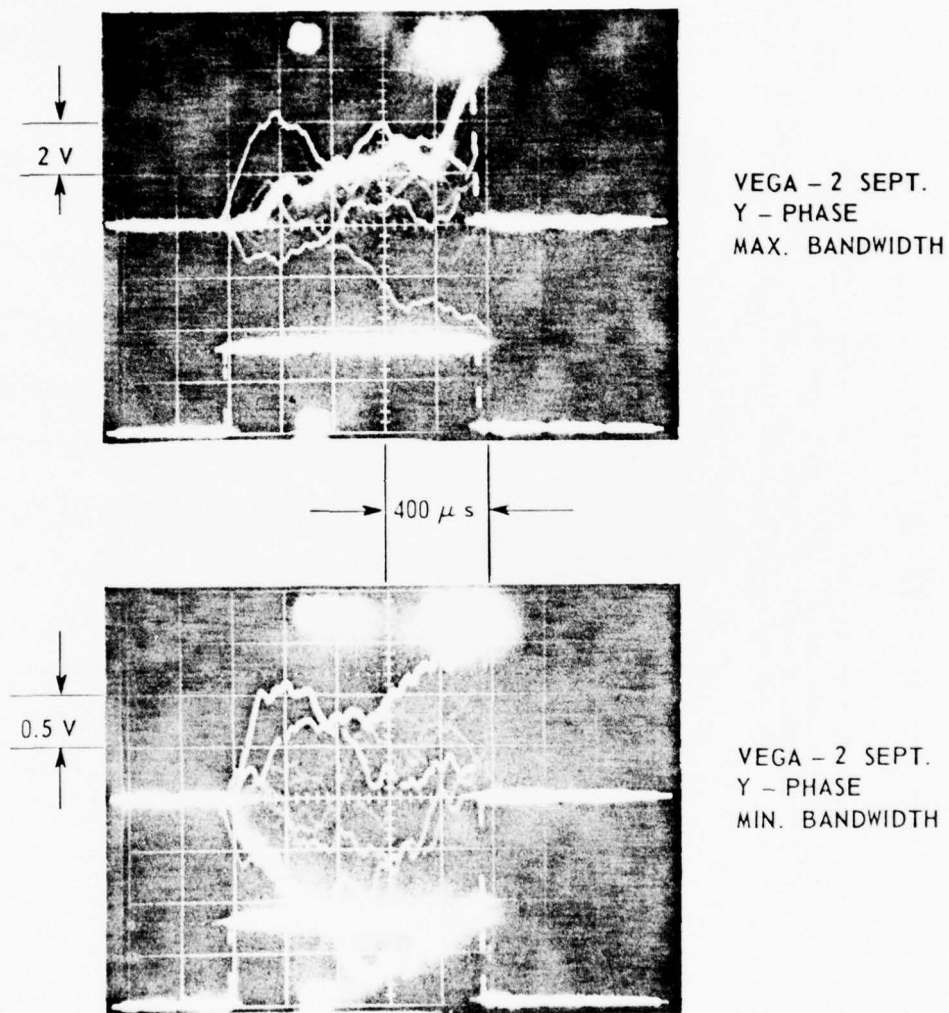
Figure 26. RTAM-Reduction in High-Frequency (S/N)



TABLE 6. MTF PERFORMANCE

	High-Frequency MTF (S/N) Reduction Factor	Required No. of Frames for (S/N) = 10	Fraction of H. F. Signal Due to MTF
Current RTAM			
31 Aug: Vega (m = 0.03)	0.25	500	0.21
2 Sept: Vega (m = 0.03)	0.15	1500	0.13
2 Sept: Altair (m = 0.75)	0.08	3800	0.07
2 Sept: Deneb (m = 1.26)	0.07	5000	0.06
Theoretical RTAM (m = 1)	0.45	125	0.35

Note: All values are nominal and are based on visual estimates of the data.



G6196

Figure 27. RTAM-PTF Data. Source was Vega ( $m \approx 0$ ) on 2 September. Upper trace is with maximum bandwidth and lower trace is with minimum bandwidth.

function of frequency) from each realization. Tracking induced image wander would be somewhat more complicated to handle because it is dynamic. However, the dynamics of the mount are such that little motion can occur with a bandwidth greater than 10 Hz. Therefore, if subsets of data corresponding to total collection times of less than 0.1 sec were normalized to eliminate the least-square fit of the average phase to a linear phase taper plus the (assumed) known systematic error, much of this telescope wander should be eliminated. If this procedure did not prove to be adequate, it would also be possible (in principle) to derive the required wander effect from a time-synchronized recording of the mount shaft angle encoder error signals.

The effect of system noise is to add a statistical fluctuation to the signal which is already random due to the atmosphere. Because one interesting question regarding phase is the type of statistics it obeys, noise will act as a spurious signal which, if large enough, can mask the atmospheric effect. Increasing the number of frames reduced will not minimize this effect, but only refine the estimates of the combined statistics. Hence if useful information is to be obtained, either the noise must be small or a set of noise evaluation experiments and/or theory (as a function of operational parameters) must be carried out so that this effect can be deconvolved from the combined data. The amount of noise seen in the MTF would suggest that the former is an unlikely situation.

The most difficult problem to deal with is the loss of phase-lock in the detection process. This occurs whenever the MTF drops below some critical level which is unknown at this time. The result of this phase-lock loss is that a random and unknown amount of phase shift is added to the output. In fact if the MTF does not rise above this threshold, the phase output will apparently be due entirely to noise. Because the effect of the atmosphere is to depress the MTF at all frequencies but the very lowest, the possibility exists that the only real atmospheric phase information which can be obtained from the RTAM will be at spatial frequencies below the seeing induced cutoff. If this is indeed the case, the phase outputs will be of little utility.

## REFERENCES

1. Miller, M. G. and Kellen, P. F., Turbulence Characterization and Control, Interim Technical Report, Contract #F30602-75-C-0012 (Avco Everett Research Laboratory, Inc.), Rome Air Development Center Technical Report #RADC-TR-75-185 (July 1975), (A015759).
2. Miller, M. G., Zieske, P. L. and Dryden, G., Turbulence Characterization and Control, Final Technical Report, Contract F30602-75-C-0012 (Avco Everett Research Laboratory, Inc.), Rome Air Development Center Technical Report #RADC-TR-76-189 (June 1967), (A027155)
3. Giuliano, C. R., et al., Space Object Imaging, Final Technical Report, Contract #F30602-74-C-0227 (Hughes Research Laboratory), Rome Air Development Center Technical Report #RADC-TR-76-54 (March 1976), (A023497).
4. Fried, D., J. Opt. Soc. Am. 56, 1372 (1966).
5. Papoulis, A., Probability, Random Variables and Stochastic Processes (McGraw-Hill, N. Y. 1965), 245.
6. Middleton, D., An Introduction to Statistical Communication Theory, (McGraw-Hill, N. Y. 1960), 426.
7. Actually, the random fluctuation is more appropriately modeled as having a small, but non-zero mean (see reference 8). However, this should not significantly effect the first order analysis.
8. Korff, D., Dryden, G. and Miller, M. G., Optics Comm. 5, 187 (1972).
9. Gaussian voltage statistics are assumed.
10. Karo, D. and Schneiderman, A., J. Opt. Soc. Am. 66, 1065A (1976).
11. Ochs, G. R., Lawrence, R. S., Wang, T. and Zieske, P., SPIE Proceedings 75, 48 (1976).
12. Ochs, G. R., Wang, T., Lawrence, R. S. and Clifford, S. F., Applied Optics 15, 2504 (1976).
13. Lawrence, R. S. and Strohbehn, J. W., Proc. of IEEE 58, 1523 (1970).
14. Yura, H., Aerospace Technical Report #TR0077(2756)-1, 1976.
15. Lawrence, R. S., private communication.

16. Hufnagel, R. E., OSA Topical Meeting on Optical Propagation Through Turbulence (Boulder, Colorado, 1974), paper WA1.
17. Bufton, J. L., Appl. Opt. 12, 1785 (1973).
18. Koprov, V. M. and Tsuang, L. R., Atmos. and Oceanic. Phys. 22, 1142 (1966).
19. Schneiderman, A. and Karo, D., OSA Topical Meeting on Speckle Phenomena (Pacific Grove, California, 1976), paper ThC6 and private communication.
20. Miller, M. G. and Kellen, P. F., AAS/SAO/SPSE Topical Meeting on Imaging in Astronomy (Cambridge, Mass., 1975), paper WB 3.
21. Kelsall, D., J. Opt. Am. 63, 1472 (1973).
22. Dainty, J. C. and Scaddan, R. J., Mon. Not. R. Astr. Soc. 170, 519 (1975).
23. Based on an analysis similar to that given by F. Roddier (reference 20, paper ThC6), A. Schneiderman and D. Karo (reference 11, pg. 70) and M. G. Miller (reference 19, paper ThC4).
24. MacGovern, A., private communication.



APPENDIX A  
SEEING MONITOR DATA

Notes

1. All data points correspond to the average value of a 1350 member ensemble of short exposures (one millisec) taken over a period of approximately 8.25 min.
2. All data except that of 12 and 13 May were taken with a 1200 Å filter centered at 6200 Å. The data of 12 and 13 May was not spectrally filtered. Theoretical scaling was used to reduce to the effective wavelength of 5000 Å.
3. The data of 9-13 July has been corrected for zenith angle dependence using the theoretical scaling. The rest of the data was not corrected because small zenith angles (less than 30°) were used and hence the correction is small.
4. The times given are approximate ( $\pm 5$  min) local Hawaiian Standard Time. The dates given are those of the starting time.

TABLE A-1. SEEING MONITOR DATA - SUMMARY

Date	Time Period HST	No. of Points	$r_0$ @ Mean	5000 Å: cm Range
11 Nov 1975	2240 - 0030	6	9.6	7.9 - 10.7
12	1950 - 2240	9	9.9	8.5 - 11.1
14	2110 - 2400	9	11.7	10.8 - 12.9
15	1930 - 2230	10	11.4	10.2 - 13.0
17	1950 - 2240	9	7.7	6.8 - 9.8
18	2050 - 2350	9	11.3	9.7 - 13.2
19	2020 - 2310	9	8.7	6.9 - 10.5
21	1930 - 2220	8	8.6	6.6 - 12.4
6 Dec 1975	0100 - 0350	9	9.4	9.0 - 9.7
8	0200 - 0450	9	14.1	10.0 - 17.8
12 May 1976	2250 - 0040	6	10.7	10.1 - 11.4
13	2120 - 2300	6	12.1	10.3 - 13.1
27	2230 - 2320	3	5.6	5.3 - 5.9
10 June 1976	2110 - 2220	4	7.0	5.3 - 8.1
18	2120 - 2400	10	7.8	7.1 - 8.7
21	2030 - 2230	12	7.6	7.9 - 9.0
24	2150 - 2350	12	10.5	9.1 - 11.3
29	2250 - 0050	12	12.2	11.6 - 13.3
30	2120 - 2320	12	6.0	5.5 - 6.9
6 July 1976	2300 - 0100	12	7.6	6.2 - 8.4
8	2330 - 0130	12	9.6	8.1 - 11.6
9	2100 - 0210	9	8.2	7.1 - 9.0
12	0150 - 0450	18	11.1	7.6 - 14.4
13	0050 - 0420	13	8.7	8.0 - 9.6

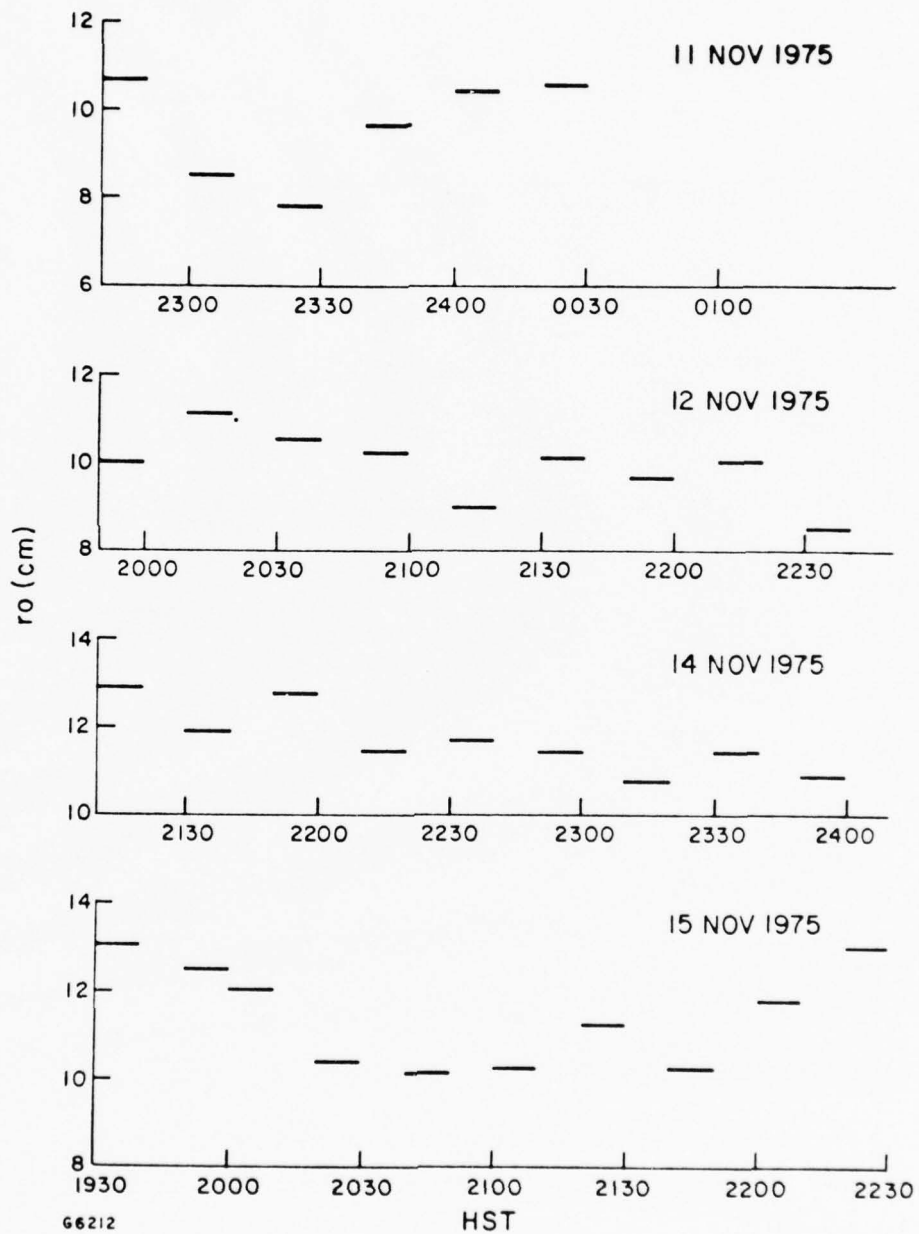


Figure A-1. Seeing Monitor Data - 11, 12, 14 and 15 November 1975. The horizontal bars indicate the averaging period.

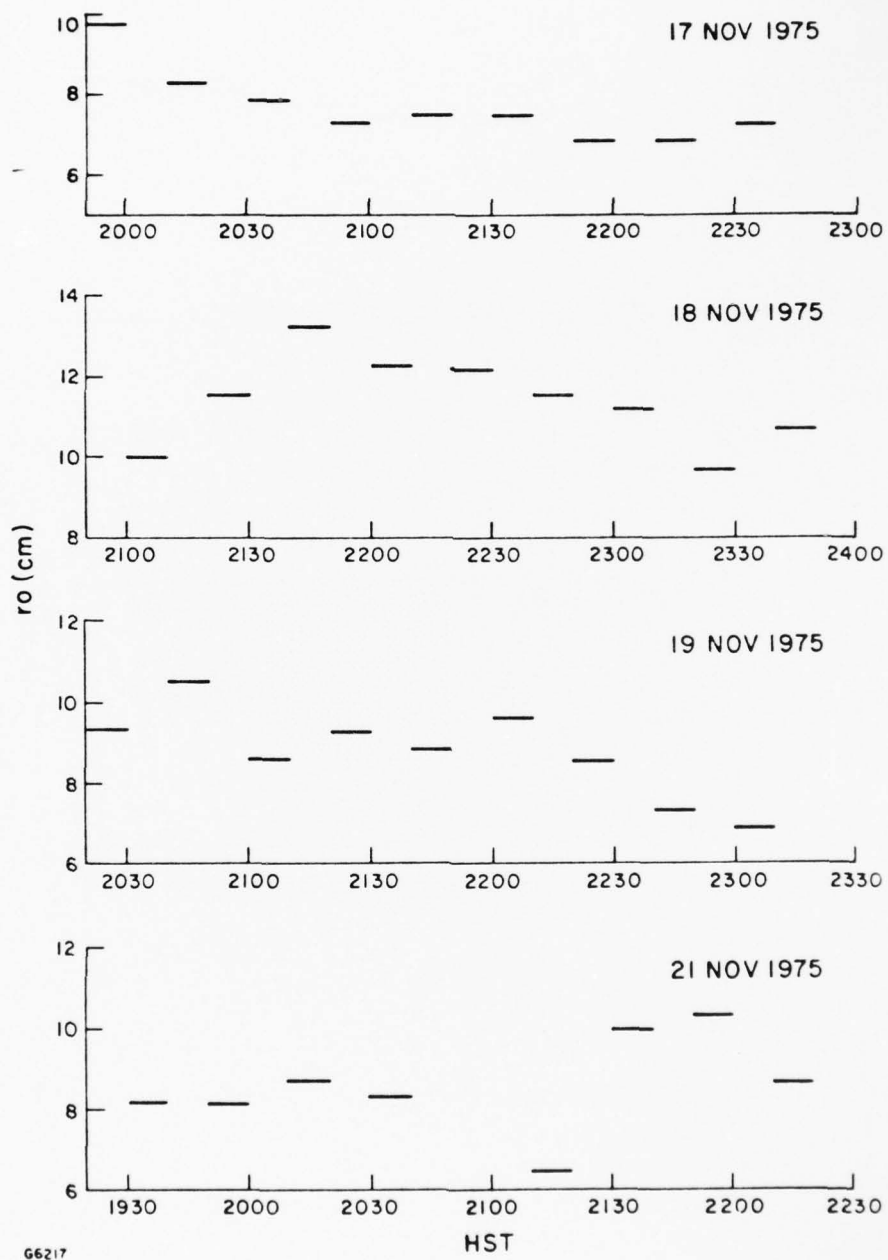


Figure A-2. Seeing Monitor Data - 17, 18, 19 and 21 November 1975. Same as A-1.



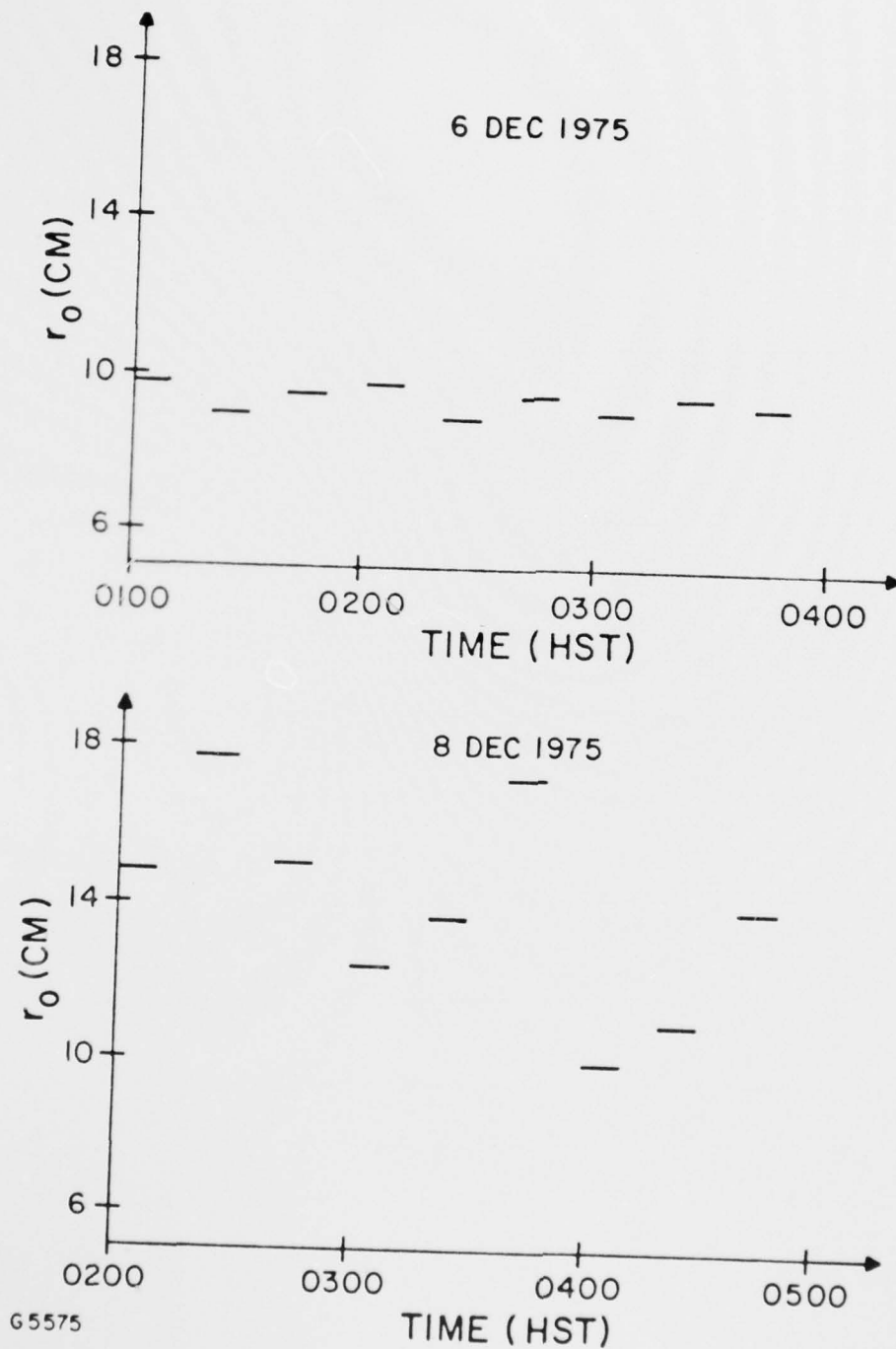


Figure A-3. Seeing Monitor Data - 6 and 8 December 1975. Same as A-1.

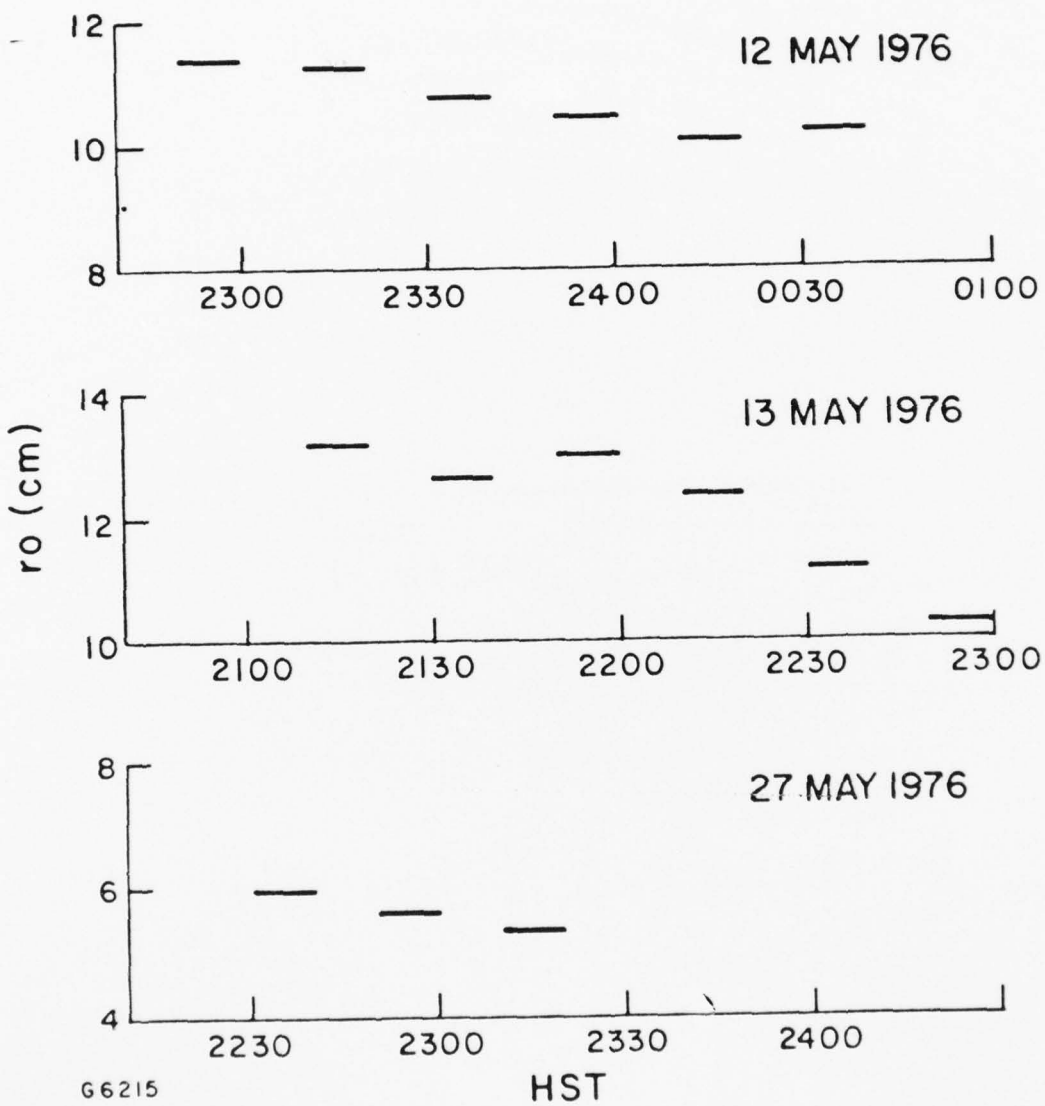


Figure A-4. Seeing Monitor Data - 12, 13 and 27 May 1976. Same as A-1.

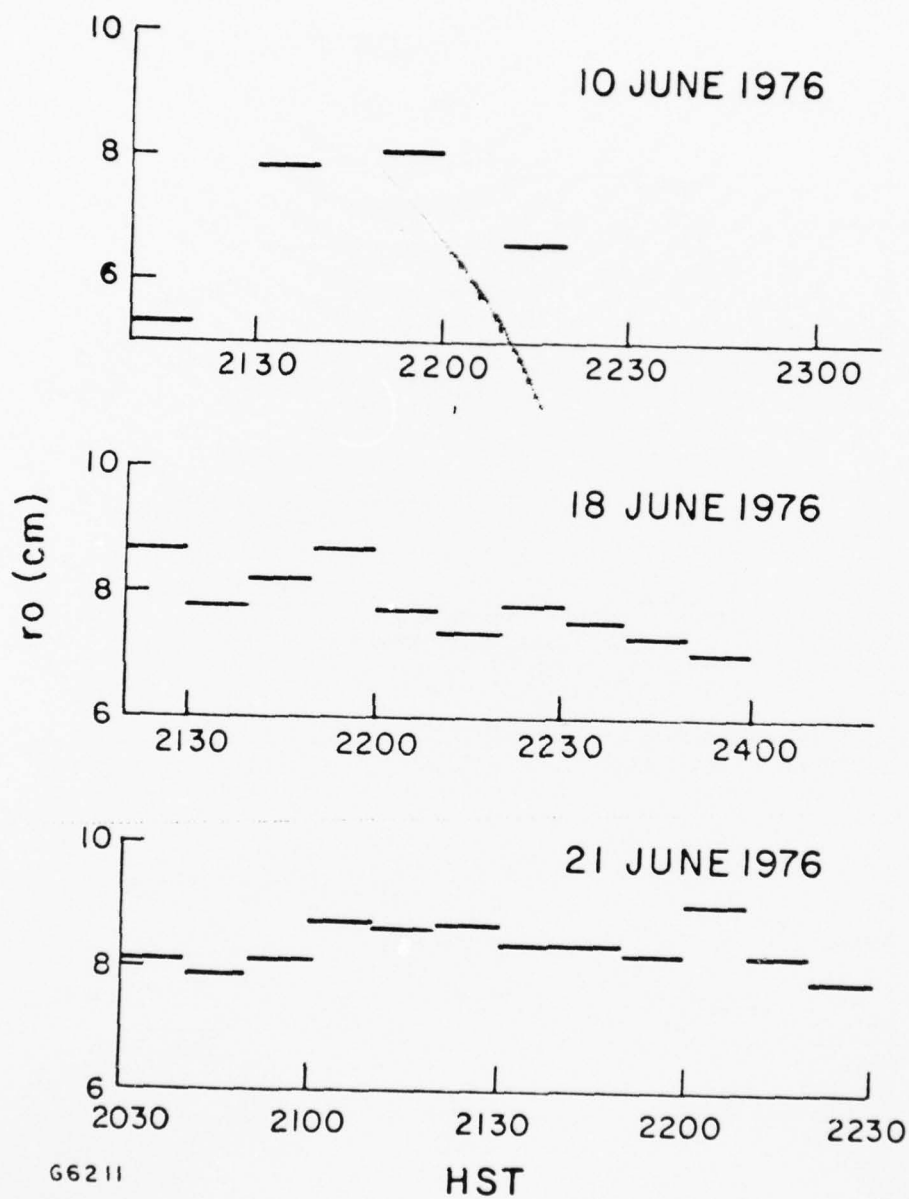


Figure A-5. Seeing Monitor Data - 10, 18 and 21 June 1976. Same as A-1.

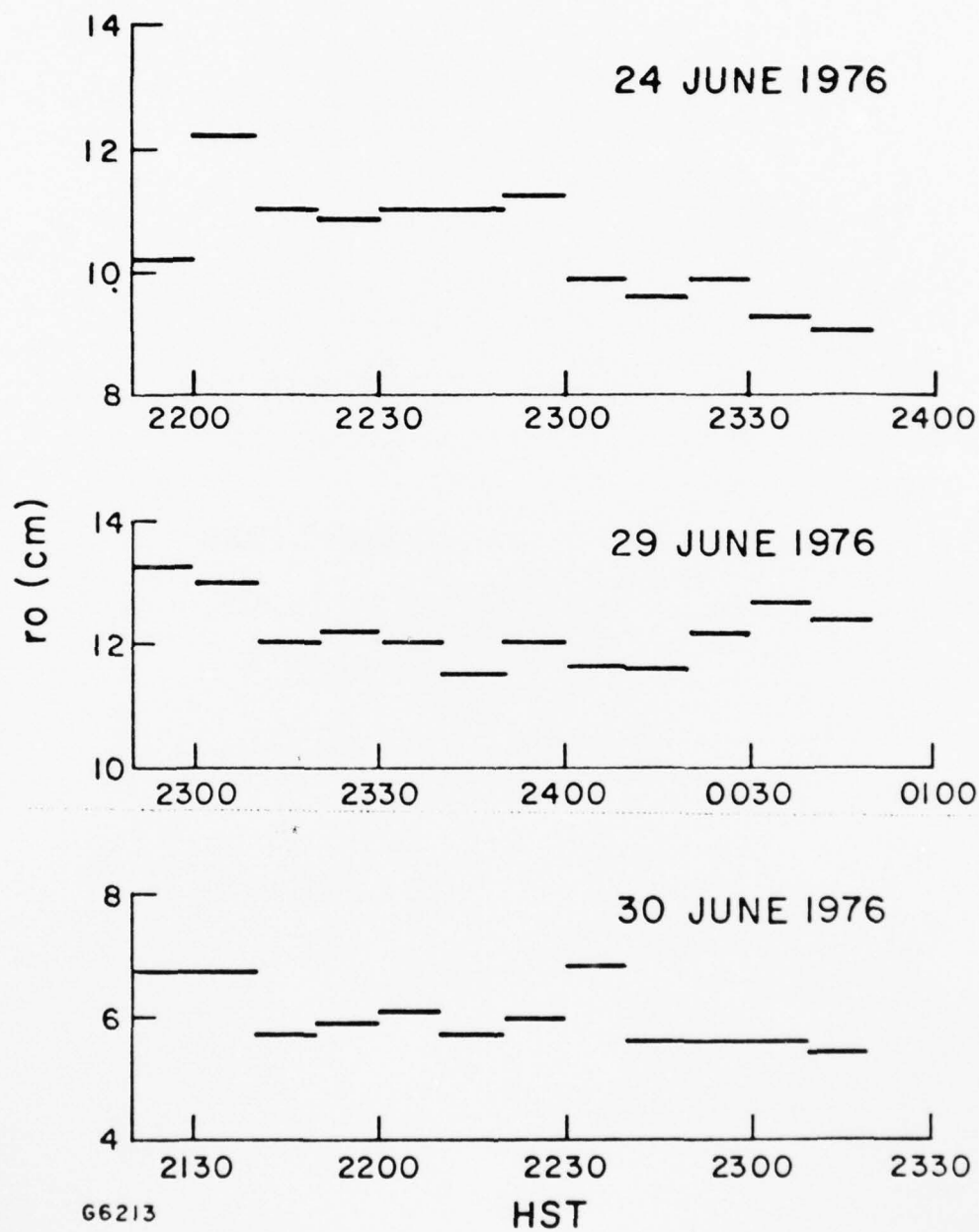


Figure A-6. Seeing Monitor Data - 24, 29 and 30 June 1976. Same as A-1.

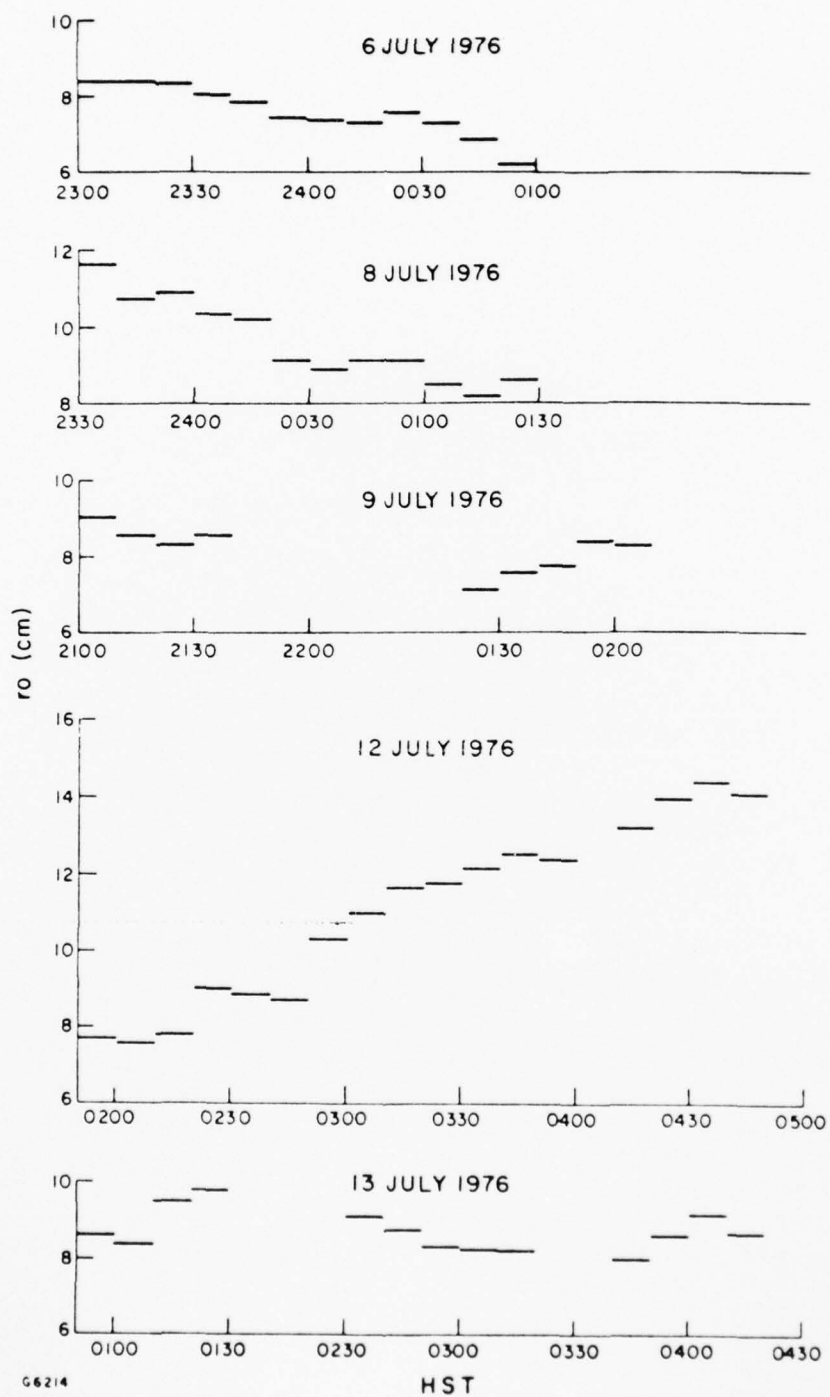


Figure A-7. Seeing Monitor Data - 6, 8, 9, 12 and 13 July 1976. Same as A-1.



APPENDIX B  
STAR SENSOR DATA

### Notes

1. The basic data obtained corresponds to ensembles of approximately 40 twenty-four second averages taken during a twenty minute time period. These data are then reduced for the turbulence profile and 20 min. averaged  $\sigma_1^2$ .
2. The reported  $\sigma_1^2$  is the mean and range of the 20 min. averages taken on each night.
3. The times given are approximate local Hawaiian Standard Time. The dates given are those appropriate for the beginning of each night's data collection run.
4. The data has not been corrected for zenith angle. Typically this angle was less than  $30^\circ$  so that the correction should be small. No spectral filtering was used.
5. Yield refers to the number of valid profiles divided by the total number of profiles collected during an evening. To be valid, a profile must have a standard deviation to mean ratio of the twenty-four second log-amplitude variances of 0.20 or less. Values larger than this indicate a high level of non-stationarity in the atmosphere during the twenty minute collection cycle. Only valid profiles are reported.
6. No valid profiles were collected on 11 and 12 November due to mechanical and electrical failures in the device. Seven of the ten profiles taken on 19 November were invalid due to saturation of the photo-multiplier tubes.
7. The seven value of  $C_n^2(i)$ ,  $i = 1 \dots 7$ , are for the nominal altitudes (above the site) of 2.25, 3.75, 5.25, 7.5, 9.75, 12.75 and  $> 14.5$  km, respectively. SD/M is the standard deviation to mean ratio of the ensemble of twenty-four second variances.

TABLE B-1. STAR SENSOR DATA - SUMMARY

Date	Time Period HST	Yield	No. of Samples	$\sigma_1^2$ ( $\times 10^{-4}$ )	
				Range	Mean
11 Nov 1975	2200 - 0040	0/8	-	-	-
12	1920 - 2220	0/9	2	5.50 - 5.54	5.52
14	2010 - 0030	7/12	15	2.78 - 6.22	4.16
15	1930 - 2310	10/11	13	1.55 - 3.98	2.68
17	1910 - 2250	4/11	12	2.79 - 18.2	7.92
18	1950 - 2350	11/12	12	2.28 - 5.03	3.76
19	1940 - 2320	0/10	4	2.04 - 28.3	18.2
21	2010 - 2250	5/7	8	5.17 - 8.21	6.00
6 Dec 1975	0020 - 0400	9/11	12	4.51 - 10.4	6.88
8	0140 - 0500	3/10	10	2.13 - 5.71	3.24
16 April 1976	0020 - 0440	7/12	12	5.25 - 12.8	8.13
23	2350 - 0530	12/16	16	2.58 - 7.02	4.45
29	2000 - 2305	2/6	5	3.62 - 9.12	4.83
5 May 1976	2210 - 0030	3/7	7	2.12 - 5.85	3.84
6	2150 - 2350	4/6	6	3.54 - 8.25	6.08
12	2240 - 0040	3/6	6	3.37 - 5.22	4.49
13	2100 - 2320	7/7	7	1.67 - 2.81	2.12
26	2340 - 2400	1/1	1	-	6.38
27	2050 - 2310	5/6	6	6.36 - 10.5	8.57
9 June 1976	2150 - 2310	3/4	4	2.89 - 3.43	3.14
10	2110 - 2250	2/5	5	5.09 - 6.30	5.76
18	2140 - 2300	1/4	4	4.17 - 7.61	5.58
21	2040 - 2240	4/6	6	5.24 - 9.99	6.75
24	2150 - 2350	0/6	6	5.97 - 13.4	8.78
29	2250 - 0050	4/6	6	4.03 - 7.02	5.39
30	2125 - 2325	4/6	6	5.59 - 8.89	7.30
6 July 1976	2310 - 0120	4/4	4	2.95 - 4.65	3.79
8	2330 - 0130	2/4	5	13.1 - 21.3	17.86
9	2100 - 0200	3/3	3	3.91 - 10.8	7.33
12	0150 - 0440	4/9	9	1.99 - 9.12	3.91
13	0030 - 0420	2/4	6	4.14 - 10.5	6.73

TABLE B-2. STAR SENSOR DATA-PROFILES

Date Local	Time HST	$\theta_z$ Deg	$\sigma^2$										$\sigma$	
			$C_{n^2(1)}$	$C_{n^2(2)}$	$C_{n^2(3)}$	$C_{n^2(4)}$	$C_{n^2(5)}$	$C_{n^2(6)}$	$C_{n^2(7)}$	$\times 10^{-4}$	SD/M			
14 Nov '75	2200	60	15.5	8.0	2.25	0.62	1.69	1.98	2.14	4.52	0.18			
	2320	72	20.8	18.9	14.5	2.44	0	0	0.74	3.57	0.18			
	2340	75	10.7	10.1	6.9	1.57	0.31	0	0.365	2.78	0.09			
	0020	81	53.8	18.6	0	0	0	0	1.41	4.99	0.20			
	0040	86	29.7	12.2	0.13	0	0	0	0.546	4.28	0.16			
	0120	82	34.1	13.5	0	0	0.33	1.21	0.616	4.35	0.19			
	0140	78	13.5	8.61	4.15	0.988	0.725	0.688	0.536	5.15	0.2			
			16.5	6.33	0	0.467	2.05	2.01	1.53	2.42	0.09			
15 Nov '75	1930	66	23.1	3.76	0	1.68	2.39	1.88	0.566	2.41	0.15			
	1950	70	6.8	3.24	0.845	0.183	0.151	0.19	0.572	3.28	0.07			
	2030	78	6.04	3.55	2.09	1.78	0.598	0.572	0.803	2.48	0.14			
	2050	81	7.05	3.59	1.1	0.631	0.577	0.77	0.808	2.78	0.10			
	2110	81	8.51	2.45	0.915	0.338	0.227	0.182	0	2.84	0.19			
	2130	79	5.95	3.47	2.58	1.73	0	0	0.852	2.79	0.17			
	2150	77	8.55	2.25	0	0.241	2.57	2.58	0.74	2.74	0.15			
	2210	73	14.0	4.77	0	0.17	0	0	0.858	3.98	0.13			

TABLE B-2. (CONTINUED)

	2250	65	17.3	9.03	2.3	0	0	0	1.26	2.74	0.14
17 Nov '75	1910	74	3.37	7.31	9.64	7.07	3.9	2.65	0	2.79	0.14
	1930	76	13.6	5.79	0.61	2.19	2.51	1.86	0.24	3.16	0.13
	1950	79	16.8	6.7	0	2.05	4.77	3.36	0.87	3.97	0.10
	2050	79	9.66	8.26	7.21	6.46	2.39	0.97	0	5.70	0.19
18 Nov '75	1950	58	11.7	8.48	6.13	3.07	0.173	0.443	1.65	4.54	0.06
	2010	63	25.8	14.3	3.24	4.68	6.0	4.96	0.114	5.03	0.16
	2050	66	16.1	7.85	5.44	7.67	4.67	2.17	0.43	3.60	0.16
	2110	71	16.4	7.84	1.23	1.53	2.29	2.46	0.072	2.78	0.10
	2130	75	24.7	10.4	1.4	1.15	0.74	0.45	0.41	2.28	0.08
	2150	80	33.1	9.62	4.7	1.26	0.602	0.92	0.95	3.77	0.15
	2210	84	28.5	9.11	3.52	3.63	1.47	2.29	1.16	3.88	0.19
	2230	88	21.6	8.36	1.52	0.32	2.39	2.48	0.89	4.47	0.12
	2250	82	19.3	6.92	1.74	0.87	1.97	2.27	1.24	4.09	0.15
	2310	80	14.6	6.27	0.65	1.17	1.95	1.13	0.31	3.73	0.17
	2330	75	18.8	11.2	3.17	1.24	0.71	0.86	0.11	2.71	0.18
21 Nov '75	2030	81	7.36	8.7	9.13	5.79	3.78	1.66	0.95	5.69	0.12



TABLE B-2. (CONTINUED)

2050	82	10.9	2.96	0	2.11	3.14	2.07	1.18	6.82	0.10
2110	80	16.4	5.79	0.07	2.27	1.18	0.98	0.91	4.72	0.15
2130	81	69.9	18.8	0	1.15	2.19	2.01	1.09	5.17	0.17
2210	88	115.0	50.2	4.68	0	0.75	1.65	2.85	6.81	0.15
6 Dec '75	73	10.8	5.44	3.22	5.25	5.49	3.94	1.92	6.2	0.13
0040	76	12.7	6.75	6.05	12.2	9.54	6.27	1.42	8.24	0.18
0100	78	4.07	0.63	0.51	9.25	10.4	8.24	1.09	7.41	0.15
0120	78	11.0	2.9	0.41	12.5	14.4	10.6	2.1	10.4	0.15
0140	76	10.0	6.58	5.98	14.4	13.3	8.83	0.50	9.61	0.18
0200	74	9.26	6.65	5.16	4.91	4.88	4.83	3.23	8.21	0.15
0220	70	14.7	5.51	0.18	8.29	10.3	8.25	1.79	7.07	0.18
0300	82	37.4	14.5	2.41	12.1	10.1	6.39	0	4.91	0.15
0320	80	6.19	9.49	11.2	10.7	6.8	5.23	10.7	4.51	0.12
8 Dec '75	71	10.0	5.8	3.72	4.77	3.01	1.93	0.19	2.13	0.17
0320	80	9.09	5.18	2.2	3.18	3.05	2.48	0.78	2.65	0.13
0400	72	4.52	5.14	6.23	7.02	5.05	2.89	0.18	2.88	0.17

TABLE B-2. (CONTINUED)

16 April '76	0040	84	0.45	12.2	18.9	9.73	4.78	1.99	0.88	8.11	0.13
	0100	82	0	4.45	8.64	9.28	5.86	4.07	1.69	8.30	0.13
	0120	81	1.43	2.21	4.0	6.33	4.79	4.11	1.57	8.49	0.10
	0140	78	13.1	14.9	12.2	7.92	9.46	7.95	2.46	10.6	0.15
	0240	66	0	9.03	15.0	15.7	12.2	6.56	0.10	6.03	0.18
	0300	60	0	0	5.35	13.4	11.6	6.75	0	5.85	0.10
	0420	72	0	3.78	7.01	7.85	8.07	0	1.99	5.73	0.19
23 April '76	2350	82	19.5	6.39	0	3.38	3.35	2.62	0.86	4.20	0.13
	0010	87	43.4	29.4	12.5	0	0	0.24	2.07	4.23	0.13
	0030	87	35.3	17.5	2.97	0	1.02	1.67	2.11	4.51	0.20
	0050	83	27.2	10.7	0	0	0	0.485	1.91	3.76	0.15
	0130	74	55.0	13.8	0	0.36	4.37	3.68	2.93	6.67	0.12
	0150	69	30.6	14.3	4.43	2.83	1.96	1.73	1.99	4.67	0.12
	0210	64	50.8	25.1	9.09	8.12	3.69	1.14	0.489	6.49	0.19
	0330	65	21.9	7.23	0	0.30	1.11	1.06	1.31	2.58	0.15
	0410	70	3.75	3.30	4.51	5.62	4.68	2.61	0.99	4.49	0.13
	0430	72	23.4	7.02	0	1.05	1.44	1.16	1.47	3.11	0.11

TABLE B-2. (CONTINUED)

0450	72	15.9	3.62	0	1.17	0.97	1.21	1.47	2.73	0.19
0510	71	15.3	5.26	0	0.75	1.68	2.01	1.22	2.62	0.13
29 April '76	2000	12.2	3.11	0	1.26	2.22	1.24	2.10	9.12	0.20
2225	67	2.03	1.39	0.85	0.68	1.75	2.18	1.42	3.62	0.12
5 May '76	2210	14.9	6.71	1.02	0.43	0.44	0.27	0.47	2.12	0.16
2250	79	67.3	17.7	0	0	0.83	2.0	0.75	3.56	0.18
2320	86	17.6	36.2	39.7	15.1	6.04	0.51	0	5.85	0.20
6 May '76	2210	8.18	7.94	0	0	1.03	1.07	0.79	5.95	0.20
2230	75	2.78	0.78	0	1.42	2.11	2.0	0.41	8.25	0.16
2250	80	1.38	1.22	2.45	4.47	2.92	1.73	0	7.05	0.20
2330	87	4.49	2.03	2.59	0.16	0.56	0.89	0.48	3.54	0.16
12 May '76	2300	3.9	2.73	2.08	1.72	0.71	0.18	0.26	4.70	0.17
2320	85	6.34	2.15	0	0.37	0.22	0.18	0.50	3.37	0.20
0020	75	5.88	2.77	1.63	1.77	1.45	0.47	0.87	4.13	0.18
13 May '76	2100	5.23	1.36	0	0.02	0.60	0.77	0.80	1.67	0.14
2120	66	3.1	1.17	0	0.55	1.12	1.23	0.59	2.35	0.20
2140	70	3.84	1.5	0	0	0.29	0.35	0.52	1.73	0.14

TABLE B-2. (CONTINUED)

	2200	75	3.09	1.65	0.65	0.84	1.04	0.68	0.32	2.81	0.15
	2220	80	4.48	2.39	0.72	0	0	0.15	1.06	2.18	0.20
	2240	84	4.09	2.27	0.80	0.22	0.83	0.64	0.75	2.31	0.17
	2300	87	4.99	1.09	0	2.42	1.66	0.66	0	1.79	0.14
26 May '76	2340	69	2.62	0.28	0	2.79	3.96	3.75	2.7	6.38	0.17
27 May '76	2050	72	38.2	39.1	30.9	9.9	7.17	2.89	0.63	8.12	0.20
	2110	77	21.3	16.2	15.3	10.9	3.62	0	1.11	6.79	0.16
	2130	82	33.9	19.2	12.0	8.93	2.54	0	2.34	9.7	0.16
	2210	86	28.4	13.9	3.49	4.05	2.89	3.0	2.94	6.94	0.13
	2230	83	22.9	8.21	0	4.43	5.6	3.99	1.32	6.36	0.13
9 June '76	2150	80	8.96	4.59	1.95	2.58	2.78	1.58	0.53	3.43	0.14
	2230	73	5.084	2.34	1.32	3.18	2.34	1.23	4.45	2.89	0.12
	2250	68	6.71	3.81	1.65	2.03	2.78	2.13	0.91	3.07	0.11
10 June '76	2130	86	3.55	1.51	0	1.03	2.03	3.2	2.31	5.58	0.14
	2210	76	0	0.44	3.82	4.57	3.01	0.74	0.72	5.08	0.17
18 June '76	2220	65	66.9	43.0	25.8	16.5	6.24	1.07	0	4.76	0.19
21 June '76	2040	87	53.6	46.1	29.0	3.54	4.1	2.21	1.87	6.03	0.19

AD-A038 632

AVCO EVERETT RESEARCH LAB INC EVERETT MASS  
TURBULENCE ENVIRONMENT CHARACTERIZATION.(U)  
MAR 77 M G MILLER, P L ZIESKE

F/G 4/1

UNCLASSIFIED

RADC-TR-77-70

F30602-76-C-0054  
NL

2 OF 2  
ADAD38632



END

DATE  
FILMED  
5-77

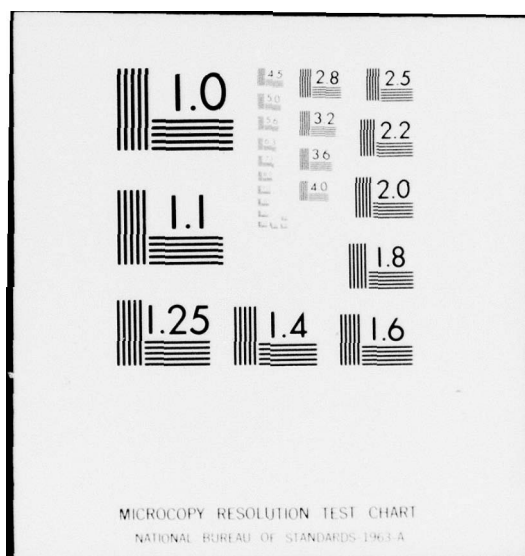




TABLE B-2. (CONTINUED)

2130	76	57.8	44.1	25.4	3.36	2.14	0.78	1.8	5.24	0.14
2150	72	14.7	14.2	10.3	7.93	6.81	5.69	1.83	6.00	0.12
2230	62	20.0	8.48	4.52	11.0	8.29	7.87	3.91	9.99	0.14
29 June '76	2250	0	0	0.67	3.89	3.37	1.86	0.42	5.05	0.11
2310	67	1.34	0	0	3.45	3.08	2.25	0.88	4.03	0.17
0010	72	0.54	1.29	1.49	2.52	1.68	2.02	0.53	6.21	0.18
0030	72	0.97	0.87	1.45	1.65	1.14	0.81	0.99	4.10	0.16
30 June '76	2145	39.4	25.0	8.87	1.06	5.97	6.41	3.41	8.89	0.19
2205	76	59.9	15.1	0	0	4.1	2.3	2.3	7.27	0.13
2225	72	40.3	19.1	5.09	1.8	1.19	0.07	2.05	6.12	0.12
2305	63	28.0	9.47	0	0	2.36	4.09	2.77	5.59	0.17
6 July '76	2310	12.3	5.0	0	1.35	2.23	1.92	0.29	2.96	0.17
2330	71	7.52	5.66	5.55	3.87	1.07	0	0.13	2.95	0.18
0040	69	25.4	15.5	8.96	9.19	4.79	2.28	0	4.65	0.12
0100	67	39.1	9.67	0	12.4	7.05	2.54	0	4.53	0.14
8 July '76	2330	0	0	5.74	13.0	11.3	8.24	3.04	15.8	0.15
0030	69	0	6.48	23.4	31.9	26.1	16.0	2.33	21.4	0.15

TABLE B-2. (CONTINUED)

9 July '76	2100	65	1.92	1.68	0.79	2.07	4.77	3.85	0.66	10.8	0.15
	2120	61	1.28	3.45	12.0	9.77	3.24	0.54	0	7.3	0.11
	0140	58	7.51	13.7	18.0	14.5	6.31	5.5	-	3.91	0.13
12 July '76	0310	53	9.1	5.44	2.52	2.16	1.95	1.55	1.06	2.70	0.19
	0340	45	17.9	10.3	3.2	0	0.27	1.17	1.93	3.3	0.16
	0400	41	4.44	4.1	4.14	4.87	3.62	2.04	0.12	3.00	0.14
	0420	36	1.48	7.27	11.4	2.57	4.13	2.54	0.64	3.16	0.18
13 July '76	0050	63	0	0.75	10.5	21.5	21.1	1.48	2.15	10.5	0.18
	0230	60	7.94	4.61	2.9	6.17	4.16	4.87	0.82	4.14	0.15

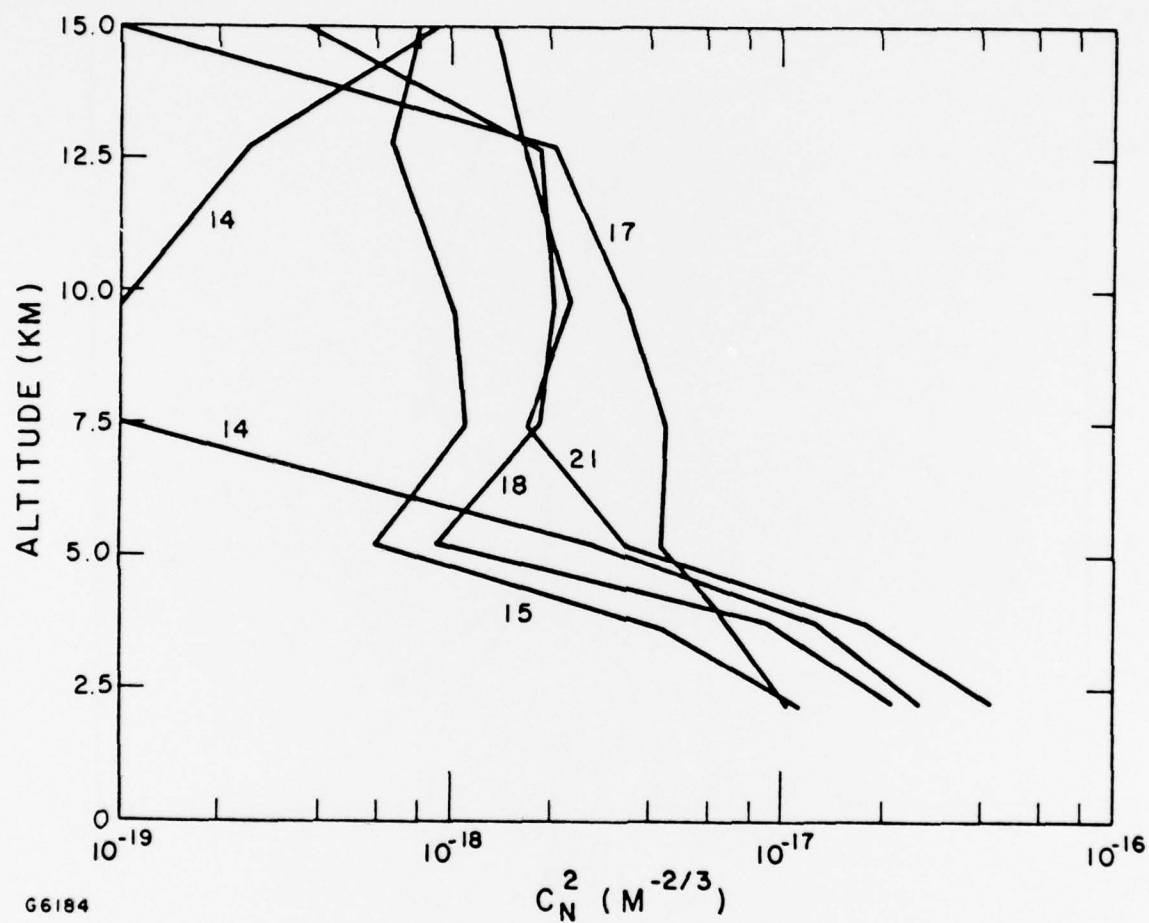


Figure B-1. Star Sensor Nightly Averaged Profiles - November 1975. Altitude is in height above the observatory. Each profile is an average of all valid data collected on a specific night. The width of the weighing functions are not shown.

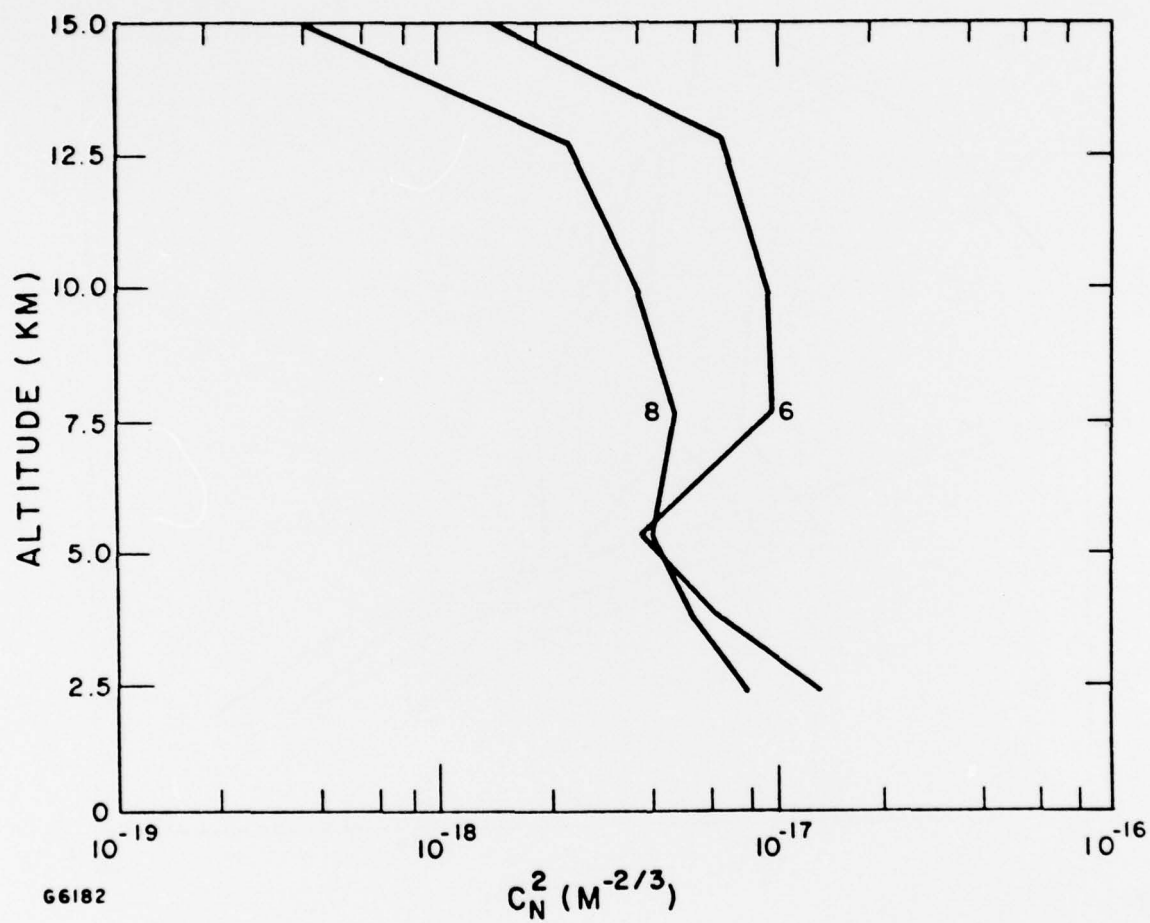


Figure B-2. Star Sensor Nightly Averaged Profiles - December 1976.  
Same as B-1.

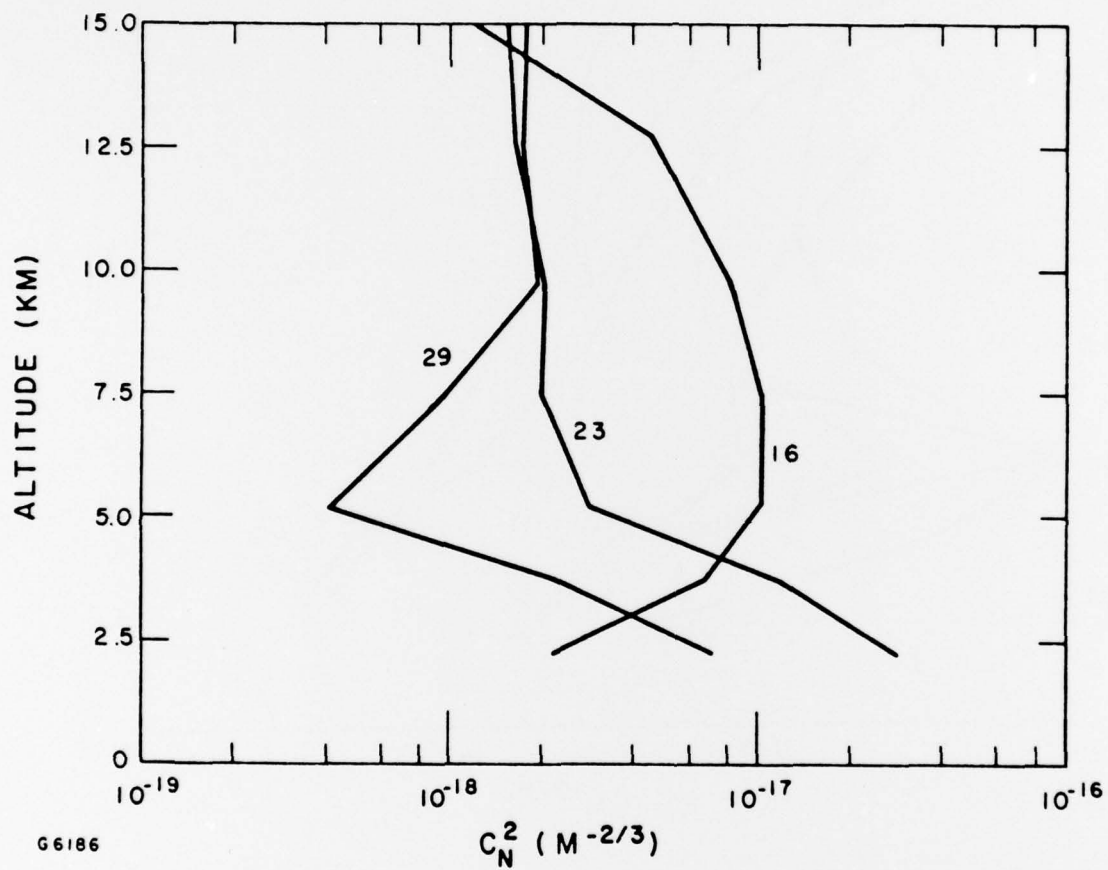


Figure B-3. Star Sensor Nightly Averaged Profiles - April 1976. Same as B-1.

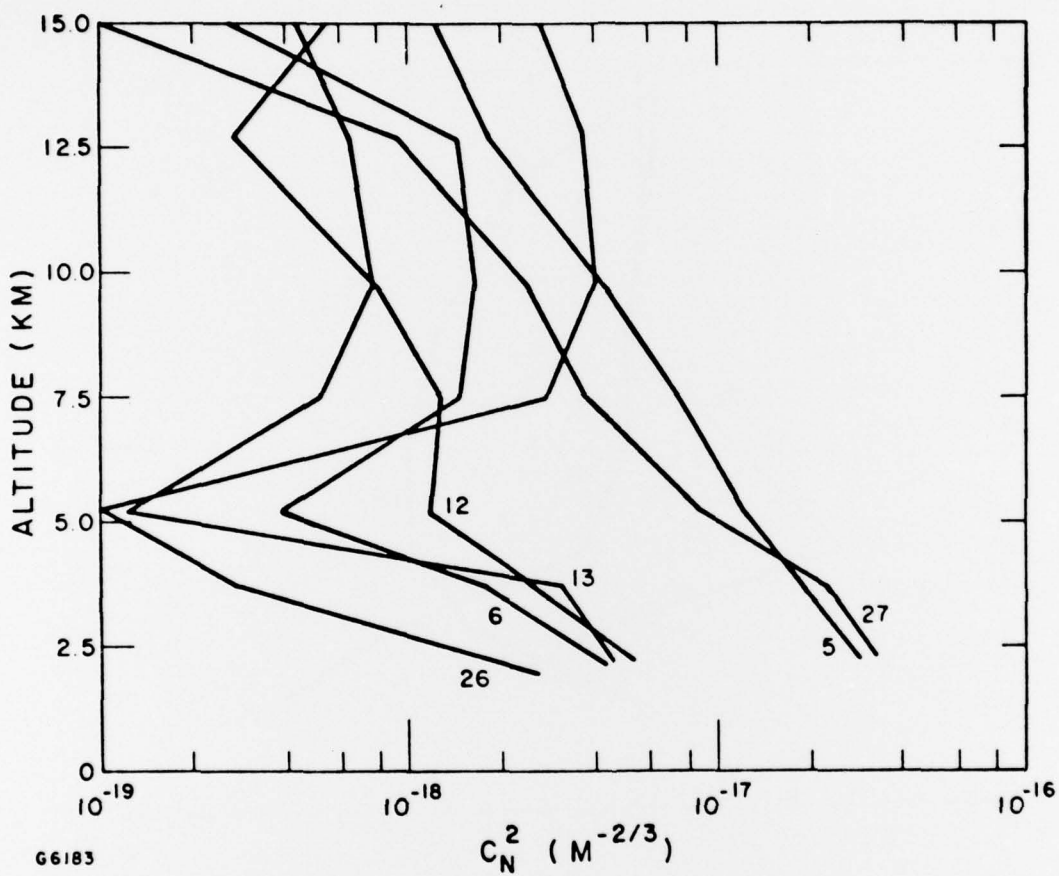


Figure B-4. Star Sensor Nightly Averaged Profiles - May 1976. Same as B-1.



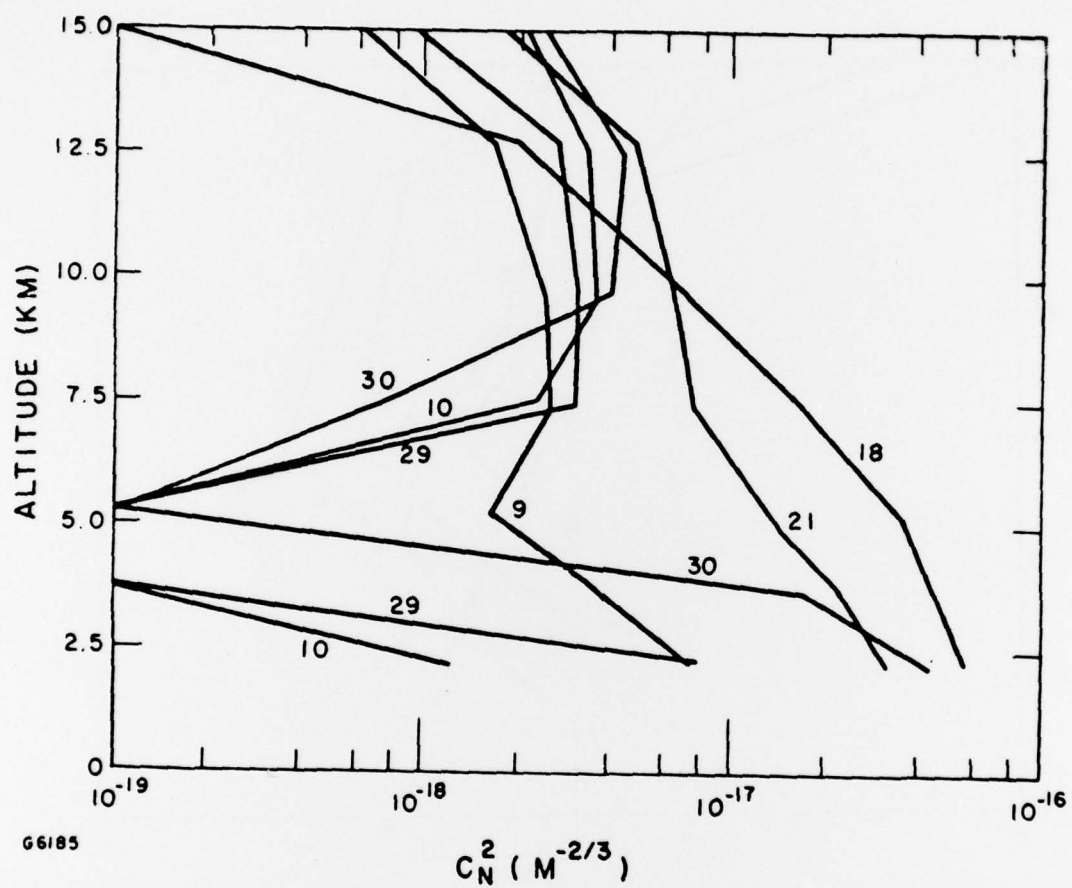


Figure B-5. Star Sensor Nightly Averaged Profiles - June 1976. Same as B-1.

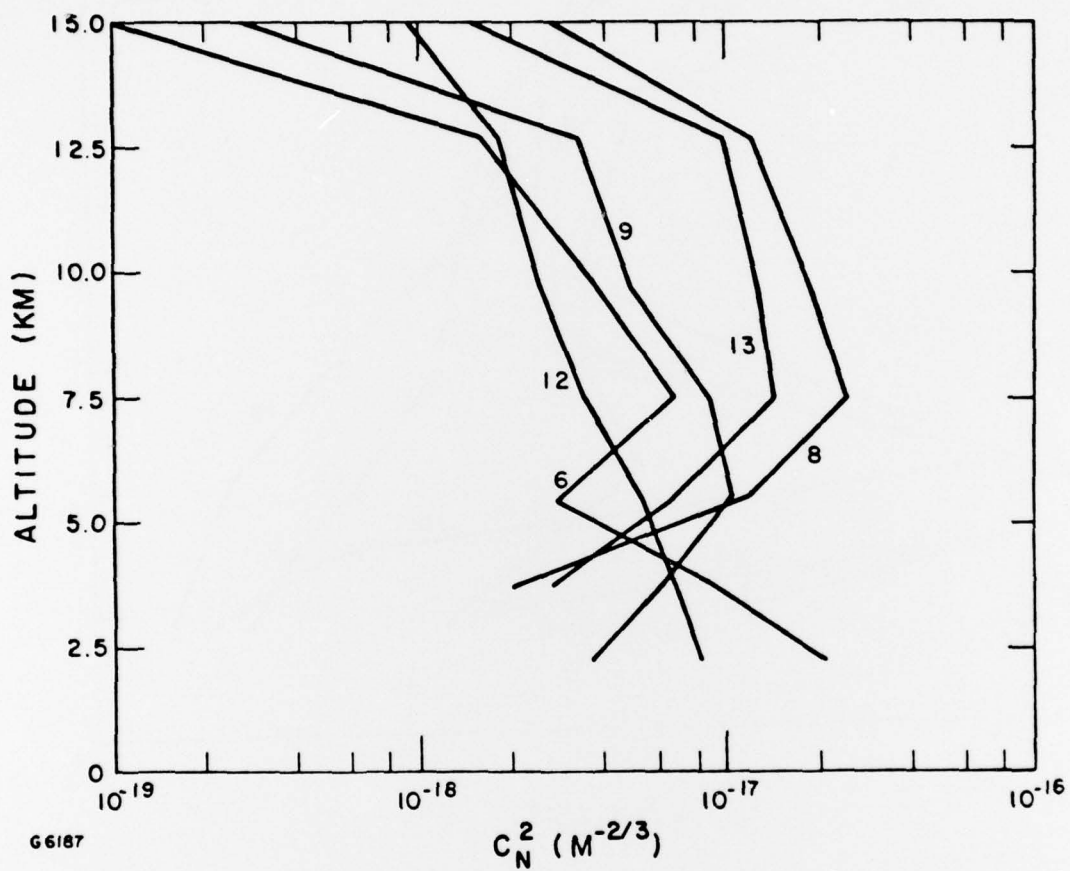


Figure B-6. Star Sensor Nightly Averaged Profiles - July 1976. Same as B-1.

APPENDIX C  
METEOROLOGICAL DATA

### Notes

1. All data points correspond to the average value of a 1350 member ensemble taken over a period of approximately 8.25 min.
2. The times given are approximate ( $\pm 5$  min.) local Hawaiian Standard Time. The dates given are those of the starting time.
3. Only one of the six calculated values of  $C_n^2$  is reported. This value was selected on the basis of wind direction and proper operation of the probes. The upwind probe pair closest to normal to the wind direction is the preferred set.
4. Radiosonde data is from the USWB station at Hilo, Hawaii, approximately 110 miles south-east of AMOS. Launch time was 0200 HST. Data reported corresponds to the night of each data run.

TABLE C-1. MICROTHERMAL DATA-SUMMARY

Date	Time HST	No. of Points	Cn2 (M - 2/3) x 10 <sup>-15</sup>	
			Mean	Range
14 Nov 1975	2110 - 2410	18	2.89	0.775 - 6.62
15	1930 - 2230	18	9.17	4.67 - 16.1
17	1950 - 2250	18	2.28	0.94 - 3.09
18	2050 - 2350	18	7.01	1.28 - 13.3
19	2020 - 2320	18	7.25	1.36 - 16.2
21	1930 - 2130	18	6.90	1.09 - 16.6
6 Dec 1975	0100 - 0400	17	1.16	0.48 - 4.02
8	0200 - 0500	18	5.16	1.38 - 10.5
Total		143	5.26	0.48 - 16.6

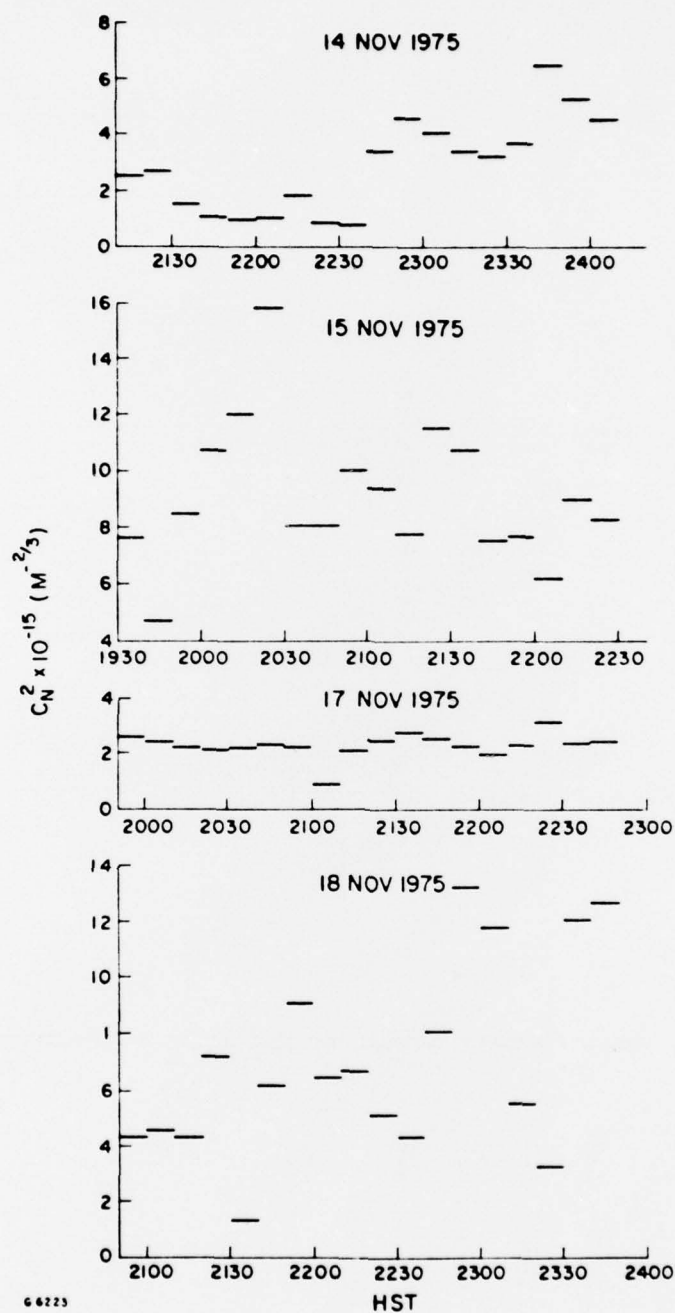


Figure C-1. Microthermal Data - 14, 15, 17 and 18 November 1975. The horizontal lines indicate the averaging period.



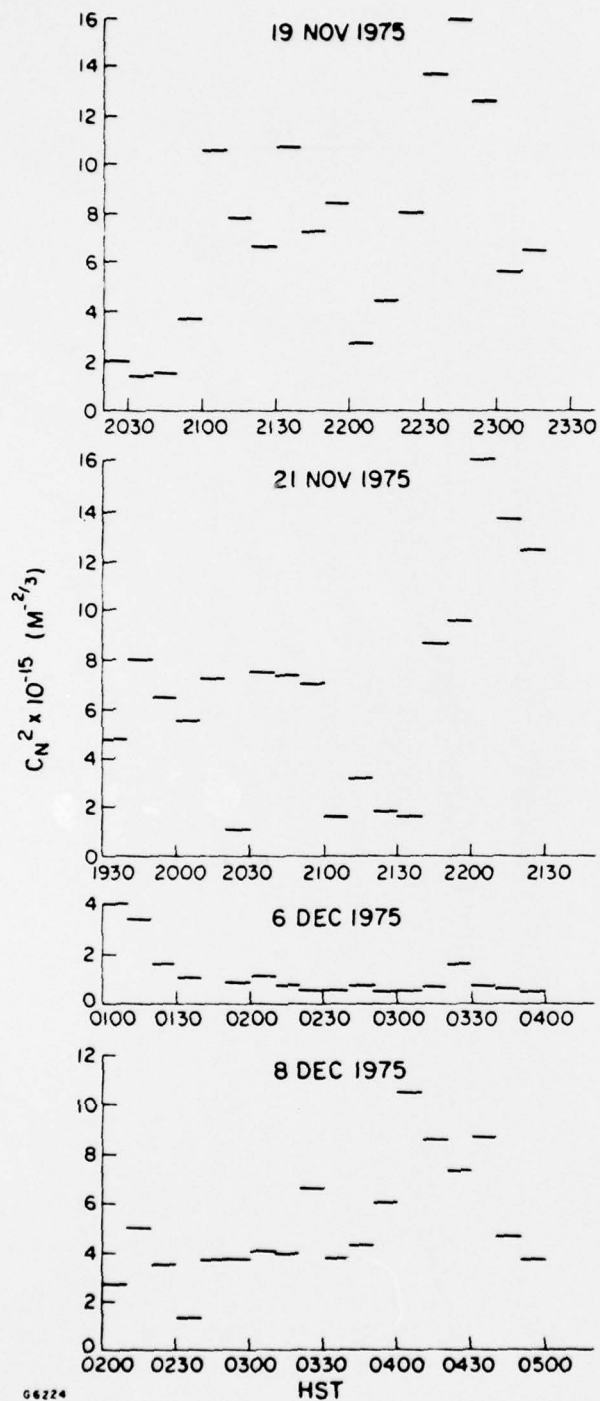


Figure C-2. Microthermal Data - 19 and 21 November and 6 and 8 December 1975. Same as C-1.

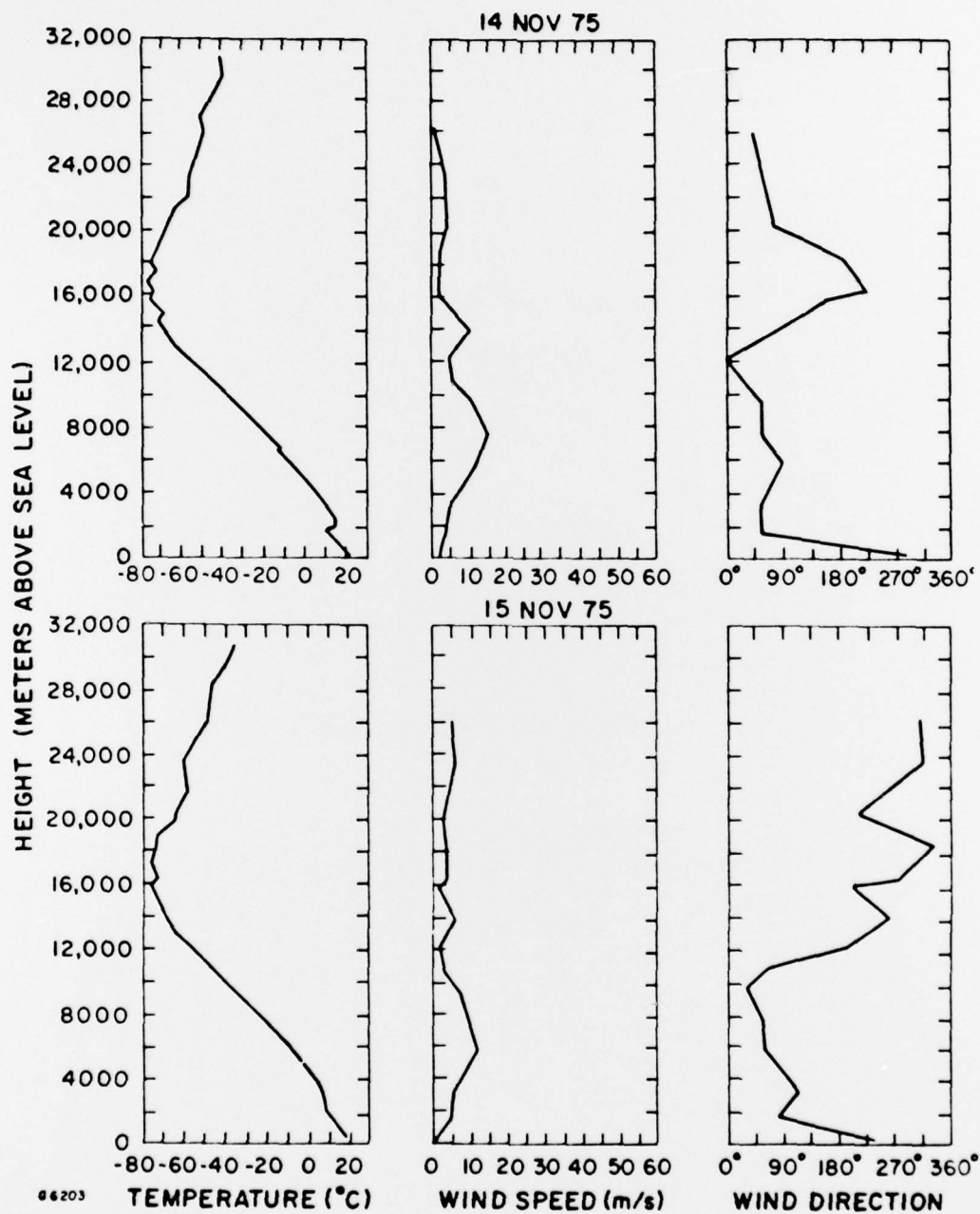


Figure C-3. Meteorological Data - 14 and 15 November 1975. Based on radiosonde data taken at Hilo, Hawaii at 0200 local time. The date indicates the mission date of Table C-1.

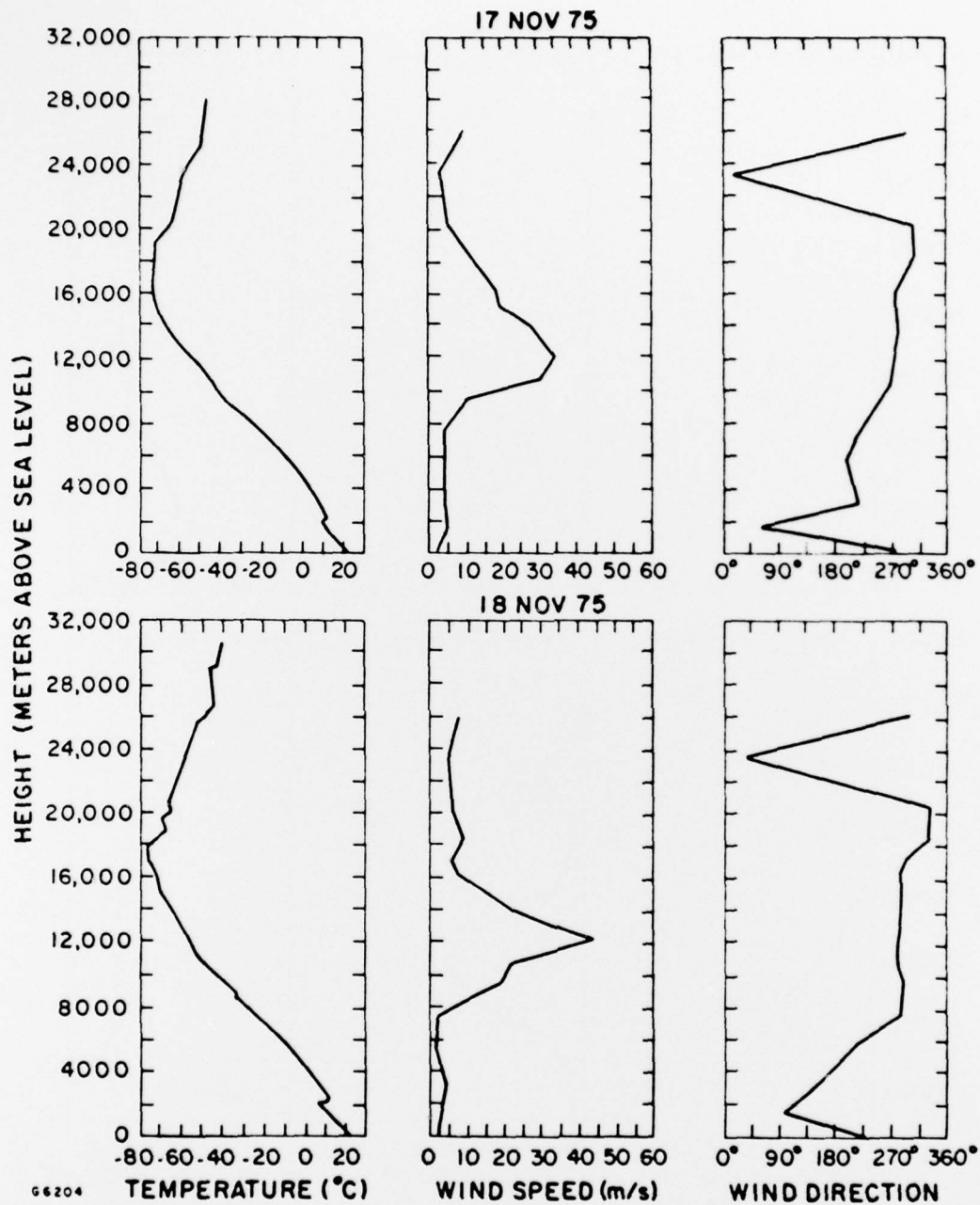


Figure C-4. Meteorological Data - 17 and 18 November 1975. Same as C-3.

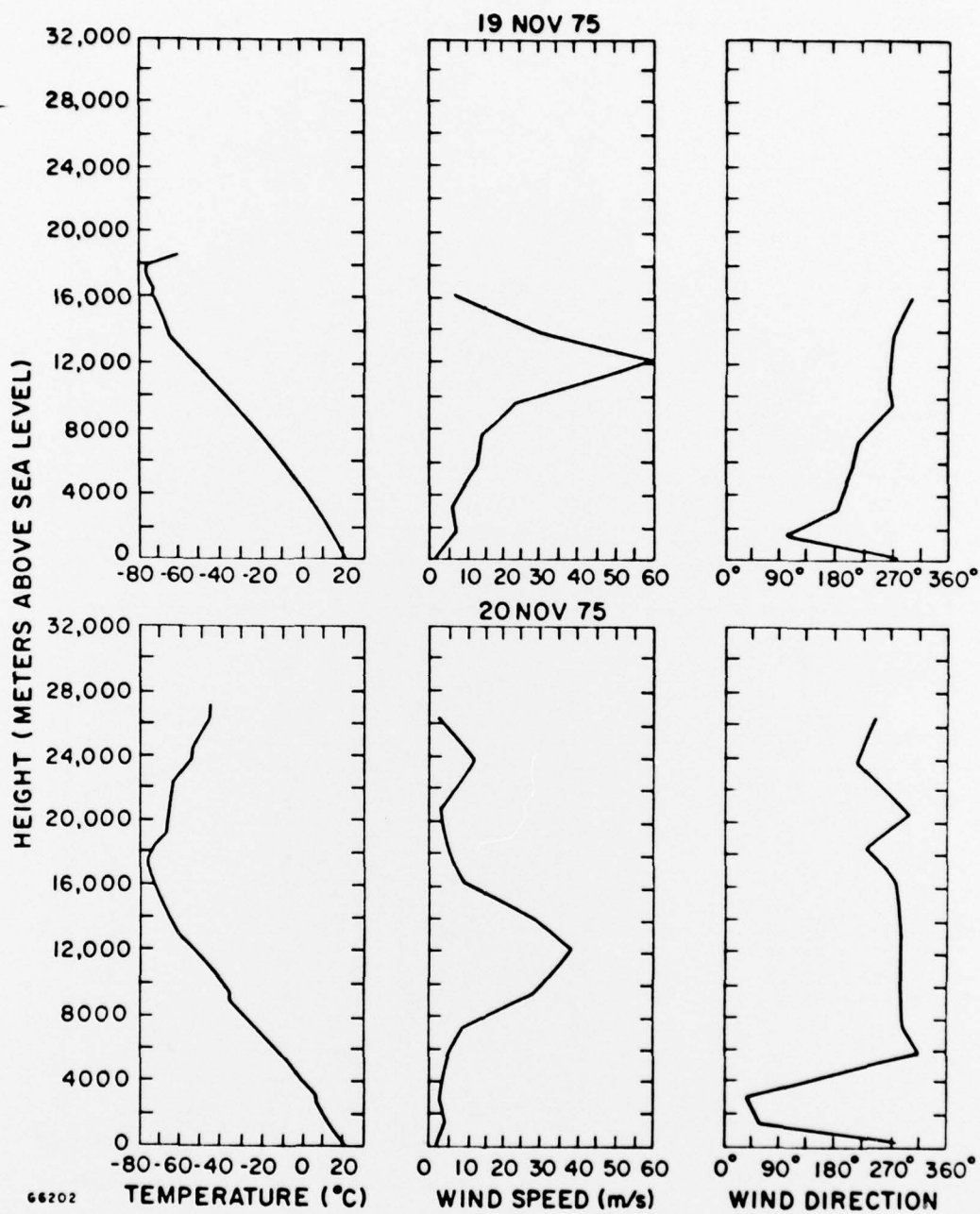


Figure C-5. Meteorological Data - 19 and 20 November 1975. Same as C-3.

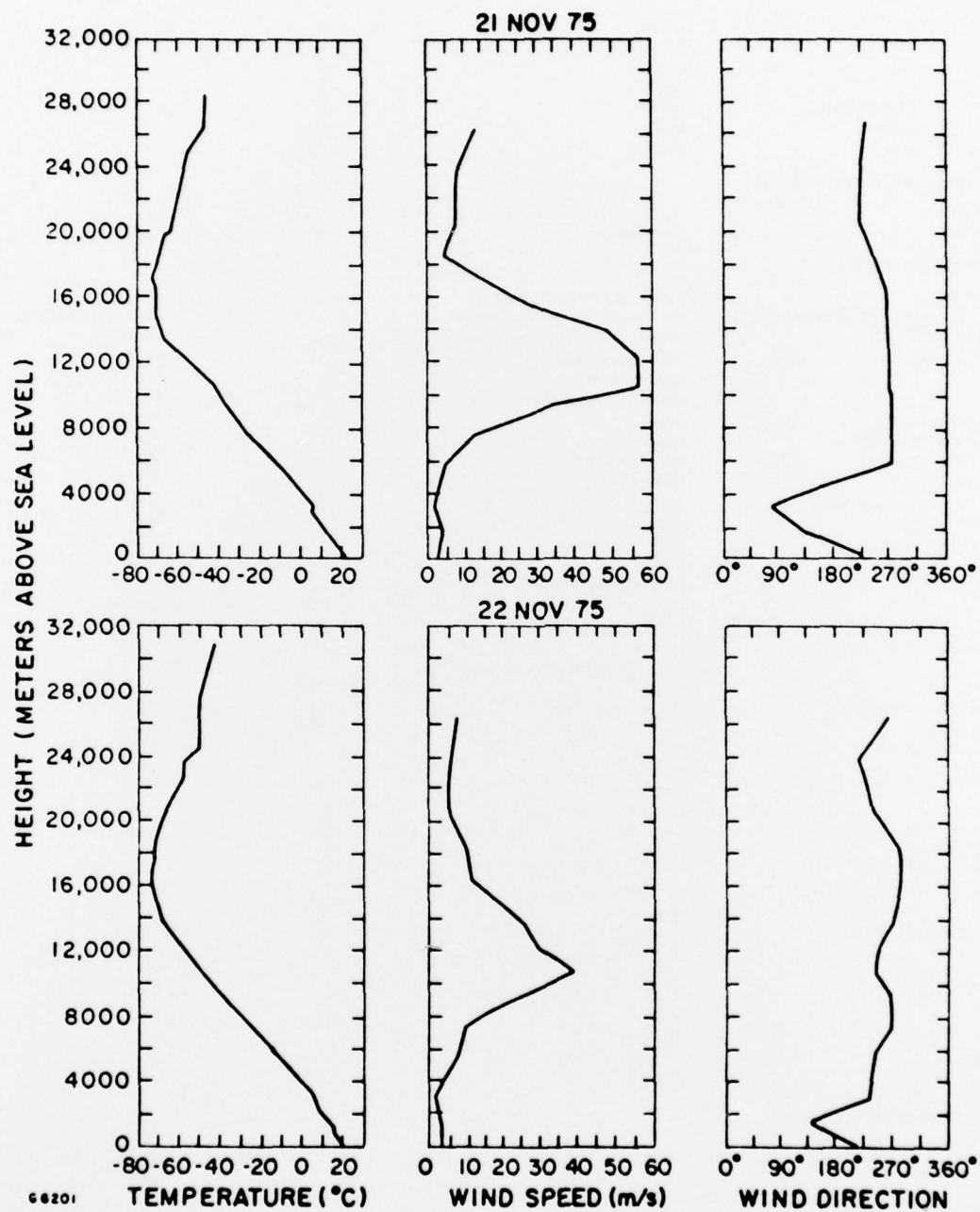


Figure C-6. Meteorological Data - 21 and 22 November 1975. Same as C-3.



# METRIC SYSTEM

## BASE UNITS:

Quantity	Unit	SI Symbol	Formula
length	metre	m	...
mass	kilogram	kg	...
time	second	s	...
electric current	ampere	A	...
thermodynamic temperature	kelvin	K	...
amount of substance	mole	mol	...
luminous intensity	candela	cd	...

## SUPPLEMENTARY UNITS:

plane angle	radian	rad	...
solid angle	steradian	sr	...

## DERIVED UNITS:

Acceleration	metre per second squared	...	m/s
activity (of a radioactive source)	disintegration per second	...	(disintegration)/s
angular acceleration	radian per second squared	...	rad/s
angular velocity	radian per second	...	rad/s
area	square metre	...	m
density	kilogram per cubic metre	...	kg/m
electric capacitance	farad	F	A·s/V
electrical conductance	siemens	S	A/V
electric field strength	volt per metre	...	V/m
electric inductance	henry	H	V·s/A
electric potential difference	volt	V	W/A
electric resistance	ohm	...	V/A
electromotive force	volt	V	W/A
energy	joule	J	N·m
entropy	joule per kelvin	...	J/K
force	newton	N	kg·m/s
frequency	hertz	Hz	(cycle)/s
illuminance	lux	lx	lm/m
luminance	candela per square metre	...	cd/m
luminous flux	lumen	lm	cd·sr
magnetic field strength	ampere per metre	...	A/m
magnetic flux	weber	Wb	V·s
magnetic flux density	tesla	T	Wb/m
magnetomotive force	ampere	A	...
power	watt	W	J/s
pressure	pascal	Pa	N/m
quantity of electricity	coulomb	C	A·s
quantity of heat	joule	J	N·m
radiant intensity	watt per steradian	...	W/sr
specific heat	joule per kilogram-kelvin	...	J/kg·K
stress	pascal	Pa	N/m
thermal conductivity	watt per metre-kelvin	...	W/m·K
velocity	metre per second	...	m/s
viscosity, dynamic	pascal-second	...	Pa·s
viscosity, kinematic	square metre per second	...	m/s
voltage	volt	V	W/A
volume	cubic metre	...	m
wavenumber	reciprocal metre	...	(wave)/m
work	joule	J	N·m

## SI PREFIXES:

Multiplication Factors	Prefix	SI Symbol
1 000 000 000 000 = 10 <sup>12</sup>	tera	T
1 000 000 000 = 10 <sup>9</sup>	giga	G
1 000 000 = 10 <sup>6</sup>	mega	M
1 000 = 10 <sup>3</sup>	kilo	k
100 = 10 <sup>2</sup>	hecto*	h
10 = 10 <sup>1</sup>	deka*	da
0.1 = 10 <sup>-1</sup>	deci*	d
0.01 = 10 <sup>-2</sup>	centi*	c
0.001 = 10 <sup>-3</sup>	milli	m
0.000 001 = 10 <sup>-6</sup>	micro	μ
0.000 000 001 = 10 <sup>-9</sup>	nano	n
0.000 000 000 001 = 10 <sup>-12</sup>	pico	p
0.000 000 000 000 001 = 10 <sup>-15</sup>	femto	f
0.000 000 000 000 000 001 = 10 <sup>-18</sup>	atto	a

\* To be avoided where possible